Engineering Protein Electrophoresis through Surfactant Design

Mónica Ospinal Jiménez

A dissertation
submitted in partial fulfillment of the
requirements for the degree of

Doctor of Philosophy

University of Washington

2013

Committee:

Danilo C. Pozzo, Chair

Hong Shen

Daniel T. Schwartz

John C. Berg

Guozhong Cao

Program Authorized to Offer Degree:

Department of Chemical Engineering

University of Washington

Abstract

Engineering Protein Electrophoresis through Surfactant Design

Mónica Ospinal-Jiménez

Chair of the Supervisory Committee:
Professor Danilo C. Pozzo
Department of Chemical Engineering

Protein separations have important applications in the medical industry. In the absence of physical symptoms, early detection of protein markers for disease can significantly decrease the morbidity and mortality of diseases like cancer, and Alzheimer's. New proteomic approaches are becoming a promising path in the advancement of diagnosis and determination of effective treatments for disease.

The specific molecular structure of a denatured protein is a key factor for the development of reliable protein separations. In polyacrylamide gel electrophoresis (PAGE), protein-surfactant interactions play an important role in the identification of proteins. Studies on protein-surfactant complexes have shown that the nature of the binding forces and related interactions originate primarily from the hydrophobic and ionic interactions between proteins and charged surfactants. However, limited information is available to directly correlate the structure of protein-surfactant complexes to their electrophoretic migration. The overall goal of this study is to develop a fundamental structural understanding of protein-surfactant complexes while aiming towards optimizing protein separations. This work focuses on protein denaturation studies using anionic surfactants with different chain architectures.

The structural characterization by small angle scattering analysis shows that, based on the architecture of the surfactant, protein-surfactant complexes primarily form pearl-necklace or elongated structures. Working with different surfactant chain structures reveals that probing of structural parameters is essential to the rational improvement of efficiency and resolution in protein electrophoresis. Here, we start to decipher the relationship between surfactant chemistry, macroscopic separation and structural parameters of various protein-surfactant complexes to enable the future design of engineered surfactant formulations.

TABLE OF CONTENTS

LIST OF FIGURES

Figure **Page**

LIST OF TABLES

Table **Page**

List of Acronyms

α: α-lactabulmin

$\triangle A$: Delta absorbance

μ_e : Electrophoretic mobility

$\triangle \rho$: Electron or scattering density difference between the particle and the solvent

1D : One dimensional gel electrophoresis

2-BOS : Sodium 2-butyloctyl sulfate

2D : Two dimensional gel electrophoresis

2-EHS : Sodium 2-ethylhexyl sulfate

3,7-DMOS : Sodium 3,7-dimethyloctyl sulfate

A: aprotinin

A_0: Background signal

A_c: Instrument constant (DLS)

A_L : Absorbance of left circularly polarized light

a_o : Effective head group area

A_R : Absorbance of right circularly polarized light

b_i : Bound coherent scattering of an atom i

bkg: Background intensity

BSA or B : Bovine serum albumin

c : Protein concentration (mg/mL)

C: Carbonic anhydrase

CD : Circular dichroism

CMC : Critical micelle concentration

CPP : Critical packing parameter

D': Diameter of a sphere

D_f : Diffusion coefficient

D_H: Hydrodynamic diameter

DLS : Dynamic light scattering

D_m: Micelle diameter

DTT : Dithiothreitol

E: Applied electric field

FWHM: Full width at half maximum

G: β-galactosidase

GIFT : Generalized Inverse Fourier Transformation

$I(q)$: Scattered intensity

I_0 : Zero angle intensity

IFT : Indirect Fourier transformation

k : Boltzmann constant

k_i : Incident radiation

k_s : Scattered radiation

l : Aliphatic hydrocarbon tail length

L : protein-surfactant complex length

l : Pathlength

MRE : Mean residue ellipticity

MRW : Mean residue weight

Mw: Molecular weight

N : Number of particles

n : Number of amino acids

n_L : Total number of carbon atoms in the longest segment

n_m : Number of terminal methyl groups

NMRSD: Normalized root-mean-square deviation

n_T: Total number of carbon atoms in the aliphatic chain

O: Ovalbumin

$P(q)$: Form factor

P: Phosphorylase

PAGE : Polyacrylamide gel electrophoresis

PDB: Protein data bank

PDDF or *P(r)*: Pair-distance distribution function

PFC_4S : potassium perfluorobutane sulfonate

PFC_6S : Potassium perfluorohexane sulfonate

PFC_8S : Potassium perfluorooctane sulfonate

q : Scattering vector

r : Distance within an object

r': r-distance in the x-axes in the PDDF

r_1: Magnitude of distance r

r_e : Classical radius of the electron

R_g : Radius of gyration

R_H: Hydrodynamic radius

r_m *:* Micelle radius

$S(q)$: Structure factor

S : Nearest neighbor distance between micelles

SANS : Small angle neutron scattering

SAS : Small angle scattering

SAXS : Small angle x-ray scattering

$SC_{10}S$: Sodium decyl sulfate

$SC_{12}S$: Sodium dodecyl sulfate

$SC_{14}S$: Sodium tetradecyl sulfate

$SC_{16}S$: Sodium hexadecyl sulfate

SC_6S : Sodium hexyl sulfate

SC_8S : Sodium octyl sulfate

SC_xS : Sodium alkyl sulfates

SDS : Sodium dodecyl sulfate

SLD or ρ_i : Scattering length density
T: Temperature

Trp: Tryptophan

v : Hydrocarbon tail volume

V : Scattering volume

$v_{complex}$: Protein complex velocity

v_m : Atomic molecular volume

$V_{particle}$: Particle volume

Z_i : Atomic number of atom i

θ : Scattering angle

θ_e : Ellipticity

λ : Incident radiation wavelength

μ : Viscosity of the fluid

τ : Time shift

Γ: Decay constant

ACKNOWLEDGMENTS

Without a doubt this is the most important page in the whole document. It is here where I can write what I "want" and not what I "should". The place where my memories became tangible and I can materialize the names of those who I met in this adventure.

I would like to thank to my Advisor Danilo Pozzo, for his guidance, mentoring, support and for his patience during this journey. But most importantly I would like to thank Danilo and Marvi for letting me observe that it is possible to successfully mix love to science, success, hard work and family. Thanks to both of you.

I also would like to thank members of my committee, Prof. John Berg, Prof. Hong Shen, Prof. Dan Schwartz and Prof. Guozhong Cao for their support, guidance and inspiration.

My start at UW wasn't smooth; it started with limited English, chickenpox and a deep homesickness from Puerto Rico and Colombia. But with time, layers of clothes and new good friends I started to enjoy this journey, to love the weather, to like the city and everything around, including the non-stop raining days. Because of that, I would like to express my most sincere gratitude to: Valerie, Renata, Rob, Katie, Kjersta, Carolynn, Suhasini, Leila, Pablo, Jeff, Greg, Mike, Saran, Sathana, Christina, Karen and Joyce. They offered me their friendship, interesting conversations, encouragement, guidance, comic relief, smiles, hugs, and from whom I have learned immeasurably. Most importantly, they gave me the sense of family in this foreign land.

I appreciate the enthusiasm and effort of the undergraduate students who contributed to this research including, Epiphany Nfr, Kevin Kohlmeier, Christina Ellias, Mitchel Smith and Chantelle Jacques. I am deeply grateful to those who helped me edit this dissertation: Christina, Renata, Rob, Karen, Heidi and Pablo.

Finally, I want to acknowledge the key element that my family plays in this adventure. Mi Mama, mi Papa, Mario, Jorge, Leidy, Marisel, Omayra and Jessica, your love and endless source of moral and emotional support made it possible for me to reach this professional milestone. Mario thanks for all the times that you drove me home at very late hours. But most important for being a continuous inspiration in my life. You are the most science-passionate person I have ever met and I want to continue learning from you.

"God has been present from beginning to end of this project"

DEDICATION

To Miriam Jimenez Garcia, (Para ti mami), who without being an engineer,
supported me the best and filled my days (literally)
with her love, enthusiasm, courage, and hope.

CHAPTER I

PROTEIN SEPARATIONS

The characterization of the genome opened the opportunity to pay attention to the significance of proteins, which are key factors in all biological functions[1]. The vast number of proteins in humans and their functional significance are the key elements to motivate biological studies focused in protein biomarkers[2]. Serum analysis, which involve the study of the richest source of biological markers, can entail the detection of around a million of proteins[3]. Thus, efforts that contribute to the enhancement of techniques that differentiate proteins should improve the ability to detect diseases in earliest stages; this helps with the diagnosis and risk assessment. One of the biggest challenges in protein identification is increasing the fidelity in the detection of low-abundance proteins that are shadowed by high-abundance proteins and the improvement of the separation of membrane proteins[1,4,5]. The identification of the proteins contained in body fluids allows diagnosing the appearance or vanishing of biomarkers that are related with diverse biological activities. Table 1.1 contains the name of some proteins that have been labeled as potential biomarkers for diseases.

Table 1. 1. Protein markers and diseases[3,6–9].

Protein names	**Disease**
CA 125	Cancer
Fibulin-3 (Fib3-1, Fib3-2), follistatin-like (FSTL1)	Osteoarthritis
Haptoglobin, Apolipoprotein A-IV, PRO2044 (unnamed protein)	Guillain-Bárre syndrome
14-3-3, transthyretin, serotransferrin, gelsolin	Creutzfeldt-Jakob disease
Apolipoprotein-A1, clusterin, haptoglobin	Bladder transitional cell carcinoma

Protein analyses are done primarily by matrix-assisted laser desorption/ionization mass spectrometry (MALDI-MS), high performance liquid chromatography (HPLC) and gel electrophoresis[10,11]. Despite the high technology developed by some of these methods, there are still challenges identifying certain proteins. This is a real concern in the biological field, which is in need of more sensitive protein detection[4–6,9]. Among the mentioned techniques, gel electrophoresis is probably one of the easiest and most used approaches to separate proteins, and its improvement is one of the main motivations of this thesis. It is not surprising that refinements in protein separation will contribute to improvement of analytical techniques in terms of sensitivity, robustness, practicality and cost. Our efforts in particular, are focused on improving protein separations through an engineering approach in which polyacrylamide gel electrophoresis (PAGE) is improved by manipulating the nanostructure of protein-surfactant complexes.

1.1 Protein separation by gel electrophoresis

Polyacrylamide gel electrophoresis (PAGE) is one of the most used and practical techniques to separate proteins and DNA. It is used in molecular biology, genetics, and forensics fields[12]. Some of the assumptions made in this technique are: an identical charge per unit of mass in the protein-surfactant complexes, a constant ratio of protein to sodium dodecyl sulfate (1.4g of $SC_{12}S$ /g of protein) and that protein separation occurs because of differences in molecular size[13,14]. Although gel electrophoresis is quite practical and very well characterized, the separation of low-abundance proteins and membrane proteins is still challenging[4,15].

Figure 1.1 shows a schematic of a typical 1D gel electrophoresis, in which a protein is denatured by heat and stabilized by the addition of a reducing agent (dithiothreitol or DTT) and a surfactant. Researchers have studied a variety of anionic and cationic surfactants to be used in gel electrophoresis, however the anionic sodium dodecyl sulfate (SDS or $SC_{12}S$) is the preferred and most used surfactant[13,16,17].

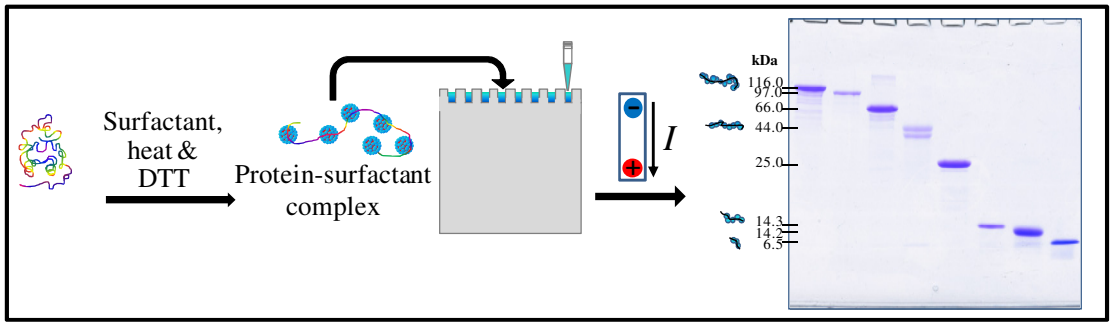

Figure 1. 1. Schematic of one dimensional (1D) gel electrophoresis.

Once the denatured protein is mixed with the surfactant, the protein-surfactant sample is loaded into the polyacrylamide or agarose gel wells. Then, under the

application of an electric field, each protein-surfactant complex travels through the gel at a different pace that is related to the intrinsic characteristic of the proteins such as their mass (SDS-PAGE) or their isoelectric points (isoelectric focusing, IEF). In the schematic of Fig.1.1, the protein-surfactant complexes migrate according to their molecular weight. The smaller proteins move faster through the gel and are located at the bottom of the gel (i.e., last band at 6.5 kDa), whereas the bigger ones move slowly and are trapped at the top of the gel (i.e., first band at 116 kDa).

Similarly, in order to maximize identification results obtained with this technique on complex mixtures, two consecutive analyses of 1 dimensional (1D) gel electrophoresis can be done. Thus, the results of the first 1D gel electrophoresis are analyzed by a second property in an additional polyacrylamide gel system in a process known as two-dimensional gel electrophoresis (2D PAGE). The use of this approach maximizes protein detection because of the use of a second property in an additional direction to spread proteins over a larger gel area. Some of the alternatives for a 2D analysis are combining separations by protein size, charge (isoelectric focusing, IEF), migration of native protein and surfactant-surfactant interaction[1,18].

Studies related to the migration of proteins through a gel cover a wide range of areas such as the type of surfactant, the experimental conditions, the migration mechanisms and the protein-surfactant interactions[19]. This thesis is mainly focused on gaining a fundamental understanding that correlates the macroscopic separation of proteins with surfactants and their nano-structures. Specifically, this thesis will cover the interactions of a series of proteins of diverse size and composition with sodium alkyl sulfates, sodium branched sulfates and potassium perfluorinated sulfonates.

1.2 Surfactant self-assembly generalities

Surfactants, the acronym given to the term surface active agents, are some of the most versatile molecules used in the pharmaceutical and biological industry[20,21]. Surfactants are also called soap, detergent or amphiphile molecules. They are characterized by the presence of a hydrophobic tail (water hating) and a hydrophilic head group (water loving). The hydrophobic and hydrophilic sections are usually composed respectively by an aliphatic chain of varied length and an ion such as: $-SO_4^-$, $-SO_3^-$, -OH, $-COO^-$ and $-NH_3^+$ among others. Surfactants are classified as anionic, cationic, zwitterionic or nonionic according with the intrinsic characteristics given by their head group. Within these classification, ionic surfactants are the most used in proteomic applications because of their strong and effective interactions at low concentrations with proteins[22]. Sodium dodecyl sulfate (SDS or $SC_{12}S$), an anionic surfactant of twelve carbons, is the preferred and most studied surfactant to conduct protein separations[13,23–29].

Surfactants are widely used in the fields of chemical engineering and biochemistry because of their tendency to self-assemble[20]. The formation of micelles is a spontaneous process that occurs at a specific concentration that is known as the critical micelle concentration (CMC). The shape of micelles depends primarily on the surfactant architecture and it is established by molecular parameters. In a diluted state with minimal interactions between aggregates, the shape of micelles can be estimated using the surfactant packing parameter, also referred as surfactant parameter, surfactant number or critical packing parameter (CPP). This dimensionless factor CPP (Eq. 1.1), relates the hydrocarbon tail volume (v), the aliphatic hydrocarbon tail length (l) and the effective head group area (a_o)[20,30,31]. Israelachvili reported that the CPP of sodium dodecyl sulfate

($SC_{12}S$ or SDS) is 0.37 and that $SC_{12}S$ monomers pack into slightly nonspherical micelles[30]. However, other studies have shown that samples of $SC_{12}S$ at high concentrations favor the formation of elongated ellipsoids[32,33].

$$CPP \approx \frac{v}{l \cdot a_o} \qquad \textbf{(1. 1)}$$

A summary of the typical CPP values and their expected structures and shapes are shown in Table 1.2.

Table 1. 2. Self assembled structures for different surfactant monomers[20].

Critical packing shape	Self-assembled structures	Critical packing parameter
Cone 	 Spherical	CPP ≤ 1/3
Truncated cone 	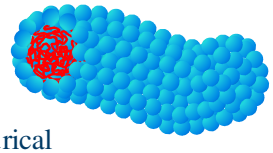 Cylindrical	1/3 < CPP < 1/2
Truncated cone 	Curved bilayers 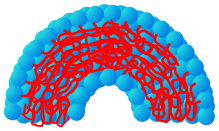	1/2 < CPP < 1
Cylinder 	Flat bilayer 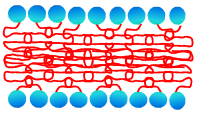	CPP ≈ 1

Assuming room temperature and no voids within the micelle, the v and l_c (in nm^3 and nm respectively) for a saturated aliphatic chain can be estimated using Equations 1.2 and 1.3, where n_T corresponds to the total number of carbon atoms in the aliphatic chain, n_m is the number of terminal methyl (CH3) groups, and n_L is the total number of carbons

along the longest segment [31,32]. To the best of our knowledge, there is no established method to calculate the CPP for branched surfactants. In most cases, the only observation about this topic is always referred to the anticipated large hydrocarbon tail volumes and therefore larger CPP[17].

$$v \approx \left(27.4 n_m + 26.9 \cdot \left(n_T - n_m\right)\right) \times 10^{-3} \qquad \textbf{(1. 2)}$$

$$l_c = 0.154 + 0.1265 \cdot \left(n - 1\right) \qquad \textbf{(1. 3)}$$

From CPP calculations it is clear that different surfactant structures could satisfy the same critical packing parameter. However, the structure with the smallest aggregation number will be the favored choice[30]. Thus, changes in the tail length or relative sizes for the head group will promote modifications in the CPP, for example, from spheres to cylindrical micelles. It is also expected that variation in the hydrophobic tail such as branching, will modify the shape of the micelle due to the larger tail volume. Similarly, the presence of fluorine in the surfactant tail also modify the micelles packing shape due the bulky size of the fluorine atoms when compared to hydrogen[32]. In this thesis work, the calculated CPP for linear, branched and fluorinated surfactants ranges between 0.36 and 0.5. Therefore, many structural shapes from spherical to cylindrical can be expected. In this work, scattering results have confirmed the self-assembly of linear, branched and fluorinated surfactants into spheres and ellipsoidal-like structures. Also, it was established that the architecture of the surfactant can modify not only the structure of free micelles but also the shape of the protein-surfactant complexes[34,35].

1.3 Protein-surfactant complexes

A protein-surfactant complex is a charged macromolecule that originates from the association of a surfactant with a protein either in its native or denatured state. The most common use of this term makes reference to the protein denaturation process in which an unfolded protein is stabilized by a surfactant. The physical mechanisms that control the association of micelles to native or denatured proteins include hydrophobic forces, electrostatic interactions, hydrogen bonding and Van der Waals attractions[11,13,36]. The study of protein-surfactant complexes is important because of the role that they play in food technology, pharmaceutical and detergent industries in addition to the biological field. The importance to this last discipline is usually related to protein purification, solubilisation and extraction of membrane proteins and protein identification [11,19].

Two of the main areas in protein-surfactant separation studies are the interactions between proteins and surfactants and the mechanisms that describe the electrophoretic migration of charged particles through a fixed network. Some of the approaches to describe the migration of polyelectrolytes during gel electrophoresis include the free-volume, the Slater-Guo and the reptation models[19]. The free-volume is the simplest migration model and it is suitable to describe the migration of globular particles, such as native proteins. However, this approach does not integrate the hydrodynamic interactions, gel flexibility and random barriers as factors affecting particle migration. The Slater-Guo model proposed a deviation of the free-volume model in which periodic obstacles are considered along the migration of the particles through the gel. However, neither of these two models can effectively describe the electrophoresis phenomenon for large flexible particles, which is the best definition to describe the migration of protein-surfactant

complexes through a gel. Back in the 1970's two independent research groups approached for the first time the electrophoretic migration of linear polyelectrolyte like the movement of a snake in thick grass[37,38]. This introductory idea inspired additional theoretical predictions such as models for the biased reptation with and without fluctuations, which have been used before to explain the migration of proteins-surfactant complexes through a sieving matrix[19,39].

Each of the models detailed above have postulated specific theories to describe the migration of particles that have different shapes. We hypothesize that the migration mechanisms could be influenced by the shape of the charged particles (i.e. protein-surfactant complexes). Therefore, fundamental studies focused on identifying the nano-structure and the interactions between protein and surfactants can potentially contribute to a better understanding of the migration mechanism of these charged complexes.

Based on structural parameters it is not surprising that the migration of protein-surfactant complexes through a gel is better described by models such as the reptation than the free-volume. Upon the protein denaturation process, surfactant starts binding the protein, turning it into a more elongated flexible complex. Protein conformation upon denaturation with surfactants can be rather complex and changes in protein conformation are not fully understood[39].

On the other hand, given the variability in the protein composition and the dynamic nature of the association of surfactant to the protein backbone during protein denaturation, diverse forms of protein-surfactant complexes could be anticipated. Fig. 1.2 shows five schematics examples of three different shapes that protein-surfactant

complexes could adopt upon denaturation: pearl-necklace (left), ellipsoidal (top-right) and rod-like (bottom-right) complexes. Protein-surfactant conformation of these types have been shown previously and are the result of multiple and extensive analyses performed by a combination of spectroscopy, microscopy, kinetics, rheology and small angle scattering techniques [14,34,35,40–42].

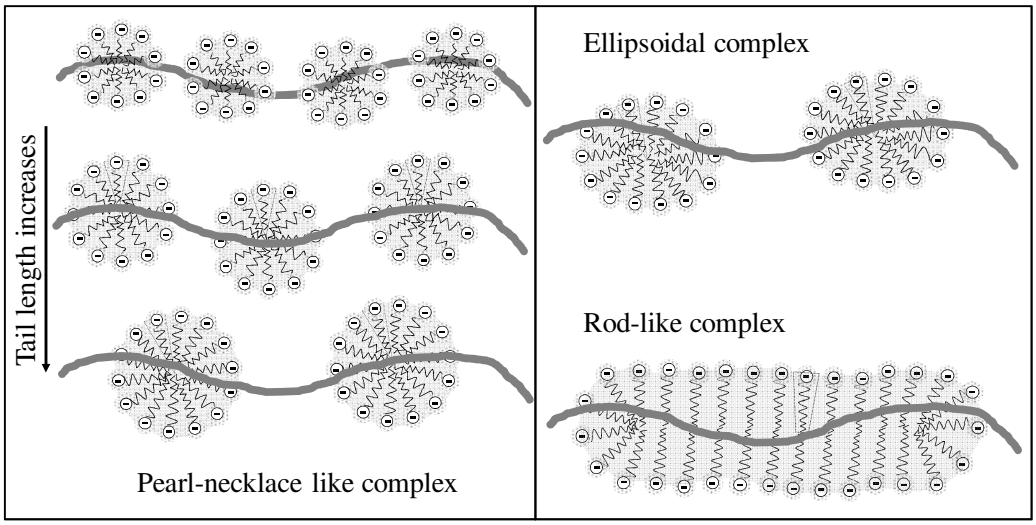

Figure 1. 2. Schematic of protein-surfactant complexes of different shape.

In the left side of Fig.1.2, three alternatives of pearl-necklace structures are described. These pearl-necklaces represent the expected interaction of three surfactants of different tail length to the same protein. The main difference between the pearl-necklace complexes are the size and number of micelles attached to the protein backbone. Thus, as the surfactant tail length decreases, the protein-surfactant complex could be more densely decorated by smaller micelles. The right side of Fig. 1.2 illustrates the shape of ellipsoidal and rod-like complexes. Surfactants with alternative architecture such as branching or fluorinated could induce the formation of these alternative shapes [43]. Thus, we expect that the difference in surfactant architectures will form diverse micelle shapes

and that this will also cause variations in the shape of the protein-surfactant complex. We hypothesize that long tailed, branched or bulky tailed surfactants could form more elongated and packed protein-surfactant complexes since the CPP increases.

The study of the interactions of native proteins denatured by surfactants of diverse architectures contributes not only to our fundamental understanding of protein separations, but also provide basic knowledge to better describe the overall hydrodynamics of protein-surfactant complexes with diverse shapes.

1.4 Protein-surfactant interactions

The interactions of a surfactant when binding to proteins depend to a great extent on the molecular parameters of the surfactant, such as the charge of the head group and the length of the hydrophobic tail. Other important parameters include the surfactant concentration, the solvent composition and the nature of the biomolecules in study [44]. Previous studies have shown that, at lower surfactant concentrations, electrostatic interactions dominate the initial surfactant adsorption and that hydrophobic interactions play a dominant role when the surfactant concentration increases. Similarly, the class of surfactant (anionic, cationic and zwitterionic) and its intrinsic characteristics plays an important role in the interactions with proteins[22]. On the other hand, the linear association of amino acids in a protein, which is called primary structure or sequence, confers unique interactions with surfactants based on their localized properties (positively charged, negatively charged, uncharged, hydrophobic and hydrophilic).

In general terms, surfactant and protein adsorption have been studied by isothermal titration calorimetric, circular dichroism, small angle scattering and

fluorescence spectroscopy among other complementary techniques[11,13,40,45–48]. The adequate use of these methods provides insights on the preferential adsorption regions and the thermodynamics of the interactions from which it is also possible to evaluate the nano-structural shapes and structural parameters of protein-surfactant complexes.

Studies on the interactions of protein and surfactants have improved understanding of the binding stages, their stoichiometric and the kinetics[11]. To this date, the findings of Reynolds and Tanford, related with the saturation of sodium dodecyl sulfate ($SC_{12}S$ or SDS) in proteins, is still the accepted guideline and basis for the assumptions used in the conduction of protein-surfactant electrophoresis analysis (e.g. constant binding of ~1.4 grams of surfactant/gram of protein)[13]. Also, through isothermal titration calorimetry, changes in the protein secondary structure upon surfactant binding have revealed the efficacy or limitation of certain surfactants to denature proteins [47]. Other important findings include protein flexibility, clustering and quantification of structural parameters[22].

Ruso and others have suggested that, for proteins denatured at room temperature, electrostatic and hydrophobic forces play the dominant role in binding[26,49–51]. They describe the protein-surfactant denaturing mechanism as a three-step process: first, the surfactant adsorbs through electrostatic interactions; this binding occurs primarily in regions with net opposite charge. Secondly, the surfactant causes the protein structure to expand. Lastly, after protein expansion, the hydrophobic regions become accessible and surfactant is adsorbed primarily by hydrophobic interactions. In contrast, thermal and chemical protein denaturation is often described in terms of the efficiency of breaking disulfide bonds, the thermal unfolding of the polypeptide and the stabilization of the

exposed hydrophobic areas by the surfactant. For proteins prepared for electrophoresis analysis, which typically includes boiling of the samples, addition of a reducing agent and the adsorption of surfactant implies that both thermal/chemical and surfactant denaturation processes could occur[25].

Although the multiple characterizations and studies in the field have explained intriguing phenomena occurring during the interactions between model proteins and surfactants, it is still necessary to continue expanding the field using surfactants of different architectures other than sodium dodecyl sulfate ($SC_{12}S$ or SDS). In doing so, it will be possible to better understand how the large variety of proteins interact with different surfactants, including the unfolding of globular proteins and the stability of membrane proteins upon interaction with alternative surfactants[11]. In addition, the growing production and use of environmental friendly surfactants will encourage further studies on their interactions with proteins given their technological and biological importance.

1.5 Objectives and Approach

While sodium dodecyl sulfate ($SC_{12}S$) is the main denaturing agent in gel electrophoresis, the use of alternative surfactants is an area of much interest because it provides the advantages of identifying proteins that are not feasible with $SC_{12}S$-PAGE [1,15,52–55]. The ideal protein separation implies the technical ability to resolve proteins separated by gel electrophoresis with great fidelity and reproducibility. A few studies have initiated the search for alternative surfactants either from a macroscopic separation point of view or from the analysis of the nano-structure in these complexes[52,56–60]. The

unique contribution and novelty of this work lies in the direct correlation of the structural changes occurring in protein-surfactant complexes with the changes in their macroscopic separations in order to gain fundamental understanding in the interactions of proteins and alternative surfactants. Also, studies with branched and fluorinated surfactants used as denaturing agent are new and of much interest for the design of novel surfactants. The goal of this work is brought to bear for both the development of new surfactant molecules and to elucidate the role of surfactant architecture in protein separations.

In this dissertation, the interactions between proteins and three different types of surfactants are examined: linear, branched and fluorinated. First, the experimental techniques that are used in this work are described in Chapters II and III. Then, Chapter IV presents the results of protein denaturation by a series of linear alkyl sulfates. With this systematic study it is shown that the effect of the surfactant tail length in the structure of the complexes and in protein gel electrophoresis is significant. Chapter V investigates the effect of tail branching in sodium short-tailed alkyl sulfates in protein denaturation. This work shows the modification of macroscopic separations by using branched surfactants and also highlights the unique role of these surfactants in the disruption of the protein's secondary structure. Finally, Chapter VI contains the results of using fluorinated surfactants as alternatives to enhance the binding interactions between proteins and short-tailed linear surfactants during protein gel electrophoresis.

1.6 References

(1) Verrills, N. M. *Clin. Biochem. Rev.* **2006**, *27*, 99–116.
(2) Gibbons, G. H.; Liew, C. C.; Goodarzi, M. O.; Rotter, J. I.; Hsueh, W. A.; Siragy, H. M.; Pratt, R.; Dzau, V. J. *Circulation, Journal of the American Heart Association* **2004**, *109*, 47–58.

(3) Ahmed, N.; Oliva, K. T.; Barker, G.; Hoffmann, P.; Reeve, S.; Smith, I. A.; Quinn, M. A.; Rice, G. E. *Proteomics* **2005**, *5*, 4625–4636.
(4) Rabilloud, T.; Chevallet, M.; Luche, S.; Lelong, C. *Proteomics* **2008**, *8*, 3965–3973.
(5) Gorg, A.; Weiss, W.; Dunn, M. *Proteomics* **2004**, *4*, 3665–3685.
(6) Jin, T.; Hu, L.-S.; Chang, M.; Wu, J.; Winblad, B.; Zhu, J. *European Journal of Neurology* **2007**, *14*, 563–568.
(7) Brechlin, P.; Jahn, O.; Steinacker, P.; Cepek, L.; Kratzin, H.; Lehnert, S.; Jesse, S.; Mollenhauer, B.; Kretzschmar, H. A.; Wiltfang, J.; Otto, M. *Proteomics* **2008**, *8*, 4357–4366.
(8) Mobasheri, A. *Osteoarthritis and Cartilage* **2012**, *20*, 1451–1464.
(9) Li, H.; Li, C.; Wu, H.; Zhang, T.; Wang, J.; Wang, S.; Chang, J. *Proteome Science* **2011**, *9*, 1–11.
(10) Samyn, B.; Sergeant, K.; Memmi, S.; Debyser, G.; Devreese, B.; Van Beeumen, J. *Electrophoresis* **2006**, *27*, 2702–2711.
(11) Otzen, D. *Biochimica et Biophysica Acta* **2011**, *1814*, 562–591.
(12) Kayser, M.; De Knijff, P. *Nat. Rev. Genetics* **2011**, *12*, 179–192.
(13) Reynolds, J. A.; Tanford, C. *Proceedings of the National Academy of Sciences of the United States of America* **1970**, *66*, 1002–1007.
(14) Reynolds, J. A.; Tanford, C. *The Journal of Biological Chemistry* **1970**, *245*, 5161–5165.
(15) Brown, E. G. *Analytical biochemistry* **1988**, *174*, 337–348.
(16) Rabilloud, T. *Journal of proteomics* **2010**, *73*, 1562–72.
(17) Chattopadhyay, A. K.; Mittal, K. L. Surfactants in Solution. *Surfactant science series* **1996**, *64*, 415.
(18) Bergh, G. Van Den; Arckens, L. *Expert Review Proteomics* **2005**, *2*, 1–10.
(19) Viovy, J.-L. *Reviews of Modern Physics* **2000**, *72*, 813–872.
(20) Berg, J. *An Introduction to Interfaces & Colloids. The Bridge to Nanoscience*; World Scientific Publishing Co. Pte. Ltd.: Singapore, 2010; p. 785.
(21) Schramm, L. L. *Surfactants : Fundamentals and Applications in the Petroleum Industry*; Cambridge University Press: Cambridge, UK, 2000.
(22) Ananthapadmanabhan, K. P.; Dickinson, E.; Goddard, E. D.; Lindman, B.; Strauss, U. P.; Thalberg, K.; Tirrel, M.; Winnik, F. M. *Interactions of Surfactants with Polymers and Proteins*; CRC Press, Inc.: Florida, USA, 1993.
(23) Shapiro, A. L.; Viñuela, E.; Maizel, J. V. *Biochemical and Biophysical Research Communications* **1967**, *28*, 815–820.
(24) Weber, K.; Osborn, M. *The Journal of Biological Chemistry* **1969**, *244*, 4406–4412.
(25) Mattice, W.; Riser, J. M.; Clark, D. S. *Biochemistry* **1976**, *15*, 4264–4272.
(26) Gimel, J. C.; Brown, W. *The Journal of Chemical Physics* **1996**, *104*, 8112–8117.
(27) Sonia F. Santos Hannes Fischer, Rosangela Itri, D. Z. *Journal of Colloid and Interface Science* **2003**, *262*, 400–408.
(28) Narayanan, J.; Abdul Rasheed, A. S.; Bellare, J. R. *Journal of colloid and interface science* **2008**, *328*, 67–72.
(29) Pozzo, D. C. *Langmuir* **2009**, *25*, 1558–1565.
(30) Israelachvili, J. *Intermolecular and Surface Forces with application to colloidal and biological systems*; Second.; Academic Press: London, 1985.
(31) Evans, F. D.; Wennerstrom *The colloidal domain where physics, chemistry, biology and technology meet*; 1st ed.; VCH Publishers, Inc.: New york, USA, 1994; p. 515.
(32) Tanford, C. *J. Phys. Chem* **1972**, *76*, 3020–3024.

(33) Bezzobotnov, V. Y.; Borbély, S.; Cser, L.; Faragó, B.; Gladkih, I. A.; Ostanevich, Y. M.; Vass, S. *J. Phys. Chem* **1988**, *92*, 5738–5743.
(34) Ospinal-Jimenez, M.; Pozzo, D. C. *Langmuir* **2011**, *27*, 928–935.
(35) Ospinal-Jiménez, M.; Pozzo, D. C. *Langmuir* **2012**, *28*, 17749–17760.
(36) Privalov, P. L. *Critical Reviews in Biochemistry and Molecular Biology* **1990**, *25*, 281–306.
(37) Lumpkin, O. J.; Zimm, B. H. *Biopolymers* **1982**, *21*, 2315–2316.
(38) Lerman, L. S.; Frisch, H. L. *Biopolymers* **1982**, *21*, 995–997.
(39) Dolnik, V.; Gurske, W. A. *Electrophoresis* **2011**, *32*, 2893–2897.
(40) Turro, N. J.; Lei, X.-G.; Ananthapadmanabhan, K. P.; Aronson, M. *Langmuir* **1995**, *11*, 2525–2533.
(41) Chen, S.-H.; Teixeira, J. *Physical Review Letters* **1986**, *57*, 2583–2586.
(42) Jones, M. N. *Biochemical Journal* **1975**, *151*, 109–114.
(43) Tiddy, G. J. T. Concentrated surfactant systems. *Modern Trends of Colloid Science in Chemistry and Biology* **1985**, 148–156.
(44) Tanford *The hydrophobic effect: formation of micelles and biological membranes*; John Wiley & Sons: New york, USA, 1973.
(45) Vivian, J. T.; Callis, P. R. *Biophysical Journal* **2001**, *80*, 2093–2109.
(46) Lindner, P.; Zemb, T. *Elsevier Science B.V.* **2002**.
(47) Nielsen, A. D.; Arleth, L.; Westh, P. *Biochimica et Biophysica Acta* **2005**, *1752*, 124–132.
(48) Casals, C.; Miguel, E.; Perez-Gil, J. *Biochemical Journal* **1993**, *296*, 585–593.
(49) Ruso, J. M.; Gonzáez-Pérez, A.; Prieto, G.; Sarmiento, F. *Colloids and Surfaces A* **2004**, *249*, 45–50.
(50) Ruso, J. M.; González-Pérez, A.; Prieto, G.; Sarmiento, F. *Internation Journal of Biological Macromolecules* **2003**, *33*, 67–73.
(51) Stenstam, A.; Khan, A.; Wennerstrom, H. *Langmuir* **2001**, *17*, 7513–7520.
(52) Starita-Geribaldi, M.; Thebault, P.; Taffin de Givenchy, E.; Guittard, F.; Geribaldi, S. *Electrophoresis* **2007**, *28*, 2489–97.
(53) Breyton, C.; Pucci, B.; Popot, J. In *Heterologous Expression of Membrane Proteins, Methods in Molecular Biology*; Mus-Veteau, I., Ed.; Humana Press: Totowa, NJ, 2010; Vol. 601.
(54) Chandramouli, K.; Qian, P.-Y. *Human Genomics and Proteomics* **2009**, *2009*, 1–22.
(55) López, M. F.; Patton, W. F.; Utterback, B. L.; Chung-Welch, N.; Barry, P.; Skea, W. M.; Cambria, R. P. *Analytical biochemistry* **1991**, *199*, 35–44.
(56) Rabilloud, T.; Chevallet, M.; Luche, S.; Lelong, C. *Journal of proteomics* **2010**, *73*, 2064–77.
(57) Hoffmann, H.; Kalus, J.; Thurn, H. *Colloid & Polymer Science* **1983**, *261*, 1043.
(58) Rodnin, M. V; Posokhov, Y. O.; Contino-Pépin, C.; Brettmann, J.; Kyrychenko, A.; Palchevskyy, S. S.; Pucci, B.; Ladokhin, A. S. *Biophysical journal* **2008**, *94*, 4348–57.
(59) Breyton, C.; Gabel, F.; Abla, M.; Pierre, Y.; Lebaupain, F.; Durand, G.; Popot, J.-L.; Ebel, C.; Pucci, B. *Biophysical journal* **2009**, *97*, 1077–86.
(60) Park, K.-H.; Billon-Denis, E.; Dahmane, T.; Lebaupain, F.; Pucci, B.; Breyton, C.; Zito, F. *New biotechnology* **2011**, *28*, 255–61.

CHAPTER II

SMALL ANGLE SCATTERING

Small angle scattering (SAS) is a powerful technique for research probing the structure of colloids, proteins, micelles, polymers, and porous media. Some advantages of using scattering include its non-invasive and non-destructive nature, the fact that information is averaged over the whole sample and the detailed and multi-scale analysis of shape, size, internal structure, crystallinity and porosity. Scattering techniques can use light, x-ray and neutrons to investigate structures over a size range from 1 to 1,000 nm. The work presented in this dissertation uses primarily small angle x-ray and neutron scattering (SAXS and SANS respectively) to characterize the structural features of protein-surfactant complexes in solution. A typical scattering experiment consists on the irradiation of a sample, such as colloidal particles, proteins or surfactants, by a collimated source of the selected radiation. Once the incident beam hits the sample, the radiation is transmitted, absorbed or scattered. A position sensitive detector measures the portion of the incident radiation that is scattered at different scattering angles (2θ). The information collected by the detector contains all of the structural information, which is in the form of the scattered intensity [I (2θ or q)] as a function of the scattering angle. Figure 2.1 shows a simplified illustration of a typical scattering experiment.

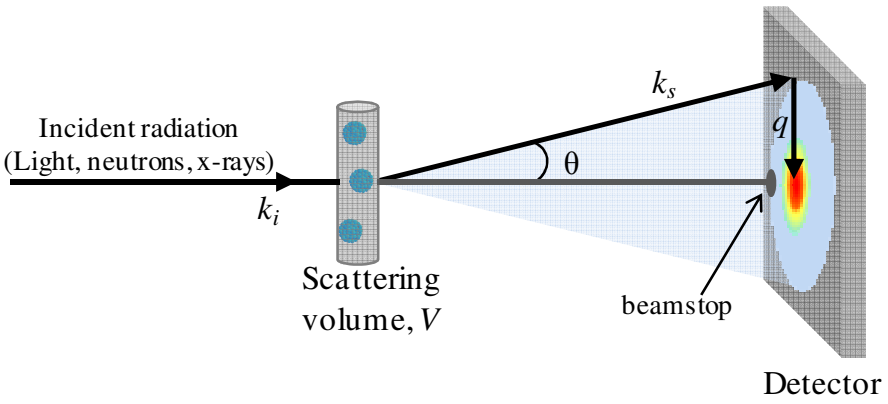

Figure 2. 1. Schematic of a small angle scattering experiment.

The scattering vector (q) is defined in terms of the propagation vectors of the incident (k_i) and scattered (k_s) radiation. In elastic scattering, both k_i and k_s, have the same magnitude ($2\pi/\lambda$) and are used to define the scattering vector in terms of the wavelength (λ) and the scattering angle (θ) (Eq. (2.1)) [1].

$$q = \frac{4\pi}{\lambda}\sin\frac{\theta}{2} \qquad \textbf{(2. 1)}$$

The scattered intensity, $I(q)$ which is a function of the shape and the size of the particles (Equation 2.2) is calculated as a function of the scattering length density (ρ_i), the form factor [$P(q)$], which is associated to the shape of single particles, and the structure factor [$S(q)$], which relates inter-particle correlations. Here, N is the number of particles, V the scattering volume, $V_{Particle}$ the particle volume, $\Delta\rho$ the scattering contrast between the particles and the solvent and bkg is the background intensity[1].

$$I(q) = \left(\frac{N}{V}\right) V_{Particle}^2 \Delta\rho^2 \cdot P(q) \cdot S(q) + bkg \qquad \textbf{(2. 2)}$$

The form factor $P(q)$ is the function that relates the scattered intensities to the geometry of an individual particle. It contains information about the shape, size and surface area of the particles. Fig. 2.2 shows the regions within a scattering profile from which different forms of structural information are obtained. At lower values of q, the radius of gyration (R_g) is obtained. In the medium range, the shape of the particles can be evaluated through the use of fitting models that provide specific characteristics, such as thickness, width, mass fractions, cross sectional dimensions, etc. Finally, at high values of q it is sometimes possible to characterize the total particle surface and to evaluate the smallest characteristic features within the particle.

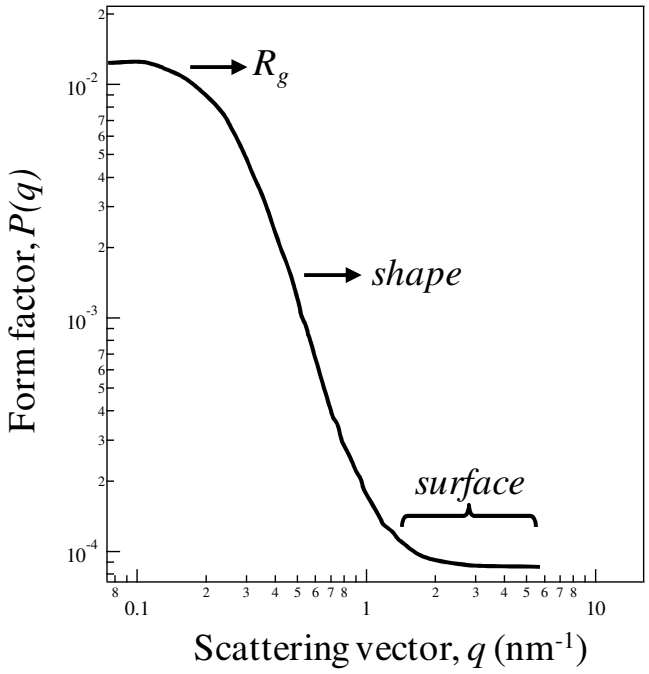

Figure 2. 2. Form factor regions in a scattering profile.

Another important component in scattering is the structure factor $S(q)$, which is related to the spatial correlation of different particles in solution. In the assumption of

infinite dilution, the particles become independent scatterers and the inter-particle correlation effects can be neglected giving the structure factor [$S(q)$] a constant value of one. In this limit, the interparticle distances are much larger than the particle dimensions. Then, the scattering data is primarily influenced by the average form factor ($P(q)$). Geometric models for $P(q)$ such as the monodisperse sphere, cylinder, fractal, parallelepiped among others can be used to extract the structural information contained in the scattering profile. The analyses of systems that cannot be represented by a single model can sometimes be treated with multiple models in different regions of q. Another alternative is to use the indirect Fourier transformation (IFT) method.

IFT is the fundamental method used to extract the pair-distance distribution function (PDDF), which is a real-space analogue of the scattering profile. Since good models are not available, this is the main analytical method that is used in this thesis to analyze the small angle scattering data (SAS) from protein-surfactant complexes. The selection of the method that is used to interpret scattering data, such as using simple models (such as cylinder, parallelepiped, spheres, etc) or a model-independent approach (IFT), also depends on the amount of information that is already known about the system and both techniques can be used complimentarily. However, in the absence of a good fitting model, performing IFT on the experimental scattering curves allows investigators to still obtain shape and structural information on the particles from the mathematical transformation of the Fourier space scattering data to real space structural parameters.

2.1 Pair distance distribution function (PDDF)

In this thesis, *P(r)*, which is one of the most consistent variable used in the literature to define pair distance distribution function (PDDF), is used in equations. The term PDDF is also used through the whole document in reference to any pair distance distribution functions. The pair distance distribution function (PDDF), which is obtained through an inverse Fourier transformation (IFT), is a probability function that is used to define contrast differences between two points separated by a distance (r) within an object [2,3]. In small angle scattering (SAS), this probability is related to local differences in neutron scattering length or electron densities (ρ_i) and yields information on the structure such as particle shape and size. PDDF is related to the probability that the points defined by the ends of a randomly placed vector of length r will have a large scattering contrast with the solvent[1]. Therefore, by using the PDDF it is possible to deduce the shape of a particle, including homogeneous and inhomogeneous structures, even though scattering models may not describe them. The calculation of a PDDF is not always simple because it can include extrapolation, smoothing and desmearing of the original data, which can potentially lead to high uncertainty. Desmearing is a correction for instrumental broadening effects.

There are two different directions that can be used to calculate these real space functions or PDDFs. When a structure's geometry and contrast is fully known, the calculation of the PDDF is simple and exact (Eq. 2.3). The PDDF can also be extracted directly from the scattering intensity but this process is more involved and can introduce errors from the transformation of potentially noisy and incomplete experimental data (Equation 2.4).

$$p(r) = \gamma(r) \cdot r^2 = \left(\int_V \Delta\rho(r_1) \cdot \Delta\rho(r_1 - r) dr_1 \right) \cdot r^2 \quad \textbf{(2. 3)}$$

$$p(r) = \frac{1}{2\pi^2} \int_0^\infty I(q).qr \sin qr \, dr \quad \textbf{(2. 4)}$$

Simple examples of PDDFs for homogeneous systems of particles with different shapes are shown in Figure 2.3. The structural symmetry of a sphere yields a bell-shaped PDDF function (Figure 2.3A). Figure 2.3B describes the PDDF of a structure composed of two neighboring spheres: this representation it is commonly used to illustrate neighboring micelles associated to a protein. The shape of this PDDF is also the emblematic plot of a pearl-necklace structure from which it is possible to extract the average distance between adjacent micelles, known as the nearest neighbor distance (*S*), the micelle radius (r_m) and the maximum length of the structure (*L*). Finally, Figure 2.3C corresponds to the PDDF of a cylindrical particle such as rod fibers, cylindrical surfactant micelle or cylindrical protein-surfactant complexes. The features in this plot allow identifying the total length (*L*) and radius of the structure (*r*). SinglebodyMC software was used to produce the PDDF of the three systems shown in Fig. 2.3 by random Monte Carlo sampling and Equation 2.3.

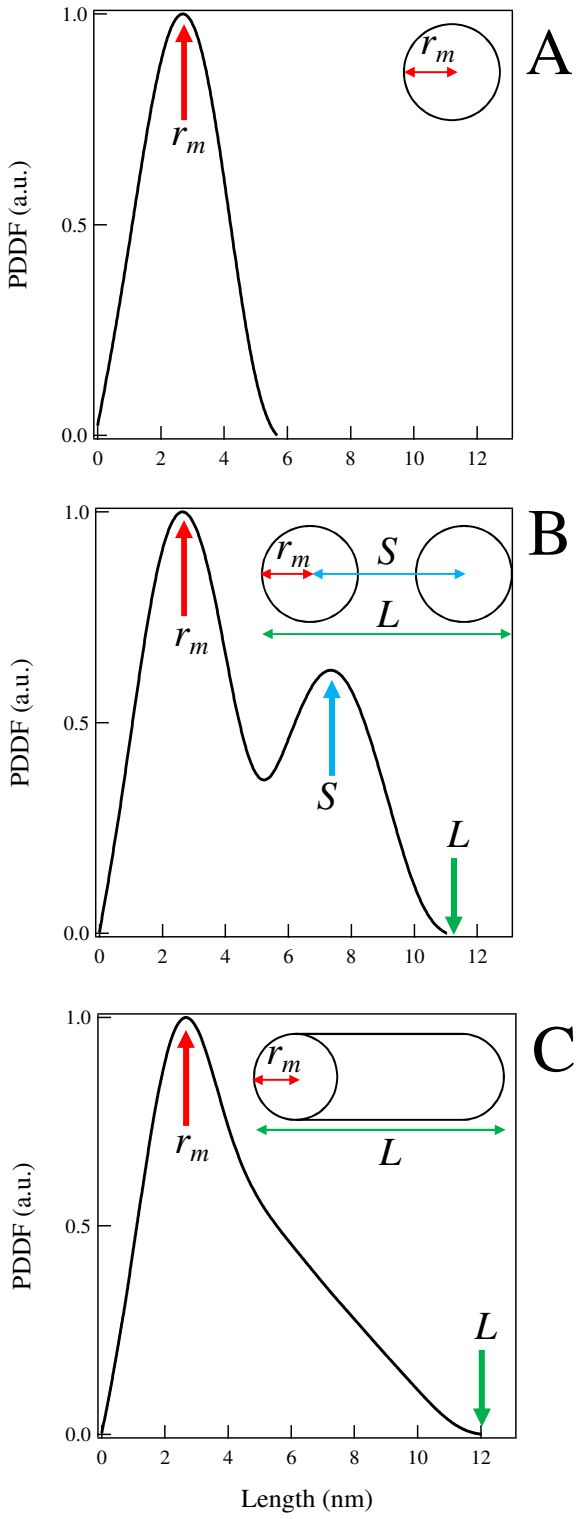

Figure 2. 3. Typical PDDFs for three different particle shapes. Spherical particles (A), pearl-necklace (B) and cylinder (C). Structural features in these PDDFs make reference to the particle radius (r), the nearest neighbor distance (*S*) and the complex length (*L*).

A real example of a typical experimental PDDF extracted from a protein-surfactant complex is illustrated in Figure 2.4. Specifically, this figure shows the representative PDDF for bovine serum albumin (BSA) denatured by sodium octyl sulfate (SC_8S), a homologue alkyl surfactant to sodium dodecyl sulfate ($SC_{12}S$) but with fewer carbons in the hydrophobic tail. From this figure, the size of the micelle (r), the distance between neighbor micelles (S) and the maximum elongation (L) of the complex can be obtained. The inset illustration guides the reader to have a better understanding of the parameters extracted from the PDDF curve.

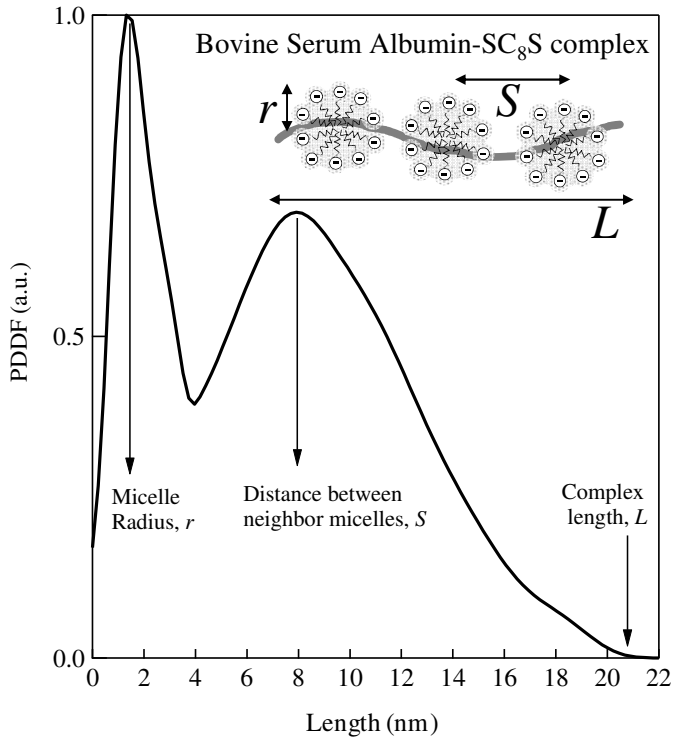

Figure 2. 4. PDDF of bovine serum albumin-sodium octyl sulfate complex [4].

The analyses of inhomogeneous systems may result in PDDFs with local minima or even negative values[2,5]. Specifically, minimum features in a PDDF curve are frequently observed during the analysis of protein-surfactant complex formed by proteins

denatured by sodium alkyl sulfates surfactants using small angle x-ray scattering (SAXS). Fig. 2.5 shows the PDDF of BSA-sodium decyl sulfate complex analyzed by two incident sources: X-ray (SAXS) and neutrons (SANS).

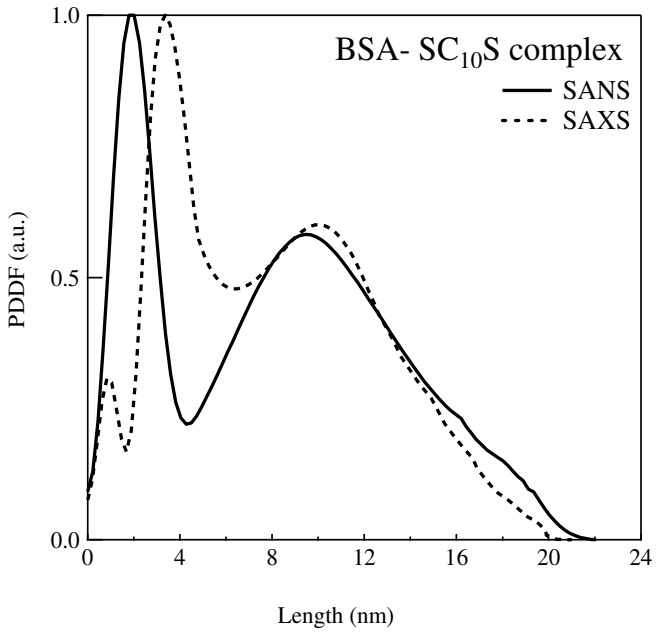

Figure 2. 5. PDDF of BSA-$SC_{10}S$ complex. Continuous line (SANS) and dotted line (SAXS).

The local minima in the PDDF obtained with SAXS data, appear because of the differences in the scattering electron densities within the micelle complexes. This effect is observed because X-rays, which are the incident radiation during SAXS, scatter from the electron cloud of the atoms. Therefore, the scattering electron densities will vary between atoms according with their differences in the atomic numbers. Specifically for this thesis, the larger electron densities of the surfactant head groups when compared to the alkyl tail and the solvent yield PDDFs that are typical of inhomogeneous core shell particles. On the other hand, in SANS analysis the resulting scattering profiles are the outcome of neutrons interacting with the nucleus of atoms. Therefore, isotopic

differences such as hydrogen and deuterium will dominate the differences in the scattering length densities between the deuterated and hydrogenated components within a sample. Then, the resulting PDDF obtained from SANS analysis of hydrogenated protein-surfactant complex dissolved in D_2O are more characteristic of homogeneous particles. The same principle holds for SAXS analyses of fluorinated surfactants due to the larger electron density of fluorine. Appendix A discusses in detail the differences in the interpretation of the PDDF from SAXS and SANS for homogeneous and in-homogeneous spherical particles.

2.2 Scattering length density (SLD)

The entire scattering intensity profile is the result of the scattering difference between the sample and the surroundings. In other words, the intrinsic characteristic of the sample and the dilution medium lead to different neutron scattering length or electron density (SLD) and these differences result in a different scattering profile, *I(q)*. The SLD (ρ) is defined as the relationship between the bound coherent scattering length of an atom (b_i) in its molecular volume (v_m). The SLDs for SANS (Eq. 2.5) and SAXS (Eq. 2.6) are obtained under the same principle, but in SAXS it is necessary to replace b_i by the product of the classical radius of the electron ($r_e = 2.81x10^{-13}cm$) with the respective atomic number (Z).

$$\rho_{neutrons} = \frac{\sum_{i=1}^{n} b_i}{v_m} \qquad \textbf{(2. 5)}$$

$$\rho_{x-rays} = \frac{\sum_{i=1}^{n} Z_i \cdot r_e}{v_m} \qquad \textbf{(2. 6)}$$

Specifically, x-rays interact with the electron cloud while neutrons interact with the atomic nuclei. Thus, the presence of atoms of different atomic number or different isotopes, such as hydrogen and deuterium make SAXS and SANS complementary in structure determination. However, given the marked difference in the interaction of neutron with hydrogen and deuterium atoms, neutron scattering (SANS) is the preferred technique to conduct contrast variation. With SANS, it is possible to differentiate regions in the system or make them more or less 'visible' to the neutrons, when deuterated water (D_2O) is used instead of distilled water (H_2O) or when deuterated or hydrogenated surfactants are used. Contrast variation with SAXS has also been successfully performed but it relies on the differences in the atomic number to promote distinctive scattering given that atoms of higher atomic number scatter the most[6]. Table 2.1 provides the scattering length and electron densities of relevant compounds in neutrons and x-ray respectively.

Table 2. 1. Scattering length densities for SANS and SAXS [7].

Compound	**Density [g/cm^3]**	**SLD $_{SANS}$ [A^{-2}]**	**SLD $_{SAXS}$ [A^{-2}]**
H_2O	1.0	-5.6 E-7	9.46 E-6
D_2O	1.1	6.33 E-6	9.36 E-6
$SC_{12}S$	1.01	3.37 E-7	9.32 E-6

Contrast variation is very useful for many systems. In particular, in the study of protein-surfactant complex, replacing the hydrogen by deuterium atoms and/or the use of heavy water as solvent allow us to obtain scattering from the unmatched components. Fig. 2.6 shows an illustration of the effect of using deuterated or hydrogenated

components in a protein-surfactant complex. Thus, SAXS and SANS can highlight different components of the same system achieving a comprehensive structural characterization.

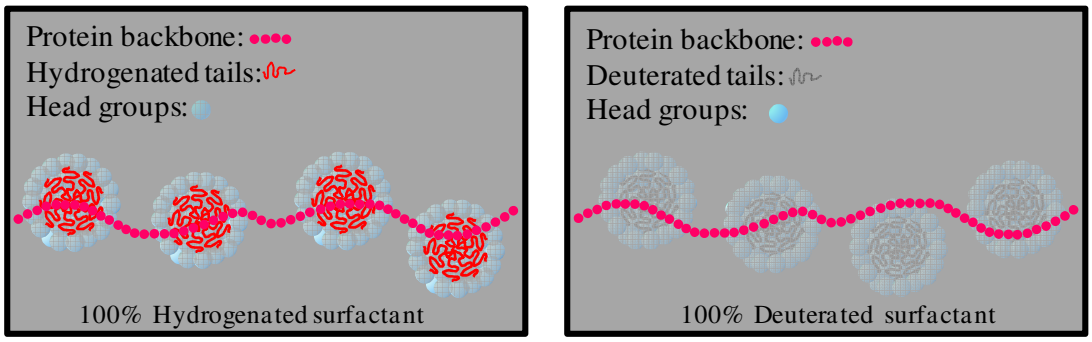

Figure 2. 6. Schematic of contrast matching for a protein-surfactant complex system.

2.3 Radius of gyration (R_g)

The radius of gyration (R_g) is an important structural parameter used in small angle techniques to describe the size of an object with arbitrary shape. It is defined as a function of the scattering length density distribution and thus also relates the distribution of mass in a particle around its center of mass. The R_g is fundamentally known as the second moment of inertia and is calculation is given in Equation 2.7 [1].

$$R_g^2 = \frac{\int \Delta\rho(r_1) r_i^2 dV_i}{\int \rho(r_i) dV_i} \qquad \textbf{(2. 7)}$$

The radius of gyration is also obtained directly from a scattering experiment through the Guinier approximation. This calculation assumes dilute systems, so that the structure factor can be neglected and assumed to be equal to one. This approximation is also valid only at low q when qR_g <1. The simple way to calculate the radius of gyration is by extracting the slope ($R_g^2/3$) from the linear region of the Guinier plot [ln $I(q)$ vs. q^2]

at low values of qR_g. Table 2.2 contains the relationship of R_g to geometric parameters for some common geometrical shapes [1,3].

Table 2. 2. Radii of gyration for typical structures [1].

Infinitely disk	**Circular rod**	**Infinite rectangular plate**	**Spherical shell**	**Sphere**
$R_g^2 = R_{gx}^2 + R_{gy}^2 = R^2/2$	$R_g^2 = \frac{R^2}{2} + \frac{L^2}{12}$	$R_g^2 = \frac{1}{3}\left[\left(\frac{W}{2}\right)^2 + \left(\frac{H}{2}\right)^2\right]$	$R_g^2 = \frac{3}{5}\frac{(R_2^5 - R_1^5)}{(R_2^3 - R_1^3)}$	$R_g^2 = \frac{3R^2}{5}$

In this thesis, the radius of gyration is used as an additional independent method to complement the structural information that is obtained through PDDF analysis and from dynamic light scattering (DLS) data. It is expected that the comparison of the PDDF, DLS and R_g of surfactant micelles will show a better similarity than for protein-surfactant complexes. This is because micelles in solution are frequently more spherical particles than protein-surfactant complexes. A Guinier analysis for a protein-surfactant complex is shown in Figure 2.7.

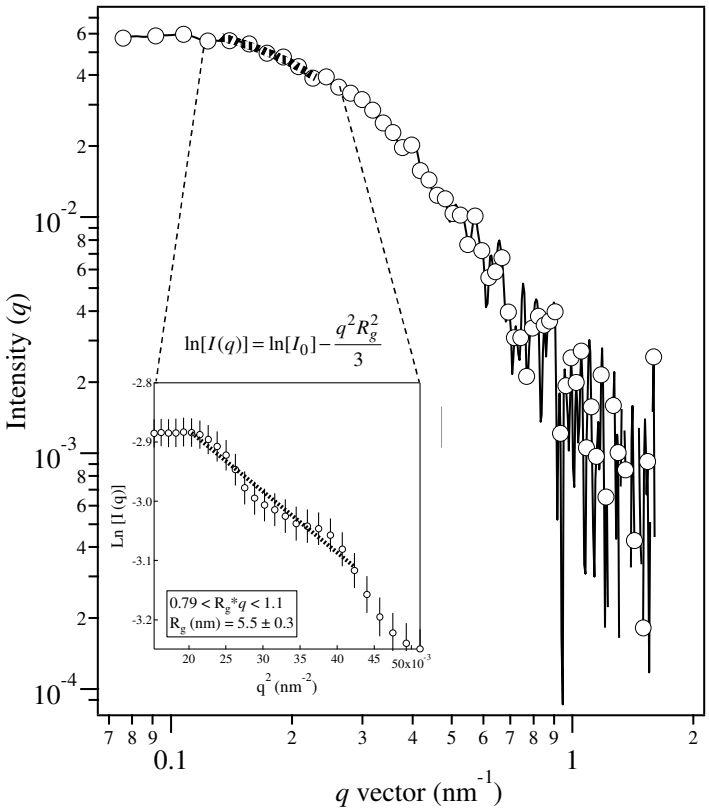

Figure 2. 7. Guinier analysis for ovalbumin-sodium dodecyl sulfate complex. R_g = 5.5 nm.

2.4 References

(1) Lindner, P.; Zemb, T. *Elsevier Science B.V.* **2002**.
(2) Fritz, G.; Bergmann, A. *J. Appl. Cryst.* **2004**, *37*, 815.
(3) O.Glatter, O. K. *Academic press* **1982**.
(4) Ospinal-Jimenez, M.; Pozzo, D. C. *Langmuir* **2011**, *27*, 928–935.
(5) Glatter, O. *J. Appl. Cryst.* **1979**, *12*, 166.
(6) Muller, K.; Laggner, P.; Glatter, O.; Kostner, G. *Eur. J. Biochem.* **1978**, *82*, 73–90.
(7) Scattering length density calculator http://www.ncnr.nist.gov/resources/sldcalc.html.

CHAPTER III

EXPERIMENTAL TECHNIQUES

This chapter will provide a short overview on polyacrylamide gel electrophoresis (PAGE), circular dichroism (CD), fluorescence spectroscopy and dynamic light scattering (DLS), which were complementary techniques used in the study of the interactions of proteins with linear, branched and fluorinated surfactants. A detailed list of the techniques with equipment specifications is shown in Table 3.1. Chapter IV, V and VI also contain meticulous description for the sample preparation and the experimental details for each study. Finally, the name and other particulars of the proteins and surfactants used in this thesis are included in Table 3.2 and 3.3 respectively.

Table 3. 1 List of techniques

Technique name	Instrument	Acronym	Details
Polyacrylamide gel electrophoresis	Mini-PROTEAN Tetra Cell	PAGE	Vertical electrophoresis system Up to 4 gels per run
Small angle x-ray scattering	SAXSess	SAXS	Cu-Ka source, q range: 0.03 nm^{-1} to 28 nm^{-1}
Small angle neutron scattering	NG7 and NG3 at NIST-CNR	SANS	Mechanical wavelength selector, q range: 0.008 nm^{-1} to 7 nm^{-1}
Dynamic light scattering	Malvern Zetasizer Nano ZS	DLS	Particle size and zeta potential, diameter range: 0.3nm to 10 μm
Circular dichroism	Jasco 720 Spectrophotometer	CD	Quartz crystal cuvette (1-mm path length). Wavelength range: 190-270 nm
UV-Vis spectroscopy	Thermo Scientific Evolution 300	UV-Vis	Light source: xenon, Wavelength range: 190-1100 nm

Table 3. 1 List of proteins and surfactants.

Name	Acronym	Molecular weight (kDa) [a]	Organism	Residues length [b]	Isoelectric point [a]	residues Trp [b]	bridges S-S [b]	Extinction coefficient (mL/g.cm)[a]	α-sheet content (%)[b]	β-sheet content (%)[b]
β-galactosidase	G	116	Escherichia coli	1023	4.6	39	0	20.9	13	39
Phosphorylase b	P	97	Rabbit muscle	843	5.8	12	3	11.8	50	14
Bovine serum albumin	B	66	Bovine serum	583	5.3	2	17	6.67	74	0
Ovalbumin	O	44	Chicken egg	385	4.5	3	4	7.25	31	31
Carbonic anhydrase	C	29	Bovine erythrocytes	260	5.8	7	0	19.0	15	30
Trypsin inhibitor	T	20.1	Soybean	172	4.5	3	2	9.94	1	40
Lysozyme	L	14.3	Chicken egg white	129	4.4	6	4	26.4	41	10
α-lactalbumin	α	14.2	Bovine milk	123	11.3	4	24	20.1	43	11
Aprotinin	A	6.5	Bovine lung	58	10.5	0	9	8.4	20	25

[a] Values provided by supplier. [b] From structure files in the protein data bank (PDB)

Table 3. 1 List of Surfactants

Surfactant name	**Acronym**	**Chemical structure**
Sodium hexyl sulfate	SC_6S	$CH_3(CH_2)_5SO_4Na$
Sodium octyl sulfate	SC_8S	$CH_3(CH_2)_7SO_4Na$
Sodium decyl sulfate	$SC_{10}S$	$CH_3(CH_2)_9SO_4Na$
Sodium dodecyl sulfate	$SC_{12}S$	$CH_3(CH_2)_{11}SO_4Na$
Sodium tetradecyl sulfate	$SC_{14}S$	$CH_3(CH_2)_{13}SO_4Na$
Sodium hexadecyl sulfate	$SC_{16}S$	$CH_3(CH_2)_{15}SO_4Na$
Sodium 2-ethylhexyl sulfate	2-EHS	$CH_3(CH_2)_4CH(CH_2CH_3)SO_4Na$
Sodium 2-butyl octyl sulfate	2-BOS	$(CH_3)_2(CH_2)_9CHSO_4Na$
Sodium 3,7-dimethyl octyl sulfate	3,7-DMOS	$(CH_3)_3(CH_2)_5(CH)_2SO_4Na$
Potassium perfluorobutane sulfonate	PFC_4S	$CF_3(CF_2)_3SO_3K$
Potassium perfluorohexane sulfonate	PFC_6S	$CF_3(CF_2)_5SO_3K$
Potassium perfluorooctane sulfonate	PFC_8S	$CF_3(CF_2)_7SO_3K$

3.1 Surfactant synthesis

Among all the surfactants used in this thesis only the 2-butyl octyl sulfate (2-BOS) and the 3,7-dimethyl octyl sulfate (3,7-DMOS) were synthesized using the method described by Missel et. al [1]. Fig. 3.1 shows a schematic of the synthesis process. Ch. IV, section 4.2.1 contains the details about the synthesis including raw materials and a brief description of the synthesis process. The others surfactants used in this thesis (hydrogenated alkyl and fluorinated) were purchased and used as received. The purity of the synthesized surfactants (Fig. 3.2) is characterized using a liquid chromatrograph-ion trap mass spectrophotometer.

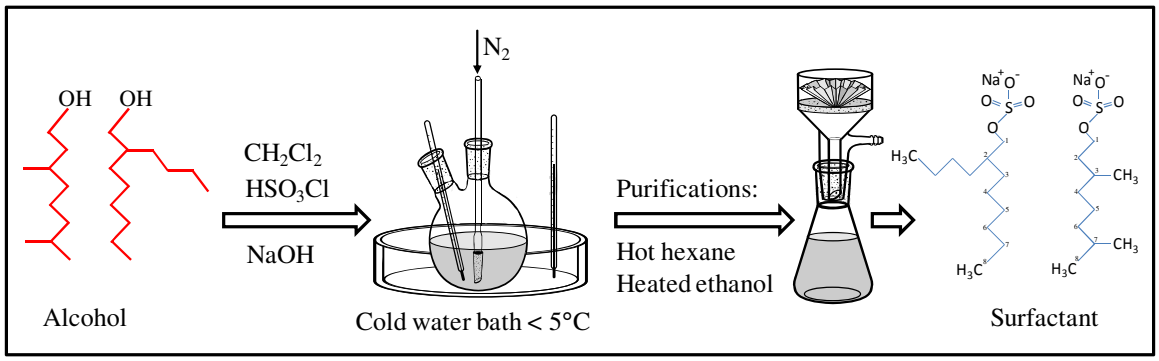

Figure 3. 1. Schematic of the surfactant synthesis used to produce 2-BOS and 3,7-DMOS.

The synthesized branched surfactants were analyzed in a Bruker Esquire liquid chromatography-ion trap mass spectrophotometer. The ion source type is electrospray ionization (ESI), a trap drive of 55 and an accumulation time of 200,000 µs were used. The reported spectra correspond to the characteristic curve of three independent analyses. The inset plot represents the mass spectrometry/mass spectrometry (MS/MS) analysis of the single-charge sulfate ion for each branched surfactant.

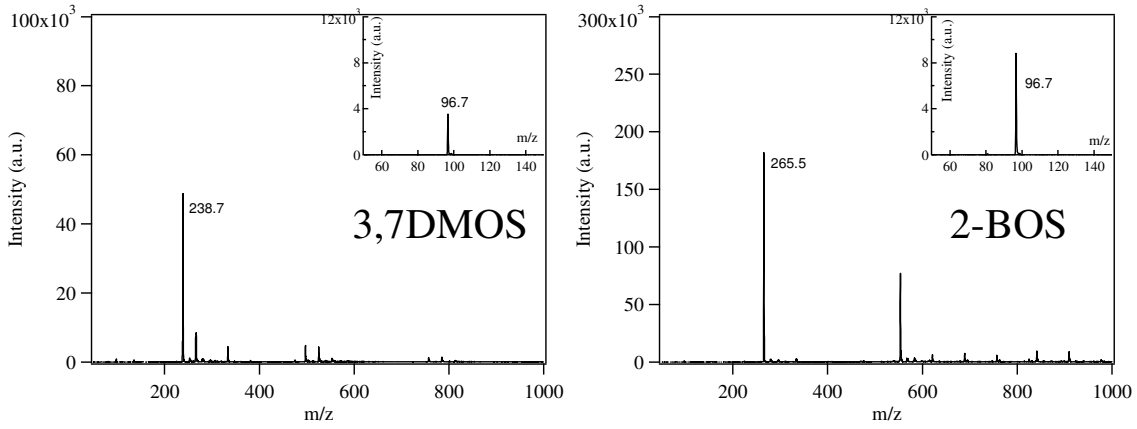

Figure 3. 2. Electrospray ionization mass spectrum of 3,7-DMOS (left) and 2-BOS (right).

3.2 Surfactant-polyacrylamide gel electrophoresis

Polyacrylamide gel electrophoresis or PAGE is one of the most used and versatile techniques to determine the molecular size of proteins. PAGE is also used to assess the purity and integrity of proteins and to quantify their presence[2,3]. In this thesis, PAGE was used to estimate the mobility of protein markers upon the binding of the selected anionic surfactants (Table 3.1 and 3.2). For reproducibility, polyacrylamide Tris-HCl precast gels were purchased from Biorad (Hercules, CA). Conveniently, these gels are made without SDS (sodium dodecyl sulfate) and allow us to study protein mobility upon the binding of any surfactant. Dithiothreitol (DTT) was used as the reducing agent to break the disulphide bonds within the protein. In gel electrophoresis charged particles move through a gel matrix (i.e. polyacrylamide, agarose) upon applying an electric field. When a particle is uniformly charged, the mobility is directly related to the molecular size. Thus, charged polyelectrolytes, such as proteins that are buried by anionic surfactants and become predominantly negatively charged would migrate to the cathode.

3.3 Circular Dichroism

Circular dichroism (CD) is a technique used to characterize the secondary structure of proteins. It is based in the chirality of the amino acids (building blocks of the protein's primary structure). The difference in the absorption (ΔA) of the right (A_R) and left (A_L) circularly polarized light in a protein sample permit to locate structural changes in the organization of the protein secondary structure. The CD spectrum of an achiral molecules shown no CD signal given that $\Delta A = 0$.

$$\Delta A = A_L - A_R \quad \textbf{(3. 1)}$$

Specifically, CD analyses allow identifying the α-helix, β-sheet, disordered and coiled motifs of a protein sample. The CD spectrum of an α-helical molecule shows three characteristic peaks: two negative peaks at ~222nm and ~208 nm and one positive peak at ~190 nm. β-sheet molecules are characterized by one positive peak at ~195 nm and one negative peak at ~215 nm. In general the positions of the β-sheet characteristic peaks can vary depending on the peptide bond geometries of the different types of β-sheet structures (i.e. parallel, sheets with twists and anti-parallel sheets). Disordered proteins exhibit a negative peak at ~ 200 nm and, sometimes, a small positive peak above 210 nm. Particularly, the CD calculations for disordered and coil conformations are challenging.

Most of the CD analyses with proteins are analyzed in the UV region. Thus, changes in the secondary structure are observed in the far UV region (260 nm to 190 nm). The CD signal in the near UV region (360 nm to 260 nm) is related with modifications in the protein tertiary structure[4]. Among all of the units used to report CD data, in this thesis the raw data, recorded in millidegrees, is converted and reported as the mean residue ellipticity or MRE (Eq. 3.2) which is a protein size independent value.

$$\theta_{MRE} = \frac{\theta_e \cdot 0.1 \cdot MRW}{c \cdot l} \quad \textbf{(3. 2)}$$

$$MRW = \frac{M_W}{n-1} \quad \textbf{(3. 3)}$$

In the above equations, θ_e is the ellipticity (raw data), c is the concentration (in mg/mL), l is the pathlength (in cm) and MRW is the mean residue weight. MRW is

defined in terms of M_w, the molecular mass of the protein (in Daltons) and n, the number of amino acids[4]. The information obtained from the CD spectra provides a quantitative analysis that can be combined with other analytical methods to characterize the conformations of a partly or fully denatured protein. In this thesis Dichroweb was the selected method to further analyze the CD spectra. Dichroweb is a web server that uses a database of experimental CD data to calculate and compare the secondary structures of an unknown protein sample[5]. This online analysis is based in 105 reference proteins grouped into eight different reference datasets (set 1, set 2, set 3, set 4, set 5, set 6, set 7 and SP175). Thus, upon the selection of a deconvolution algorithm (i.e. CONTIN, SELCON3, CDSSTR, VARSLC and K2D) the results are obtained from the minimization of the deviation between an experimental data set and the calculated spectrum. As expected the selection of the algorithm and the protein dataset can affect the outcome of the analysis. For detailed discussions in the CD theory the reader is referred to references in this chapter.[5–7]

3.4 Fluorescence

Fluorescence spectroscopy is an analytical technique that quantifies the emitted light energy of a molecule upon the excitation of a fluorophore within the sample. Fluorophores are fluorescent compounds capable of re-emitting light after light-induced excitation. Fluorescence is the result of the relaxation of a molecule from the singlet ground state (highest occupied molecular orbital, HOMO) to the singlet excited state (lowest unoccupied molecular orbital, LUMO) upon light exposition. The response of the emitted light and the wavelength is sometimes directly related to the environment in

which the fluorophore is exposed. Fluorophores are often classified as natural, organic, multichromophoric labels and semiconductor nanocrystals[8]. A simple illustration of a fluorescence process (excitation, excited-state lifetime and fluorescence emission) is shown in Figure 3.3.

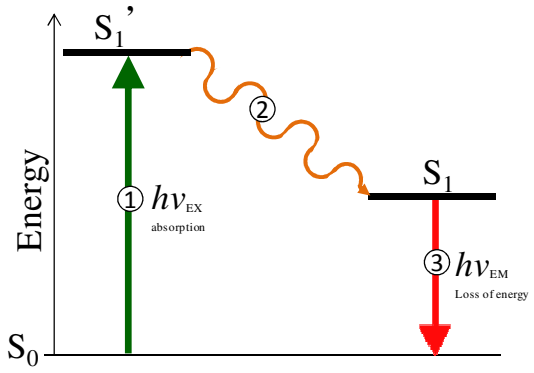

Figure 3. 3. Simplified Jablonski energy diagram.

The fluorescence signal is a function of the molar extinction coefficient, the path length, the solute concentration, the fluorescence quantum yield, the excitation source intensity and the collection efficiency of the instrument. In this thesis, a LS 55 fluorescence spectrometer from PerkinElmer was used to analyze protein-surfactant complex samples at around 0.08 mg of protein/mL using a 1 cm quartz cell. In this thesis protein samples are either excited at 285 or 295 nm (maximum absorption) and all fluorescence spectra are collected after the first emission signal (300 nm to 500 nm). Although most proteins are mainly colorless in the visible region, the presence of the aromatic residues tryptophan (Trp), tyrosine (Tyr) and phenylalanine (Phe), which are natural fluorophores, confer natural fluorescence to most proteins. Given that Trp is the most highly fluorescent residue (high quantum yields, emitted photons/exited photons), it

usually dominates the total fluorescence of proteins. Thus, changes in the fluorescence wavelength spectrum for a protein can be related to the polarity surrounding the Trp residues. In other words, by analyzing the fluorescence of a native and denatured protein it is possible to identify the changes in the environment to which the Trp residues are exposed (i.e. polar, nonpolar). Because Trp is not irreversible destroyed by light, the fluorescence intensity is cyclical.

3.5 Dynamic light scattering

Dynamic light scattering (DLS) is a technique used to characterize particles, emulsions or molecules dispersed in a liquid. As it names implies, DLS measures the fluctuations in the light scattered by the particles and relates it to the movement or diffusion of a particle in a liquid. Through DLS analysis it is possible to analyze particles sizes over a range from nm to μm in diameter. Dispersed particles in a fluid are in constant movement due to Brownian motion. However, small particles move quickly and large particles move slowly. Therefore, it is expected that smaller particles will produce fluctuations of higher frequency than the larger particles. The correlation between the intensity of light scattered by a particle at a specific time and the intensity scattered at a short time (τ) later result in the auto-correlation function $G(\tau)$. Successively, $G(\tau)$ is related to the particle diffusivity (D) through the measured decay constant (Γ) as is shown in Eq. (3.4) and (3.5) for a monodisperse spherical particle (single decay). Here, A_0 corresponds to the background signal, A_c is an instrument constant, Γ is the decay constant, τ is the time shift, q is the scattering vector, which was previously defined in Ch. II and D represents the diffusion coefficient [9].

$$G(\tau) = A_0 + A_c \exp(-\Gamma\tau) \quad \textbf{(3. 4)}$$

$$\Gamma = q^2 \cdot D \quad \textbf{(3. 5)}$$

In this thesis, the majority of protein-surfactant complex likely form particles of different shapes than a sphere. Therefore, particle radii calculated from this technique will not be perfectly accurate. However, the diffusion coefficient (D_f), which is the parameter that that is directly calculated from the correlation functions, is accurate and better value to compare protein-surfactant complexes of different shapes. Nevertheless, for spherical particles, the particle radius R_H can be obtained from the Stokes-Einstein relation (Eq. 3.6). Here, k is the Boltzmann constant, T is temperature, μ is the viscosity of the fluid and D_f is the diffusion coefficient of a spherical particle.

$$R_H = \frac{k \cdot T}{6 \cdot \pi \cdot \mu \cdot D_f} \quad \textbf{(3. 6)}$$

3.6 References

(1) Missel, P. J.; Mazer, N. A.; Benedek, G. B.; Carey, M. C. *J. Phys. Chem* **1983**, *87*, 1264.

(2) Hamdan, M.; Righetti, P. G. *Proteomics today. Protein assessment and biomarkers using spectrometry 2D electrophoresis and microarray technology*; John Wiley & Sons: Hoboken, NJ, 2005; p. 426.

(3) Chrambach, A.; Rodbard, D. *Science* **1971**, *172*, 440–451.

(4) Ann, W. B.; Janes, R. W. *Modern techniques for circular dichroism and synchrotron radiation circular dichroism spectroscopy.*; IOS Press: The Netherlands, 2009; Vol. 1.

(5) Whitmore, L.; Wallace, B. A. *Nucleic Acid Research* **2004**, *32*, W668–W673.

(6) Lees, J. G.; Miles, A. J.; Wien, F.; Wallace, B. A. *Bioinformatics* **2006**, *22*, 1955.

(7) Whitmore, L.; Wallace, B. A. *Biopolymers* **2008**, *89*, 392–400.

(8) Sauer, M.; Hofkens, J.; Enderlein, J. *Handbook of Fluorescence Spectroscopy and Imaging*; Wiley-Vch Verlag & Co. KGaA: Germany, 2011; p. 281.

(9) Berg, J. *An Introduction to Interfaces & Colloids. The Bridge to Nanoscience*; World Scientific Publishing Co. Pte. Ltd.: Singapore, 2010; p. 785.

CHAPTER IV

STRUCTURAL ANALYSIS OF PROTEIN-SODIUM ALKYL SULFATES COMPLEXES

The aim of the present chapter is to evaluate the performance of a series of sodium alkyl sulfates as denaturing agents for protein gel electrophoresis. Also, through scattering techniques is intended to assess the nano-structural changes of each of the protein-surfactant complexes. Also, macroscopic separations with each surfactant are investigated. The chapter begins with an introduction that highlights the lack of fidelity to identify proteins of similar or smaller molecular weights (< 20 kDa). Then, the hypotheses are presented and the experimental plan is discussed. In the results section, it is shown that changes in the surfactant tail length promote not only variations but improvements in the identification of proteins and also affects the way proteins and surfactants self-assemble into protein-surfactant complexes. As it turns out, this chapter shows that surfactants with shorter tail length than sodium dodecyl sulfate ($SC_{12}S$), not only improve the separation of small molecular weight proteins (<14.3 kDa), but also form larger protein-surfactant complexes.

Aspects of this chapter reproduced with permission from Ospinal-Jimenez, M., Pozzo D.C., Langmuir, 27 (3), pp 928-935. Copyright 2011. American Chemical Society.

4.1. Background

The interactions between proteins and surfactants are a key factor for the development of proteomic separations[1–6]. Several studies have been conducted in the past with the aim to increase knowledge on the fundamental principles that control complex formation between surfactants and proteins[7]. The nature of binding forces for protein-surfactant complexes are believed to originate primarily from hydrophobic and ionic interactions[1]. Sodium dodecyl sulfate (usually abbreviated as SDS but here referred as $SC_{12}S$) is one of the most extensively studied surfactant in the area of protein denaturation[3,8]. Furthermore, it has been the primary surfactant for use in analytical electrophoretic separation of denatured proteins since the initial introduction of the polyacrylamide gel electrophoresis (PAGE) technique[9,10]. This chapter aims to correlate macroscopic gel electrophoresis separations of anionic alkyl sulfate surfactants having variable alkyl chain lengths with the specific nanostructure of the protein-surfactant complex. Probing structural parameters is essential for rational improvements in the efficiency and resolution of these types of separations. Furthermore, deciphering the relationship between surfactant chemistry and structural parameters should aid in the future design of improved surfactant formulations.

Protein denaturation with surfactants occurs in a four state process as a function of detergent concentration[11]. Binding at low surfactant concentrations occurs primarily in specific high-energy sites on the protein. The next stage appears as an apparent plateau with slow increases in surfactant binding. The third state is related to massive cooperative interactions that occur during the unfolding of proteins. In the last state, the saturation of the protein is finally achieved. After full saturation, excess surfactant forms free micelles

in solution. It has been previously reported that the saturation binding for most denatured proteins and $SC_{12}S$ is relatively constant at a ratio of 1.4 g $SC_{12}S$/g protein[1]. Binding studies with fully denatured proteins and other anionic alkyl sulfates have not been studied in detail. The characterization of protein-surfactant complexes can be achieved using a variety of techniques including conductivity, spectroscopy, fluorescence and scattering among others. These techniques can provide valuable parameters such as size, shape, viscosity and surfactant diffusivities[3,8,12,13].

Three models have been previously used to describe the nanostructure of protein-$SC_{12}S$ complexes: a) the pearl-necklace model, which proposes bound spherical micelles stabilizing the protein, b) the rod-like model, which suggest that the protein wraps a rigid micellar rod and c) the "flexible helical model", which suggests that the protein wraps around a cylindrical micelle[1,2,14]. At this point, there is consensus over the necklace model occurring in $SC_{12}S$ denatured proteins under fully denatured conditions. Although $SC_{12}S$ is the most commonly used surfactant for PAGE, interest to further improves the technique has motivated studies using alternative surfactants including cationic, anionic, fluorinated and gemini surfactants[12,15–20]. Unfortunately, none of these studies directly correlate the nano-structure of the protein-surfactant complex to the macroscopic parameters of the separation. Without this link it is not possible to rationalize these results based on fundamental colloidal and transport models because critical structural details are missing. Therefore, understanding the interactions that occur between surfactants and denatured proteins is essential to guide the design of future systems for gel electrophoresis applications[6,21].

In an ideal electrophoretic separation of proteins, it would be possible to unambiguously identify all macromolecules in a highly complex mixture. However, for traditional $SC_{12}S$-PAGE it is often difficult to identify proteins that have similar molecular weights or proteins that are small (below 20 kDa)[22]. It is hypothesized that this is directly related to the type of structure of the protein-surfactant complex. Improvements in the identification of more complex protein mixtures could have overreaching implications such as, helping to understand the formation of amyloid fibrils that are associated with Alzheimer's disease[23]. Traditional PAGE techniques using $SC_{12}S$ have performed very well for common protein separations and this is the reason for their widespread adoption amongst researchers in the life sciences. However, as the proteomics field expands, it is desirable to significantly improve resolution to tackle analytical separations of higher complexity such as those encountered in the analysis of whole cell lysates and serum[24]. Research efforts in other groups have also intended to improve separations through the design of new sieving matrices, surfactant formulations and micro-fluidic devices[7]. From the results of this study, it is determined that $SC_{12}S$ is not necessarily the best performing surfactant even amongst the small family of simple alkyl sulfates. By systematically relating the quality of the separation to the nanostructure of the complex, as probed with SANS and SAXS, it is possible to rationalize the results of macroscopic separations and make predictions for the structural parameters that would be most desirable in protein-surfactant nanostructures. The primary aim of this work is not necessarily to create or identify optimal surfactant architectures but rather to identify systematic trends that can be related to structural parameters to increase our knowledge over the fundamental separation process.

Structures different from the necklace model, the consensus representation for $SC_{12}S$-denatured proteins, could potentially result in improved separations. In Ch. I, Figure 1.2 contains an illustration of three structures of protein-surfactant complexes; pearl-necklace structures (left), ellipsoidal (top right) and rod-like (bottom right) micelle complexes. It is possible that the distance between micelles increases as the surfactant tail length increases. From packing arguments, it could be argued that at certain point the tail will be long enough so that aggregation results in ellipsoidal or rod-like micelles[25]. Scattering techniques are able to identify and characterize the type of micelles mentioned above[26].

To evaluate these hypotheses, a model study that included macroscopic gel electrophoresis separations and structural analysis of protein-surfactant nanostructures in solution is designed. In this study, SAXS and SANS are used to characterize the structure of six sodium alkyl sulfates complexes with a set of model proteins with sizes ranging between 6.5 to 116 kDa. This work focuses on identifying differences in peak resolution and in the dependency of mobility with molecular weight in gel electrophoresis. Simultaneously, an extensive structural characterization of each surfactant as it associated with bovine serum albumin (BSA), (66kDa), ovalbumin (44kDa) and lysozyme (14.3kDa) using complementary small angle scattering (SAXS and SANS) is performed. Scattering techniques have been previously demonstrated to be useful in the characterization of protein-surfactant systems[5,8,15,26–32].

4.2. Materials and methods

4.2.1. Materials

Gel electrophoresis (GE) experiments are conducted using the following native proteins: β-galactosidase, phosphorylase-b, BSA, ovalbumin, carbonic anhydrase, α-lactabulmin, lysozyme, aprotinin, hemoglobin and trypsin inhibitor (protein details in Table 3.2, Ch.III). The buffers are made with trizma hydrochloride, trizma-base and glycine. $SC_{12}S$, dithiothreitol (DTT) and iodoacetamide are used to fully denature the proteins. All of the above mentioned supplies are purchased from Sigma-Aldrich (St Louis, MO).

Pre-made slab gels of 12% of polyacrylamide (without $SC_{12}S$), coomassie brilliant blue (CBB) R-250 staining solution, a precision-plus protein ladder, and a mini-protean tetra cell are used to perform the GE experiments and are obtained from Bio-Rad (Hercules, CA). The use of pre-made gels ensure reproducibility between electrophoresis experiments. More importantly, the lack of $SC_{12}S$ in the synthesis of the commercial gel allows avoiding contamination problems due to interference between $SC_{12}S$ in the gel and the specific surfactants that are used to denature the proteins. Fixer and de-staining solutions are prepared with DI H_2O, anhydrous methanol and glacial acetic acid that are purchased from Mallinckrodt chemicals (Phillipsburg, NJ). Anhydrous glycerol is obtained from J.T.baker (Phillipsburg- NJ). Sodium (hexyl 98%, octyl 99%, decyl HPLC grade, tetradecyl 95% and n-hexadecyl 98%) sulfates are purchased from Across Organics (Morris plains, NJ) and use as received. Dialysis tubing of (6-12 kDa MWCO) is purchased from Fisher scientific (Pittsburgh, PA).

4.2.2. Gel Electrophoresis

GE samples are prepared in DI H_2O using protein, buffer and DTT stock solutions. The final composition of the samples is 0.025M (trizma), 1.8M (glycerol), 0.102M (DTT) and a ratio of 3mg of surfactant/mg of protein. The samples are warmed for 4 minutes at 95 ºC before loading them into the gel. Each experiment is conducted in the mini-protean tetra cell in the presence of two buffers, an inner and outer solution. Both of them are prepared with DI H_2O, trizma at 0.025 M and glycine at 0.192 M. Additionally, the inner buffer contains 0.5 times the critical micelle concentration (CMC) of each surfactant. Finally, the gels are fixed, stained and de-stained with fixer and CBB solutions.

Gel electrophoresis method: The experiments are conducted using pre-made slab gels of 12% polyacrylamide from Bio-Rad, at a constant voltage (150 V) and with the cell immersed in a cold water bath at a temperature of ~10 °C. The fixing buffer is prepared as a mixture of 50% DI H_2O, 10% acetic acid and 40% methanol. The CBB solution stained the gel for 12 h after which the gels are washed with the fixing buffer solution to get the blue stain out. Several solvent washes are necessary until the gels are clear enough to distinguish all of the bands. Running times, conductivities, pH and temperatures are all recorded. The de-stained slab gels are scanned using a flatbed scanner and analyzed with ImageJ (National Institute of Health, USA) and the digital images are subsequently use to calculate average electrophoretic mobilities.

4.2.3. Small Angle X-Ray/Neutron Scattering

SAXS and SANS samples are initially prepare in DI H_2O. The protein samples have an initial concentration of 20mg/mL. The surfactants are also added at a ratio of 3.0 mg of surfactant to 1.0 mg of protein to ensure full saturation[1]. DTT and iodoacetamide are added in accordance with the specific number of disulfide bonds for each protein. A stoichiometric excess of 5 times is used to ensure that all disulfide bonds are broken and stabilized. After the addition of DTT the samples are warmed for 4 minutes at 95 ºC. Then, at room temperature the iodoacetamide is added and the samples are kept in darkness for 2 hours. A series of dialysis steps are then use to remove the excess surfactant. A dialysis buffer is prepared for each sample containing trizma (0.025 M), glycine (0.192 M) and surfactant at 0.7 times the CMC (Table 4.1). The surfactant concentration in the dialysis buffer is selected to minimize the scattering contribution of free micelles while also preventing the removal of surfactant from the protein complexes. After dialysis, the protein samples are freeze-dried, re-suspended in an equal volume of D_2O and diluted with D_2O buffer of identical composition to the dialysis buffer. Final protein concentrations of 0.5, 1.0, and 3.0 mg/mL are used depending on the specific sample (Table 4.1). Highly charged samples generally required more dilution. The concentrations used for scattering analysis are determined by running a dilution series for each sample. These are aimed at minimizing inter-complex interactions while maintaining adequate scattering statistics. Ideally, all samples would be analyzed at infinite dilution, but this is not possible because decreasing concentrations also reduces the scattering intensity. All protein concentrations are measured by absorbance at 280 nm in a UV-visible spectrophotometer (thermo scientific) using 6.67 (BSA), 7.25

(ovalbumin) and 26.4 (lysozyme) as the respective extinction coefficients (given in mL. $g^{-1}cm^{-1}$). Conductivity and pH are measured using a pH/Conductivity meter from Consort (Turnhout, Belgium).

Table 4. 1. Protein and surfactant concentrations for SAXS and SANS analysis

Surfactant	**Acronym**	**Protein concentrations (mg/mL)**	**Buffer surfactant concentration (mM)**
Sodium octyl sulfate	SC_8S	1	70
Sodium decyl sulfate	$SC_{10}S$	1	16.6
Sodium dodecyl sulfate	$SC_{12}S$	0.5	9.5
Sodium tetradecyl sulfate	$SC_{14}S$	0.5	0.9
Sodium hexadecyl sulfate	$SC_{16}S$	0.5	0.3

Scattering methods: SANS experiments are performed at the National Institute of Standard and Technology (NIST) Center for Neutron Research using the NG3 and NG7 instruments. Scattering data from SANS is fully reduced using Igor macros developed at NIST[33]. SAXS experiments are performed at University of Washington in a SAXSess Small-Angle X-ray Scattering instrument from Anton Paar (Graz, Austria). Image plates from Fuji (Greenwood, SC) and a Cyclone scanner from Perkin Elmer (Covina, CA) are used as a detector and reader respectively. The data is acquired, processed and analyzed with SAXSquant software. Pair distances distribution functions (PDDFs) are calculated using Generalized Inverse Fourier Transformation method through the GIFT analysis package[26,29].

4.3. Results and Discussion

Gel Electrophoresis: Complexes of proteins and alkyl sulfate surfactants are analyzed in order to understand the binding mechanism in conditions that are similar to those in a typical gel electrophoresis separation. The following results are divided in two sections: macroscopic electrophoresis separations (PAGE) and scattering analysis (SANS and SAXS). Both sets of samples use the same buffer conditions as mention in the experimental section. However, the PAGE analysis is performed over more protein-surfactant complexes than the scattering analysis. The scattering analyses are performed for three model proteins: BSA, ovalbumin and lysozyme.

PAGE experiments are analyzed by calculating average electrophoretic mobilities. These are obtained through scanning of the gels after staining. Eq.(4.1) shows the definition of electrophoretic mobility (μ_e) in terms of the applied electric field (E) and the protein complex velocity ($v_{complex}$).

$$\mu_e \approx \frac{v_{complex}}{E} \qquad \textbf{(4. 1)}$$

In order to calculate the distance traveled, a total gel dimension of 6 cm and a stacking gel region of 0.5 cm (Biorad specifications) are used. Shrinking/swelling, which occurs during staining and de-staining, is corrected by imaging the full gel and normalizing the image to the original size. The full width at half maximum (FWHM) is used to define the peak width for each band. All mobility parameters are calculated in units of (μm/s)/(V/cm).

Figure 4.1 shows the average electrophoretic mobility and the peak width for the complexes that are analyzed. In all cases there is an inverse relationship between mobility and protein molecular weight that seems to have a power-law dependency at high molecular weights. All surfactants, with the exception of sodium hexyl (SC_6S) and sodium octyl (SC_8S) sulfates result in defined separation bands. For SC_6S the results are unacceptable because none of the proteins enter the gel. For SC_8S some proteins are resolved with adequate resolution while others do not enter the gel or form large streaks in the gel. In contrast, $SC_{10}S$, $SC_{12}S$, $SC_{14}S$ and $SC_{16}S$ give reliable results that could be analyzed quantitatively. The decrease in peak width demonstrates that protein separation is significantly better when $SC_{10}S$ and $SC_{12}S$ are used (Fig. 4.1C). However, the mobilities of complexes of $SC_{12}S$ are inferior to $SC_{10}S$ in the identification of proteins smaller than 10kDa (Fig. 4.1A).

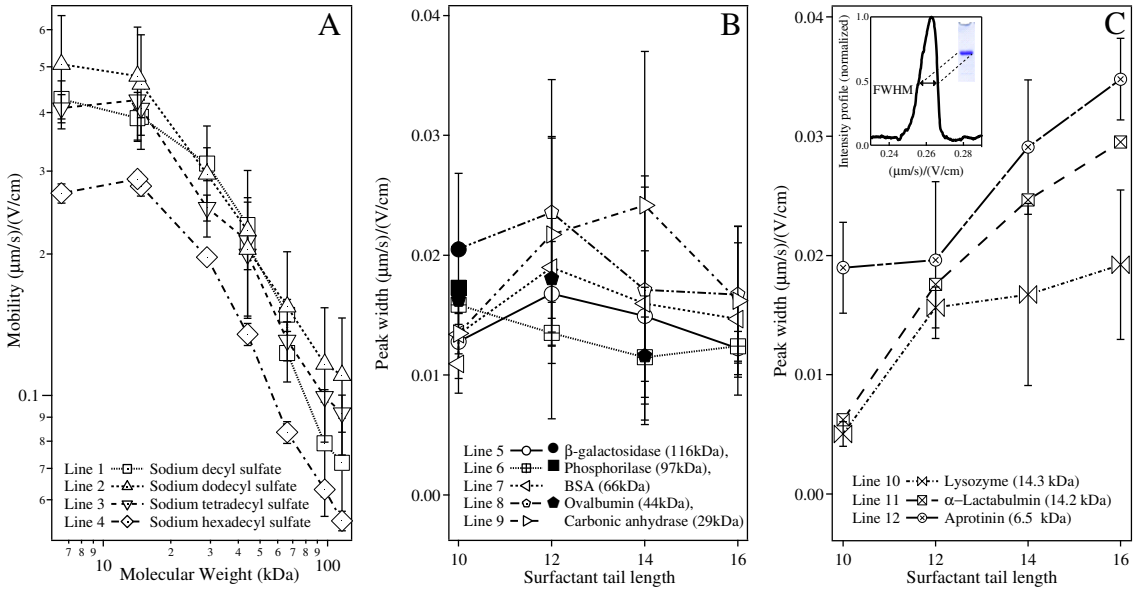

Figure 4. 1. Electrophoretic mobility (A) and peak widths of P-S complexes from 116 to 29 kDa (B) and from 14.7 to 6.5 kDa (C). Filled icons in plot B corresponds to the second bands identified. Inset in plot 1C represents the method used to measure the peak width using the FWHM.

For small proteins, mobility values show weak molecular weight dependencies. For $SC_{10}S$, the molecular weight dependency in this region is slightly stronger than for $SC_{12}S$. This is related to the use of a surfactant with smaller tail length that will also form smaller micelles. Therefore, is possible to have a larger quantity of smaller micelles attached to the backbone of the protein. Thus, the complexes may be more homogeneously coated with surfactant and potentially also more extended. It is possible that the failures of SC_6S and SC_8S are due to the fact that they are less hydrophobic molecules and bind weakly with the protein. On the other hand, surfactants with longer hydrophobic tails bind strongly to proteins due to hydrophobic interactions[17,18]. For $SC_{16}S$ the separation of the smaller proteins is worse than $SC_{12}S$ as there is anomalous migration.

The separation resolution is quantified by measuring peak width in scaled units of electrophoretic mobility. Overall, macroscopic experiments show that $SC_{10}S$ complexes result in the best resolution among all of the simple alkyl sulfates studied in this work (C_6-C_{16}). However, the improvement in resolution and molecular weight sensitivity (Fig. 4.1) is not much different than $SC_{12}S$. From peak resolution, two different trends are observed: for proteins larger (Fig. 4.1B) and smaller (Fig. 4.1C) than ~15 kDa. For small proteins, complexes consistently show better resolution when the complex is formed with surfactants of short tail. Interestingly, complexes of proteins larger than ~15 kDa are best resolved with $SC_{10}S$ and $SC_{16}S$. With $SC_{12}S$ and $SC_{14}S$ the complexes show broader peak widths. The insert plot on Fig. 4.1C describes graphically the FWHM method that is used to obtain the peak width values.

From separations with $SC_{10}S$ and $SC_{12}S$, it is found that ovalbumin samples contain two separate bands of similar intensity that are both close to the expected 44 kDa range (Fig. 4.1B, line 8). This could be due to small changes in the protein structure (e.g. glycosylation levels) or to incomplete denaturation. The dual bands merge together when larger surfactants are used until they are indistinguishable for the case of $SC_{16}S$. This serve as a simple demonstration of the higher resolution that is observed for smaller surfactants. Separations of β-galactosidase and phosphorylase with $SC_{10}S$ also result in additional protein bands that are resolved very close to each other (Fig. 4.1B, lines 5 and 6). The resolution of additional bands is associated with the fact that smaller micelles decorate the complexes more homogeneously than larger micelles from longer surfactants. Therefore, it is possible to distinguish smaller differences between molecules of similar molecular weight. The use of $SC_{16}S$ causes the total disappearance of the second ovalbumin band. This fact agrees with our statement that larger micelles do not fully decorate the protein-surfactant complex. Thus, small differences in molecular weight will not be distinguished.

Electrophoretic mobilities also show that longer surfactants significantly slow down the migration of complexes with small proteins. It is infer that this behavior is due to the relationship between micelle size and the number of micelles that associate with small proteins. Surfactants with longer tails will form large micelles. Thus, fewer micelles may be attached to the complex, as is depicted in the left side on Fig. 1.2 (Ch. I). For very small proteins is possible that the binding process results in just one micelle attached to the backbone. This assertion is corroborated with scattering experiments.

Since $SC_{10}S$ shows improved resolution over $SC_{12}S$ on smaller complexes and longer surfactants show lower resolution, it is also attempted to use SC_6S and SC_8S in PAGE separations. For experiments with SC_6S, the samples are not resolved at all and it is not possible to identify any clear band in the gels. On the other hand, experiments with SC_8S show slightly better results. In these experiments, some protein complexes never enter the gel or result in smeared bands. In contrast, some proteins such as BSA result in very sharp bands. Although some protein identification is possible with SC_8S, it is never as clear as when $SC_{10}S$ or $SC_{12}S$ is used. This effect is explained with the weakening of hydrophobic binding from the proteins and the micelles[18]. As the alkyl tail length is reduced, surfactants become increasingly more water-soluble and the driving force for protein binding is gradually lost. Additional experiments with SC_8S are also performed with variable voltage conditions without any significant improvement.

Figure 4.2 shows representative gels for PAGE separations with SC_8S (left) and $SC_{12}S$ (right). It is clearly seen that significant portions of proteins in the SC_8S gel have remained in the sample wells (ovalbumin, trypsin inhibitor and lysozyme). In contrast, in the experiment with SC_8S, the BSA complexes are separated with even sharper bands than in $SC_{12}S$. The results suggest that the micelles of SC_8S that are weakly attached to some of the proteins might be lost when the electric field is applied.

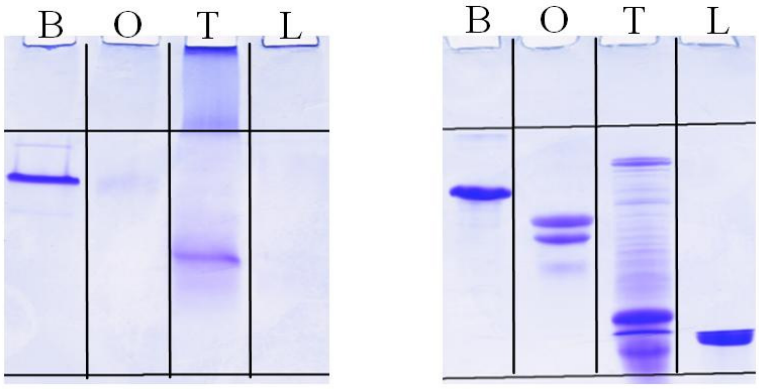

Figure 4. 2. Representative polyacrylamide gels (12%). Four proteins are separated using SC_8S (left) and $SC_{12}S$ (right). B: BSA, O: ovalbumin, T: tripsin inhibitor, L: lysozyme.

It is possible that the electrical force acting on the surfactant molecules may be similar in magnitude to the binding force of the surfactant to the micelles. Another possible explanation is that free surfactant may be electrophoretically advected to a large extent so that the local concentration around the protein-surfactant complex is significantly reduced. Here it is concluded that there is a lower practical limit where short surfactant can no longer be used because of weak protein binding interactions. For the regular series of alkyl surfactants, the limit must be close to $SC_{10}S$. Chemical modifications, such as branching and fluorination, are being explored to provide strong hydrophobic binding while maintaining the small micelle size and homogeneous protein adsorption that results in improved separation resolution.

Small angle scattering (SANS and SAXS): Three of the model proteins are analyzed with SANS and SAXS to probe their nanostructure and correlate this to their electrophoretic migration. In all cases, the samples are analyzed at room temperatures, in

D_2O buffers and in the absence of electric fields. The total protein concentration for the tested samples is shown in Table 4.1. Fig. 4.3 shows the scattering plots and the fitting approximations as obtained through the Inverse Fourier Transformation analysis for BSA, ovalbumin and lysozyme associated with various sodium alkyl sulfates. The CMC for all surfactants are evaluated in the lab with conductivity measurements using the same buffer composition that is used for the scattering analysis. PDDFs are calculated through GIFT analysis and structural parameters are obtained from these functions[26].

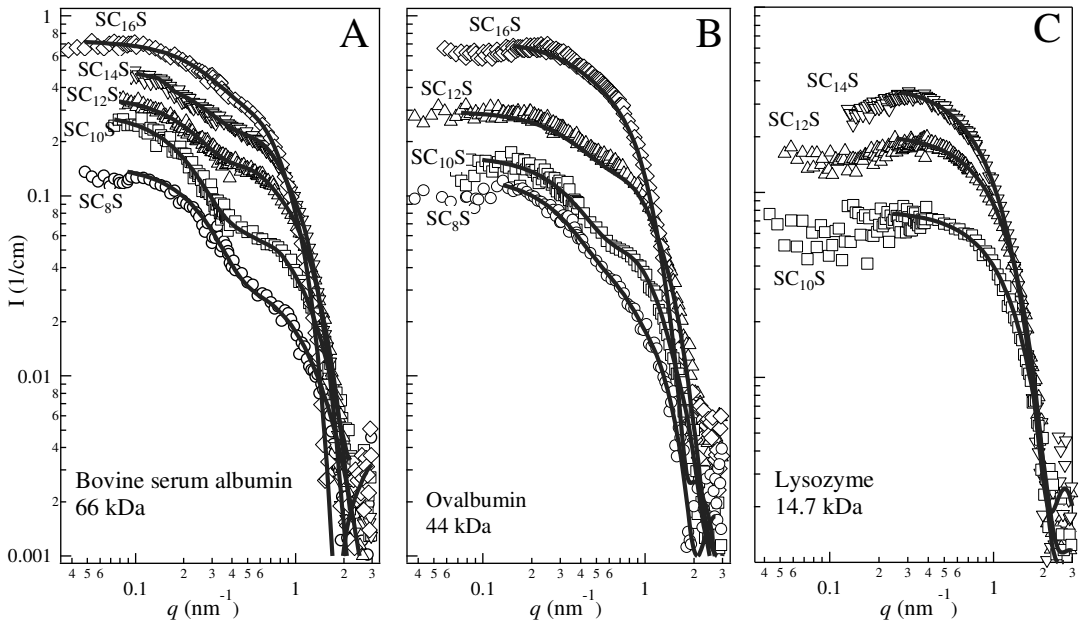

Figure 4. 3. SANS scattering intensities I (q) as function of scattering vector q for protein- surfactant complexes in solution. A) BSA, B) ovalbumin and C) lysozyme. SC_8S (○), $SC_{10}S$ (□), $SC_{12}S$ (△), $SC_{14}S$ (▽) and $SC_{16}S$ (◇). The lines through the scattering profiles are fits from GIFT analysis.

The scattering intensity, which is re-stated from Chap II, is a characteristic function of the particle shape and contrast. The scattering contrast is expressed in terms of the differences in scattering length densities $(\rho_1 - \rho_2)$ [26].

$$I(q) \approx \frac{N}{V} V_{particle}^{2} (\rho_1 - \rho_2)^2 \cdot P(q) \cdot S(q) \qquad \textbf{(4. 2)}$$

For these analyses dilute systems are used. The appropriate concentration is determined by performing a dilution series until the shape of the scattering function becomes independent on the dilution. Under dilute conditions it is possible to ignore scattering contributions from inter-particle correlations (structure factor). The scattering data are transformed into the real-space applying indirect Fourier Transformation (IFT) methods[26]. The result of this analysis is the PDDFs. Details of PDDFs calculations can be found in the literature[26,29]. Three structural parameters can be obtained directly from the PDDF. These are the average length of the complex (L), the micelle radius (r_m) and the distance between neighboring micelles (S). Fig. 4.4 shows a schematic of the PDDF for a straight linear chain of four spherical particles that are equally spaced and also for a flexible pearl-necklace chain undergoing temporal and spatial fluctuations. The radius of the micelles is obtained from the position of the first maximum (SANS) while the micelle separation is assessed from the position of the second peak. Finally, the extension of the complex is obtained from the point where the PDDF crosses the lower axis[26,29].

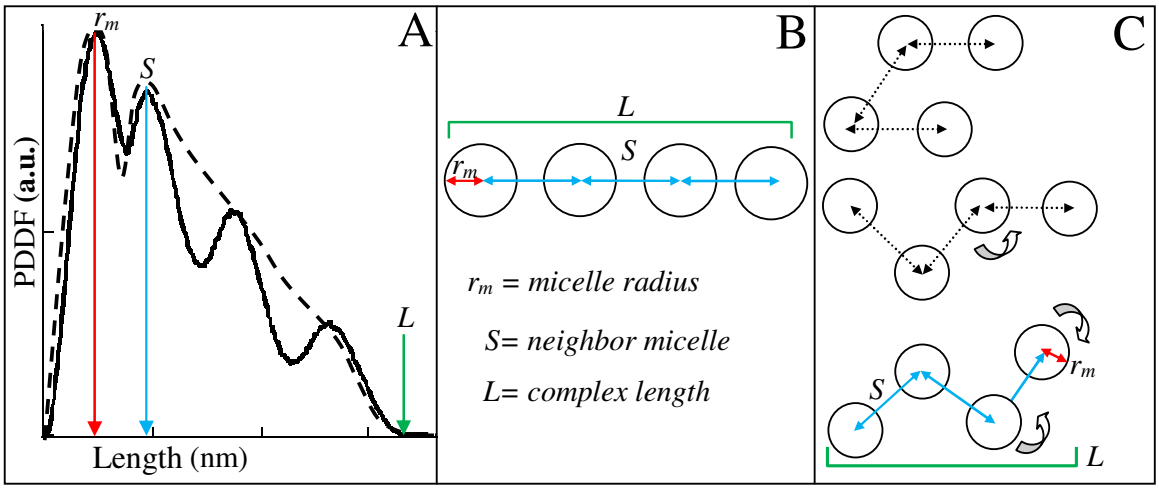

Figure 4. 4. PDDF interpretation schematic. A) PDDFs for straight chain of four equidistant solid spheres (continuous line) for a flexible, fluctuating chain (dotted line). B) Corresponding structural parameters obtained from PDDF analysis. C) Schematic of ensemble and time-averaged conformations.

PDDFs are calculated from both SANS and SAXS data using GIFT[28,29]. Figure 4.5 summarizes all of the results using four characteristic parameters: complex length, radius of the micelles, distance between neighbor micelles and radius of gyration. The radius of gyration is calculated using Guinier analysis at low angles[26].

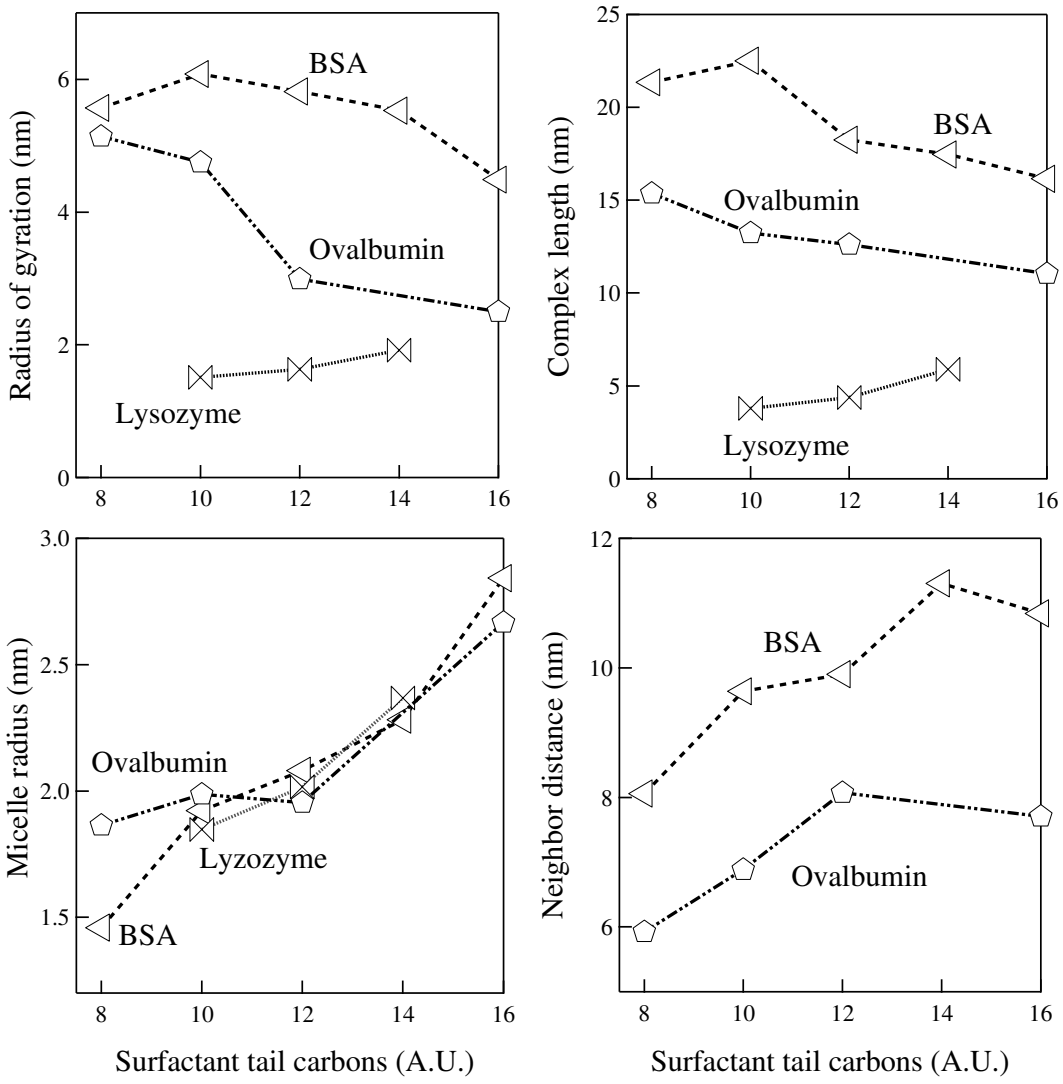

Figure 4. 5. Structural parameters for complexes of BSA (◁), ovalbumin (◇) and lysozyme (⋈) associated with sodium alkyl sulfates (from 8 to 16 carbons in the tail length).

As expected from the increasing molecular weight, the complexes of BSA have the longest lengths and radii of gyration followed by ovalbumin and lysozyme. Also as expected, the micelle radius increased with the addition of carbons to the surfactant tail. Thus, the smallest radii are for the complex of SC_8S, while the biggest radii are for the complexes of $SC_{16}S$. From the PDDF analysis, it is determined that all of the BSA and

ovalbumin complexes show the characteristic pearl-necklace structures. However, lysozyme, which is the smallest protein, did not show the expected PDDF for having neighbor micelles. Therefore, it is determined that only one micelle is associated with lysozyme for all surfactants. Furthermore, the overall length of the lysozyme complex increased proportionally with the increasing tail length of the surfactant. The largest radius of gyration and complex length is obtained when lysozyme is associated with $SC_{14}S$. Due to an unusually high scattering contribution of free micelles, it is not possible to interpret the scattering data for lysozyme associated with $SC_{16}S$. It is expected that the complex size of $SC_{16}S$ would be even larger than $SC_{14}S$. Interestingly, the behavior for BSA and ovalbumin is completely opposite. In general, it is found that the maximum extension of pearl-necklace protein-surfactant complexes decreases with increasing surfactant tail length. This suggests that smaller surfactants are able to extend the proteins to a larger extent and this could explain the higher resolution that is observed for separations involving smaller surfactants.

The two complementary scattering techniques are also used to compare and validate the structural results. An example of PDDFs obtained from SAXS and SANS is shown in Fig. 4.6. Note that there is a significant difference in the shape of the curves at lower values of distance. These differences originate from the different nature of the contrast in neutron and x-ray scattering. The PDDF of SAXS data is determined by local differences in electron density occurring within the samples. When the contrast between the solvent and a micelle core is smaller than the shell, the PDDF reflect an additional dip at short distances that is characteristic of ‘hollow’ spheres.

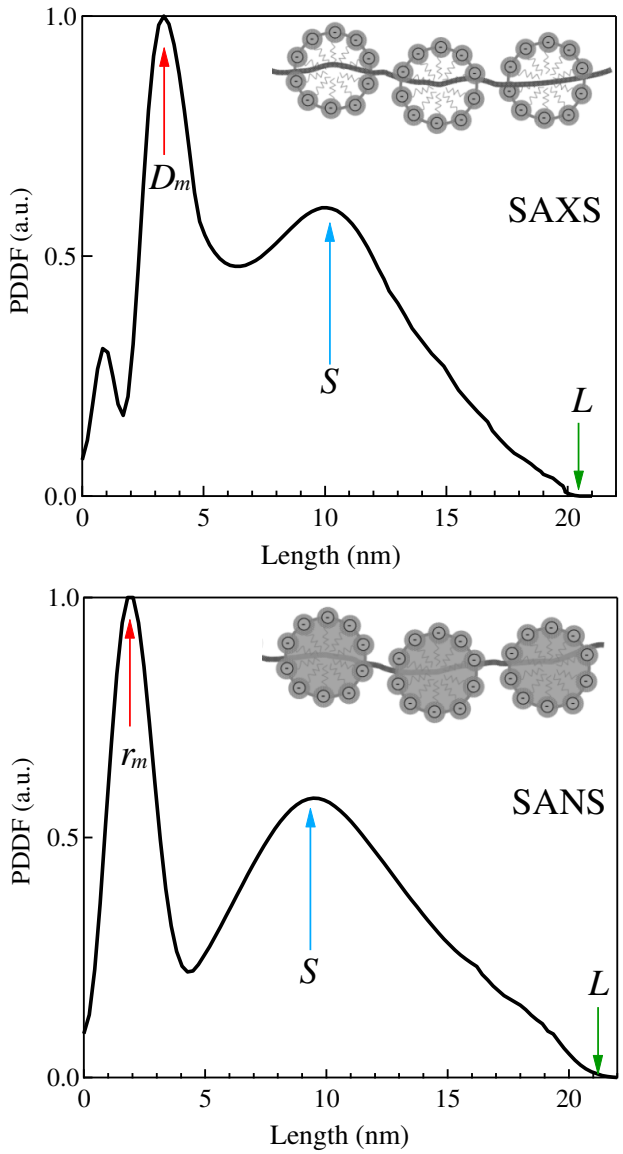

Figure 4. 6. PDDFs from SAXS (left) and SANS (right) of complex of BSA-$SC_{10}S$. The inset cartoons show schematics of SAXS (left) and SANS (right) scattering interpretation. D: micelle diameter, R: micelle radius, S: neighbor micelle and L: complex length.

In Ch. II, Eq. (2.3) and (2.4) describe the mathematical relationships that govern the evaluation of the PDDF for SAXS and SANS interpretation. In all alkyl sulfates studied here, the electron density of the head groups is significantly larger than the electron density of both the solvent and the micelle core. As a result, the PDDF can show

negative values at short distances. The protein-surfactant complexes of alkyl sulfates appear in SAXS as 'hollow' core-shell particles. In contrast, in SANS the micelles appears as 'solid' spherical aggregates because the largest contrast occurs between the hydrogenated hydrocarbon tails and the deuterated solvent (D_2O). Fig. 4.6 shows two respective cartoons that illustrate the different scattering contrasts.

When SAXS and SANS are compared, agreement between the micelle radii for all complexes is found. However, due to the lower resolution of SAXS at low angles the lengths of the largest complexes (BSA) exhibit small discrepancies with SANS. From the PDDF analysis, it seems that all protein-surfactant complexes result in the same necklace structure that has been previously associated for $SC_{12}S$. For lysozyme there is just one micelle attached to the protein backbone regardless of the surfactant tail length. Even for the longest surfactants, there are not signs for the formation of cylindrical micelles with any of the proteins. It is well known that the shape of free micelles in solution depends strongly on the surfactant architecture. The aggregate shape can be roughly predicted by calculating the critical packing parameter (CPP)[34]. The CPP is a function of the volume occupied by the hydrocarbon core, the surfactant tail length and the effective area of the head group. The value of the CPP can be used to predict the expected micellar structure in solution. Spherical micelles are expected for values lower than 0.33 and cylindrical micelles between 0.33-0.5 [34,35]. It should be noted that these are not exact limits and only serve as rough guidelines. The CPP for $SC_{12}S$ in solution is 0.37, which is in an intermediate range between cylindrical and spherical micelles. Surfactants with tails larger than twelve carbons are more likely to form cylindrical structures[36]. Figure 1.2 (Ch. I, right side) shows a hypothetical structure of alkyl surfactants with long tail.

However, the shape obtained through the PDDF analysis for $SC_{14}S$ and $SC_{16}S$ does not indicate formation of cylindrical structures. Fig. 4.7 shows a representative set of PDDFs of $SC_{12}S$ and $SC_{16}S$ associated with BSA. Both plots, SAXS and SANS, are consistent in the micelle radii, the separation distance and the complex lengths.

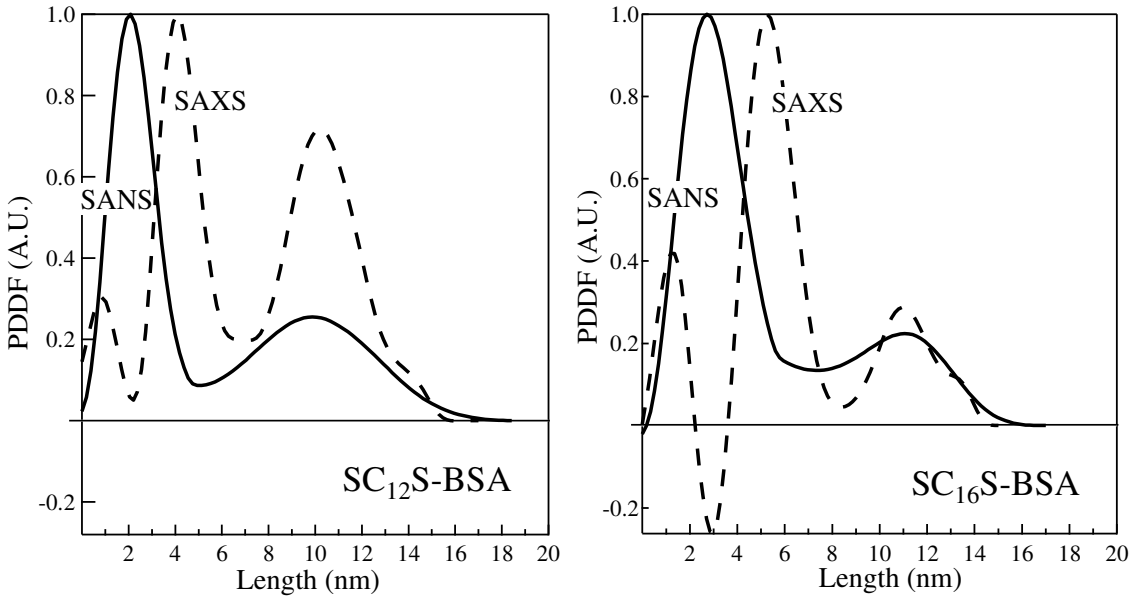

Figure 4. 7. PDDFs from SAXS (dotted line) and SANS (solid line) for BSA associated with $SC_{12}S$ and $SC_{16}S$.

Complexes of BSA, ovalbumin and lysozyme with $SC_{12}S$ are also compared in Fig. 4.8 to show the agreement of the radii and the variations in the length of the complex. From this comparison is observed that the neighbor distance seems to get slightly expanded as the molecular weight increases. The inset plot in Fig. 4.8 correspond to a zoom-in of the micelle radius region where the agreement for the micelle radii of a same surfactant associated with different proteins is confirmed. In other words, the

micelles of the same surfactant have similar shapes and sizes despite being associated to different proteins.

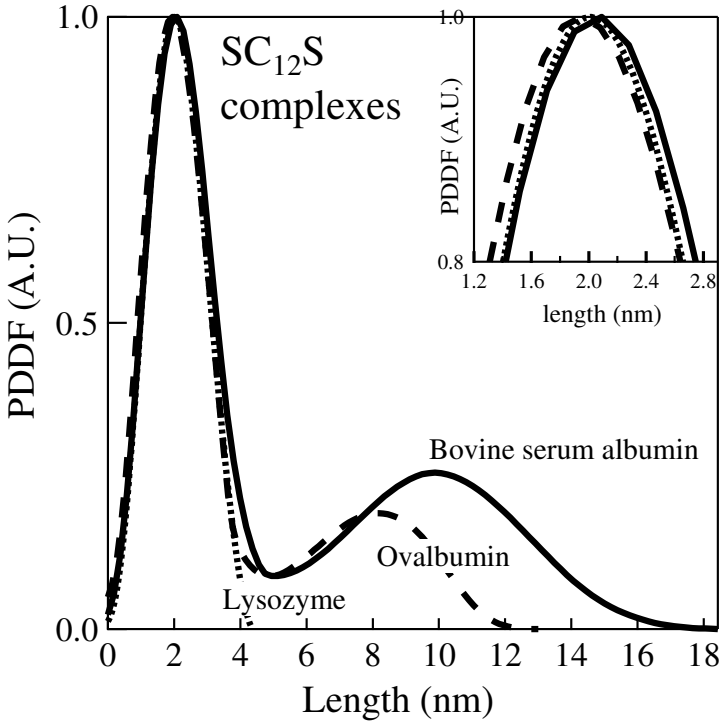

Figure 4. 8. PDDFs from SANS analysis. Comparison of three proteins associated with $SC_{12}S$. The inset shows a zoom-in for the micelle radius region.

From the scattering analysis (Fig. 4.5), it is established that increasing the surfactant tail results in larger micelles. Therefore, it is also expected that the distances between larger micelles also increase the nearest neighbor distance. However, it is noted that electrostatic repulsion between micelles is a factor that must be considered. The micelle separation distance followed the order from smallest to largest: $SC_8S < SC_{10}S < SC_{12}S < SC_{14}S$ or $SC_{16}S$ (Fig. 4.9). After twelve carbons the neighbor distance remains constant.

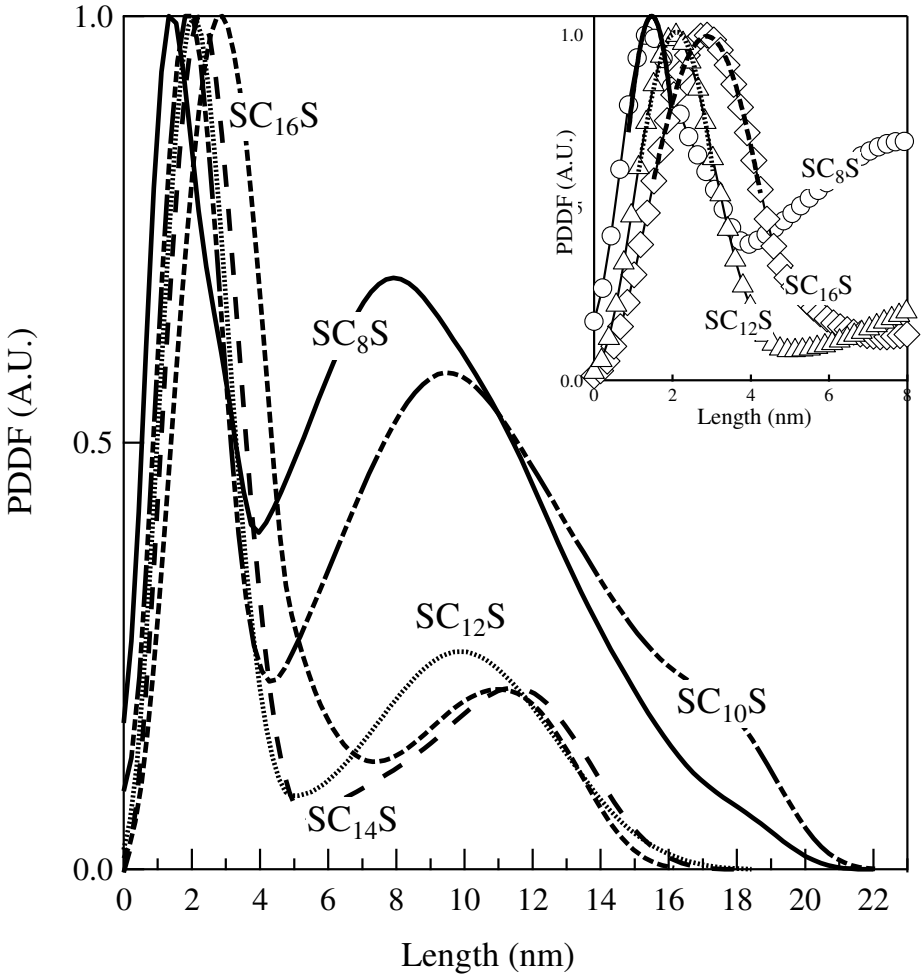

Figure 4. 9. PDDF from SANS analysis for BSA associated with five sodium alkyl sulfates. The inset shows an expanded plot of the small length region for SC_8S, $SC_{12}S$ and $SC_{16}S$ complexes with fits to the analytical function of the PDDF for a sphere.

Figure 4.9 shows a set of PDDFs of BSA associated with five sodium alkyl sulfates. It also contains a plot that magnifies the region of micelle radius. From scattering analysis it is now accepted that the necklace model is the result of multiple spherical micelles attached to the protein backbone [2,22]. The mathematical representation of a spherical object in a PDDF can be evaluated analytically as a function of *r* and *D*, which represent the r-distance in the PDDF and the sphere diameter respectively. The

following equation can be used to describe the PDDF of spherical particles where $x=r'/D'$ [29].

$$PDDF = 12 \cdot x^2 \left(2 - 3x + x^3\right) \quad \textbf{(4. 3)}$$

The experimental PDDFs are modeled with this equation in order to quantitatively verify if spherical shapes could describe well all of the associated micelles. The complexes that tend to be spherical are the ones associated with surfactants of longer tails. From the inset plot (Fig. 4.9), it is clear that the micelles of the complexes with SC_8S do not fit to Eq. (4.3). This indicates that SC_8S micelles are not spherical micelles and are likely more elongated. Aggregates of surfactant could also form other shapes such as prolate or oblate ellipsoids and rod-like micelles [37–39]. Thus, it is determined that SC_8S complexes have a shape that deviates from spherical but it has not been possible to unambiguously describe the exact shape from the current data. Still, this outcome is a motivation to pursue experiments in which shape changes are induced by modifying the chemical structure of the surfactant. Adding branches or increasing the hydrophobicity of the tail with perfluorination could induce additional structural changes in the complexes.

The results indicate that gel electrophoresis could be performed using alternative surfactants from $SC_{12}S$. Furthermore, it is demonstrated that the macroscopic separation is a strong function of the protein-surfactant nanostructure. Therefore, it is reasonable to assume that this technique could be further improved by using an engineering approach for future surfactant design. With combined gel electrophoresis and scattering analysis it is determined that the surfactant structure plays a fundamental role in a successful separation of proteins. Therefore, it is essential that tandem microscopic analyses are

used to correlate the structures to the macroscopic separations. Furthermore, these techniques could also be extended to similarly guide the design of novel sieving matrices, which are also crucial to the separation. This study would also include macro-scale and micro-scale analyses to obtain a broad overview the underlying mechanisms that control electrophoretic migration across sieving media. It has been confirmed that there is a structural reason for $SC_{12}S$ being such a great surfactant for this application but the present study also suggests that further improvements are still possible. In fact, PAGE results and scattering analysis of complexes of $SC_{10}S$ show promising outcomes for providing higher resolutions and fidelity between protein molecular weight and electrophoretic mobility especially at low molecular weights. It is also noteworthy that the design principles that are suggested in this article for surfactant formulations could also be extended to more modern separation technologies such as 2D gel electrophoresis, capillary electrophoresis and microfluidic-based separations.

Future experiments are directed to the continued use of combined SAXS and SANS analysis for alternative surfactant systems and also for analysis during the process of electrophoresis. It has also been demonstrated that in-situ scattering experiments are able to describe structural changes occurring when an electric field is applied[31]. The shape of the complexes is clearly a key factor in the choice of surfactant formulations for gel electrophoresis. This work demonstrates that a combination of analyses is critical for the design of surfactants that can go beyond the standard of $SC_{12}S$.

4.4. Conclusion and Outlook

This study has established that small angle scattering techniques are effective methods to interpret the structural changes in systems of protein-surfactant complexes used in electrophoresis. This work shows that the binding mechanisms by which the surfactants attach to the backbone of the protein is key to understanding their structure and electrophoretic migration. It is also found that most protein complexes with alkyl sulfates form 'pearl-necklace' structures. From macroscopic electrophoresis (PAGE), shows that lower surfactant tail lengths result in slight improvements in resolution but that, below $SC_{10}S$, there is a lower limit where the surfactants cannot provide a reliable separation. It is infer that surfactants with smaller tail lengths can decorate the complexes more homogeneously but also bind the protein with weaker interactions. Overall $SC_{10}S$ consistently results in the best separations of all alkyl sulfates shown here. Particularly for small proteins, $SC_{10}S$ is a substantial improvement over $SC_{12}S$, which is the most commonly used surfactant for PAGE applications. These results motivate further studies aimed at improving protein electrophoresis by designing novel surfactant architectures using engineering principles.

4.5. References

(1) Reynolds, J. A.; Tanford, C. *Proceedings of the National Academy of Sciences of the United States of America* **1970**, *66*, 1002–1007.
(2) Chen, S.-H.; Teixeira, J. *Physical Review Letters* **1986**, *57*, 2583–2586.
(3) Turro, N. J.; Lei, X.-G.; Ananthapadmanabhan, K. P.; Aronson, M. *Langmuir* **1995**, *11*, 2525–2533.
(4) Marilena Vasilescu, D. A. *Langmuir* **1999**, *15*, 2635–2643.
(5) S. Chodankar P.A. Hassan, A.G. Wagh, V. K. A. *Physica B: Condensed Matter* **2007**, *398*, 112–117.
(6) Kwak, J. C. T. In *Surfactant science series*; Marcel Dekker, INC: New york, USA, 1998; p. 482.
(7) Viovy, J.-L. *Reviews of Modern Physics* **2000**, *72*, 813–872.
(8) Sonia F. Santos Hannes Fischer, Rosangela Itri, D. Z. *Journal of Colloid and Interface Science* **2003**, *262*, 400–408.
(9) Weber, K.; Osborn, M. *The Journal of Biological Chemistry* **1969**, *244*, 4406–4412.
(10) Shapiro, A. L.; Viñuela, E.; Maizel, J. V. *Biochemical and Biophysical Research Communications* **1967**, *28*, 815–820.
(11) Jones, M. N.; Skinner, H. a; Tipping, E. *The Biochemical journal* **1975**, *147*, 229–34.
(12) Frank M. Witte, J. B. F. N. E. *the journal of organic chemistry (ACS publications)* **1987**, *52*, 6.
(13) Nelson, C. A. *The Journal of Biological Chemistry* **1971**, *246*, 3895–3901.
(14) Lundhal, P.; Greijer, E.; Sandberg, M.; Cardell, S.; Eriksson, K.-O. *Biochimica et Biophysica Acta (BBA)* **1986**, *873*, 20–26.
(15) Gul, N.; Aswal, V. K.; Chodankar, S.; Kabir-UD-DIN *Pramana- Journal of Physics* **2008**, *71*, 1027–1031.
(16) Malcolm N. Jones Edward Tipping, H. A. S. *Biochemical Journal* **1975**, *147*, 229–234.
(17) Shashank Deep, J. C. A. *Physical Chemistry Chemical Physics (PCCP)* **2001**, *3*, 9.
(18) Messina, P. V.; Ruso, J. M.; Sarmiento, F.; Prieto, G. *Journal of Physical Chemistry B* **2005**, *109*, 15566–15573.
(19) Yajuan Li Yilin Wang, X. W. *Journal of Physical Chemistry B* **2006**, *110*, 8499–8505.
(20) Rossi, S.; Ristori, S.; Martini, G.; Edwards, K.; Karlsson, G. *Langmuir* **2001**, *17*, 2340–2345.
(21) Root, B. E.; Zhang, B.; Barron, A. E. *Electrophoresis* **2009**, *30*, 2117–2122.
(22) Samsó, M.; Daban, J. R.; Hansen, S.; Jones, G. R. *European journal of biochemistry / FEBS* **1995**, *232*, 818–24.
(23) Ruiz-Peña, M.; Comas-Rojas, H.; Rodriguez-Calvo, S.; Perez-Gramatges, A. *IEE. Proc.-Nanobiotechnology* **2005**, *152*, 177–181.
(24) Peng, J.; Gygi, S. P. *Journal of mass spectrometry: JMS* **2001**, *36*, 1083–91.
(25) Myers, D. *Surfactant science and technology*; VCH Publishers, Inc.: New York, 1988.
(26) Lindner, P.; Zemb, T. *Elsevier Science B.V.* **2002**.

(27) Chodankar, S.; Aswal, V. K.; Kohlbrecher, J.; Vavrin, R.; Wagh, A. G. *Physical Review E* **2008**, *78*, 031913–1:031913–8.
(28) Fritz, G.; Bergmann, A.; Glatter, O. *Journal of Chemicals Physics* **2000**, *113*, 9733–9740.
(29) O.Glatter, O. K. *Academic press* **1982**.
(30) Narayanan, J.; Abdul Rasheed, A. S.; Bellare, J. R. *Journal of colloid and interface science* **2008**, *328*, 67–72.
(31) Pozzo, D. C. *Langmuir* **2009**, *25*, 1558–1565.
(32) Valstar, A.; Almgren, M.; Brown, W. *Langmuir* **2000**, *16*, 922–927.
(33) Kline, S. R. *Journal of Applied Crystallography* **2006**, *39*, 895–900.
(34) Israelachvili, J. *Intermolecular and Surface Forces with application to colloidal and biological systems*; Second.; Academic Press: London, 1985.
(35) Berg, J. *An Introduction to Interfaces & Colloids. The Bridge to Nanoscience*; World Scientific Publishing Co. Pte. Ltd.: Singapore, 2010; p. 785.
(36) Gargi Basu Ray Soumen Ghosh, Satya P. Moulik, I. C. *Colloid Polymer Science* **2007**, *285*, 13.
(37) Stjerndahl Maria Zhang Hailing, Menger Fredric M., L. D. *Journal of Physical Chemistry B* **2007**, *111*, 2008–20014.
(38) James Bowers Pamela J. Martin, Marcos C. Vergara-Gutierrez, C. P. B. *Langmuir* **2004**, *20*, 8.
(39) Groth C Holmberg K, Kanicky JR, Shah DO., N. M. *Journal of Surfactants and Detergents* **2004**, *7*, 9.

CHAPTER V

ANIONIC BRANCHED SURFACTANTS USED AS ALTERNATIVE DENATURING AGENT IN PROTEIN SEPARATIONS

The aim of the present chapter is to investigate the effect of branching in sodium alkyl sulfates to conduct better protein separations and to investigate their interactions with a series of proteins of diverse size and composition. The motivation and hypothesis for this study are described in the background section. The results of this study suggest that branching is indeed an alternative to enhance the hydrophobic character of a short-tailed surfactant while still forming smaller protein-surfactant complexes. Spectroscopy characterizations reveal that, when 2-butyl octyl sulfate (2-BOS) is used as denaturing agent, the secondary structure of proteins is disrupted to a much higher extent than with other surfactants.

5.1 Background

The development of technologies for protein separation and identification is a continuous goal that researchers have pursued over many years. Proteins interacting with surfactants are not only important for protein separations and for fundamental biological systems, but they also are relevant in cosmetic, pharmaceutical and food industries[1,2]. To this date, the emblematic surfactant used to denature protein is sodium dodecyl sulfate ($SC_{12}S$). Researchers have contributed with detailed characterizations of its dynamic self-

assembly, its interactions with proteins and its denaturing effect[3–6]. In spite of the success of $SC_{12}S$ in the field of protein electrophoretic separations, many authors have identified limitations such as the incorrect identification of very small molecular weight proteins (abnormal migration), the co-migration of proteins of similar molecular weight and the inability to separate membrane proteins in 2D applications[7–10]. In Chapter IV, it was found that reducing the tail length of a linear alkyl-sulfate surfactant increases the fidelity of the separation of small molecular weight proteins in terms of the formation of narrower bands and achieving a more accurate molecular weight determination[11]. Specifically, it was found that sodium decyl ($SC_{10}S$) and dodecyl ($SC_{12}S$) sulfate showed the best separations. Structural analysis revealed that sodium octyl (SC_8S) and decyl ($SC_{10}S$) sulfate formed more elongated protein-surfactant complex structures. Short tailed surfactants usually enhanced the macroscopic separation and formed larger protein-surfactant complexes. However, the linear sodium octyl sulfate (SC_8S) did not surpass the electrophoresis performance of $SC_{12}S$ or $SC_{10}S$. We suggested that this result was related to the increase of the surfactant's hydrophilic character upon alkyl tail reduction.

In this work, we investigate the interactions of surfactants having hydrophobic tails that are, overall, shorter or equal to eight carbons but which also contain one or more branches along the tail. These surfactant molecules are sometimes called Guerbet alkyl sulfates. The intrinsic hydrophobic character of these surfactants is enhanced branching, but total length can remain 'short'. We hypothesize that the binding interactions between proteins and branched surfactants will be as strong as with linear alkyl sulfate surfactants of equal number of total carbons but that the branched tails will modify the structure and the electrophoresis separations.

To the best of our knowledge, fundamental studies on the interaction of proteins with branched surfactants or on protein denaturation are unavailable. Therefore, information that can correlate the macroscopic separations of protein complexes with branched surfactants with their nanostructure is lacking. However, new alternative surfactants could help identify proteins that lack separation sensitivity when $SC_{12}S$ is used. Furthermore, we will propose surfactants that could help separate and detect membrane proteins, which are some of the most challenging protein classes due to insolubility in the absence of amphiphilic molecules. Because of the 'bulky' tail architecture of branched surfactants, we expect to form more elongated protein-surfactant complexes. This could increase fidelity in the detection of proteins during gel electrophoresis.

The three different branched surfactants are used and contain eight (sodium 2-ethylhexyl sulfate or 2-EHS), ten (sodium 3,7-dimethyl octyl sulfate or 3,7-DMOS) and twelve (sodium 2-butyl octyl sulfate or 2-BOS) carbons in the whole molecule. However, the longest segments in the tails are only six (2-EHS) and eight carbons (3,7-DMOS and 2-BOS). Similar to our previous studies, we keep the hydrophilic head group (sodium sulfate - $NaSO_4$), unchanged. The critical packing parameter for these surfactants in solution indicates that increasing the tail volume will modify the ratio of head to volume and consequently also bias the shape of the resulting micelles towards more cylindrical forms when compared to linear surfactant molecules[12,13]. Thus, we hypothesize that these features (branches) in the surfactant will also yield different shapes upon surfactant adsorption during protein denaturation.

To decipher the structural parameters and the performance of these branched surfactants we use circular dichroism (CD) and fluorescence spectroscopy to probe the secondary structure of the proteins after surfactant adsorption. Also, without any further optimization of buffer systems, we explore the use of these branched surfactants in 1D-PAGE to investigate their performance. Finally, we use small angle scattering techniques (SAXS and SANS) to probe the structural parameters of micelles in free solution and when bound to protein-surfactant complexes. Thereby, we are able to connect these different pieces of information to develop an engineering approach to design novel surfactants for electrophoretic separations.

5.2 Materials and methods

5.2.1 Branched surfactants and synthesis

Three anionic branched surfactants of the alkyl sulfate family are used (Table 5.1), 2-ethylhexylsulfate (2-EHS) is purchased from Sigma Aldrich (St. Louis, MO), while 3,7-dimethyloctylsulfate (3,7-DMOS) and 2-butyloctylsulfate (2-BOS) are synthesized according to the procedure described by Missel et al. [6]. For the surfactant synthesis and purification the following chemicals are used: 3,7-dimethyl-1-octanol, 2-butyl-1-octanol, chlorosulfonic acid and dichloromethane, which are purchased from Sigma Aldrich (St. Louis, MO). Industrial grade nitrogen is obtained from Praxair (Bellingham, WA). We also obtain sodium hydroxide from Mallinckrodt Chemicals (St Louis, MO), hexane from EMD Chemicals (Philadelphia, PA), ethanol from Decon Labs (King of Prussia, PA) and cellulose filter paper 70mm from Whatman (Piscataway, NJ).

Table 5. 1. Generalities of the studied branched surfactants

Surfactant name	Acronym	Molecular formula	Mw[a] (g/mol)	CMC[b] (M)	Structural Formula
Sodium 2-ethylhexyl sulfate	2-EHS	$C_8H_{17}NaSO_4$	232.3	0.23	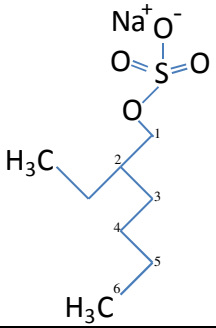
Sodium 3,7-dimethyl octyl sulfate	3,7-DMOS	$C_{10}H_{22}NaSO_4$	260.3	0.05	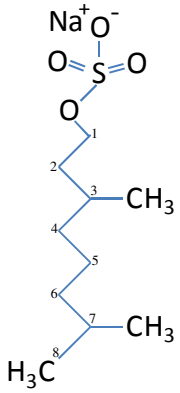
Sodium 2-butyl octyl sulfate	2-BOS	$C_{12}H_{25}NaSO_4$	288.3	0.015	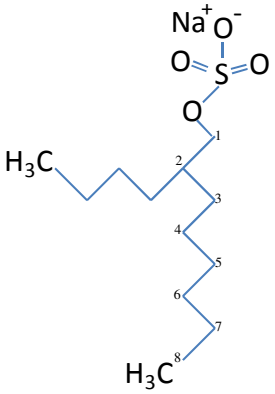

[a] Mw: molecular weight, [b] CMC: critical micelle concentration

The synthesis of 3,7-dimethyloctylsulfate (3,7-DMOS) and 2-butyloctylsulfate (2-BOS) are performed under a constant nitrogen flow and in an ice bath to control heat generation. First, the alcohol (~0.25 mol) corresponding to the desired tail is dissolved in

four times the volume of dichloromethane and the mixture is cooled down and kept at 5 °C. Then, chlorosulfonic acid (~0.25 mol) is added drop-wise while keeping the temperature below 10 °C. The mixture is stirred for 30 minutes while holding the temperature below 5 °C. Subsequently, ~250 mL of sodium hydroxide (8 M) are added drop-wise to reach a pH value between 8 to 10. The mixture is stirred and left under nitrogen until the dichloromethane is fully evaporated. The solid residue is then dissolved in hot hexane (50 °C) and filtered repeatedly to remove any un-reacted alcohol. Consecutively, the hexane-insoluble residue is dissolved in hot ethanol (50 °C) and filtered to remove inorganic salts. The final filtrate is cooled down and allowed to dry. The resulting powder corresponds to the synthesized branched surfactant. Purity is assessed by electrospray ionization mass spectrometry (Figure 3.2, Ch. III). The mass spectra are obtained in terms of intensity and the ratio of atomic mass to ion charge (m/z). Peaks at 238.7 m/z (left) and 265.5 m/z (right) in Fig. 3.2 coincide with the expected molecular weight of 3,7-DMOS and 2-BOS in the absence of the sodium ion. The inset plots in Fig. 3.2 (Ch. III) correspond to the mass analysis of the sulfate ion $(SO_4)^{-1}$ of each synthesized surfactant. Conductivity measurements at room temperature and UV-vis spectroscopy (608 nm) are also used to evaluate the critical micelle concentration (CMC) for each branched surfactant. Pinacyanol chloride, obtained from Sigma Aldrich (St. Louis, MO), is used at a concentration of at 75 μM in water as a dye for the UV-vis analysis and CMC determination [13].

5.2.2 Protein samples

Eight proteins are purchased from Sigma Aldrich (St. Louis, MO) and used as received without further purification (Table 3.2, Ch. III). Proteins are chosen based on their diverse content of secondary structure and variable molecular weight. For the analysis of secondary structure, lysozyme is not used because it aggregates when it is combined with 2-EHS. In fluorescence experiments, aprotinin is not analyzed because it does not contain tryptophan (Trp) residues.

5.2.3 Preparation of protein solutions

All proteins solutions are prepared in distilled and deionized water (18 MΩ) at a ratio of 3 mg surfactant / 1 mg of protein. This ratio is used because it is more than sufficient to fully saturate proteins when linear alkyl-sulfates are used[8,14]. Protein concentrations are corroborated by UV-Vis spectroscopy at a wavelength of 280 nm using an Evolution 300 UV-Visible spectrophotometer from Thermo Scientific (Waltham, MA). The molar extinction coefficients for all proteins are detailed in Table 3.2. (Ch. III) Dithiothreitol (DTT) is used to reduce the disulfide bonds in a stoichiometric excess of five times to the number of disulfide bonds present in each protein. Samples containing protein and branched surfactants for use in polyacrylamide gel electrophoresis (PAGE), small angle scattering (SAS) and dynamic light scattering (DLS) contain also trizma and glycine at 0.025 M and 0.192 M respectively. Samples for circular dichroism and fluorescence are prepared in the absence of trizma and glycine to avoid a high background intensity that interferes with the experiment. The precipitation

of lysozyme upon the adsorption of some the branched surfactants prevented its use in further spectroscopic investigations.

5.2.4 Polyacrylamide gel electrophoresis (PAGE)

Electrophoresis experiments are conducted in a Mini-PROTEAN tetra cell using 12% polyacrylamide commercial slab gels without $SC_{12}S$, Commasie brilliant blue dye and a protein MW standard ladder are all purchased from Biorad (Hercules, CA). Commercial slab-gels are immersed and run in trizma-glycine buffers with and without surfactant (cathode and anode, respectively). The cathode buffers are prepared at 0.5 times the CMC of each surfactant: 120 mM, 25 mM and 7.5 mM for 2-EHS, 3,7-DMOS and 2-BOS respectively. For each gel a constant voltage of 150 V is applied. Running time ranges are chosen so they are appropriate for the migration of each protein-surfactant complexes and the dimension of the gel. After running, each resulting gel is fixed (2 hr) in a volumetric mixture of methanol (40%), acetic acid (10%) and distilled water (50%). Then, each gel is immersed in Commasie brilliant blue (24 h) and washed with the fixer solution (previously described) to remove the excess of the dye. Each gel is scanned and analyzed with ImageJ to calculate the electrophoretic mobility, μ_E (Eq. 5.1) based on migration distance, total running time, voltage and length of gel. Where $v_{complex}$ corresponds to the protein-branched surfactant complex velocity and E is the applied electric field across the gel.

$$\mu_e \approx \frac{v_{complex}}{E} \qquad \textbf{(5. 1)}$$

5.2.5 Circular dichroism

Circular dichroism (CD) measurements are conducted at 25 °C in a Jasco-720 spectropolarimeter (Easton, MD) using a 0.1 cm quartz cell. Samples of protein and branched surfactants are prepared as described in the previous section at a protein concentration of 0.08 mg of protein/mL. Trizma and glycine are not added to avoid high background intensity. Samples are analyzed using the following setting conditions: scan rate 100 nm/min; accumulation (8 runs) and samples were recorded in the far-UV region (190 to 270 nm). All experiments are performed in triplicate and the presented data are representative curves.

The CD data is reported in mean residue ellipticity (θ_{MRE}), which is determined using Eq. (5.2) and (5.3)[15]. Here, θ_e corresponds to the raw CD data; *MRW* is the mean residue weight of the sample, which is calculated with the protein molecular weight (*Mw*) and the number of amino acids (*n*) within the protein. The protein concentration corresponds to parameter *c* (mg/mL) and *l* is the quartz cuvette pathlength in (mm).

$$\theta_{MRE} = \frac{\theta_e \cdot 0.1 \cdot MRW}{c \cdot l} \quad \textbf{(5. 2)}$$

$$MRW = \frac{M_w}{n-1} \quad \textbf{(5. 3)}$$

The Dichroweb online analysis is used to quantify the secondary structure of each protein-surfactant complex[16]. We use the CONTIN algorithm and the protein data set SP175 and set4 for fitting all spectra. For this analysis, only the solutions with values for the normalized root-mean-square deviation (NMRSD) lower than 0.1 will be considered

as accurate. Values of NMRSD significantly higher than 0.1 correspond to bad solutions and the results are not trustworthy.

5.2.6 Small angle x-ray scattering (SAXS)

SAXS is used to examine the structural conformation of each branched surfactant micelle and the protein-branched surfactant complexes. SAXS experiments are conducted at the University of Washington using an Anton Paar SAXSess instrument (Graz, Austria). The instrument is configured with a line-collimated CuKα x-ray source operating at a wavelength of 1.54 Å. SAXS experiments are performed on protein-surfactant complexes initially prepared at 1.5 mg protein/mL. Each sample is further diluted and analyzed to obtain dilution profiles. Thus, the SAXS analysis of the most diluted samples would satisfy the assumption that the protein-surfactant complexes are independent scatterers and that inter-particle correlation can be neglected. Each protein-surfactant sample is diluted with the correspondent surfactant solvent which is prepared in DI water at 0.7 times the surfactant CMC, 0.025 M trizma and 0.192 M glycine. Each surfactant solvent is also analyzed with SAXS to verify the absence of scattering from free micelles. Sample scattering profiles are corrected by solvent subtraction. In doing so, we confirmed the absence of the scattering contribution from any free micelle in solution. For the current instrument configuration, each protein-surfactant sample and surfactant solvent are counted for an average time of 6 hr each.

The scattering profile is given in terms of the scattering intensity ($I(q)$) and the scattering vector (q), which is a function of the incident radiation wavelength (λ) and the scattering angle (θ) (Eq. 5.4). The scattering vector q for free micelles in solution and

protein-surfactant complexes range from 0.1nm^{-1} to 10 nm^{-1} and 0.09 nm^{-1} to 4 nm^{-1} respectively. The minimum q values reached in the SAXS experiments allow us to have certainty in the maximum dimension ($D_{max} = 2\pi/q_{min}$) of the free micelles and the protein-surfactant complexes (60.8 nm and 69.8 nm respectively).

$$q = \frac{4\pi}{\lambda}\sin\theta \qquad \textbf{(5. 4)}$$

The scattering raw data is fully corrected and pair distance distribution functions (PDDF) are calculated using the *GIFT* analysis package[17,18]**.** The *GIFT* code performs an indirect Fourier transformation (IFT) of the scattering profiles to calculate a real-space analogue. By using IFT methods it is possible to evaluate the scattering data under a model-independent analysis without assuming any form-factor. Equation 5.5 defines the Fourier inversion of the scattering profile used to obtain the PDDF or $p(r)$.

$$p(r) = \frac{1}{2\pi^2}\int_0^\infty I(q)\, qr \sin(qr)\, dq \qquad \textbf{(5. 5)}$$

Through the PDDF analysis the micelle radius (r_m, first upturn in the PDDF curves), the nearest neighbor distance (S, distance between first and second upturn), and the average complex length (L, position where the PDDF curve crosses the x axes) for each micelle and protein-surfactant complex are obtained. Ch. II, discusses in more detail the interpretation of PDDF and previous works has also shown the validity of using IFT methods to extract these structural parameters from scattering data on these systems. For further details refer to literature publications[11,18–20].

5.2.7 Fluorescence spectroscopy

Fluorescence measurements of six proteins (β-galactosidase, phosphorylase b, bovine serum albumin, ovalbumin, carbonic anhydrase and α-lactalbumin) denatured by three branched surfactants are carried out at 25 °C with a PerkinElmer LS55 fluorescence spectrometer (Santa Clara, CA). For comparative purposes, the proteins are also analyzed in their native state and denatured with linear $SC_{12}S$. All protein-surfactant complexes are prepared as described in the sample preparation section at 0.08 mg of protein/mL, but without trizma and glycine. BSA and ovalbumin samples are excited at 285 nm and the other proteins at 295 nm corresponding to the maximum excitation peaks. The emission spectra are recorded over a range of 300-500 nm. All fluorescence spectra are obtained in triplicate for each protein-surfactant complex and the plots correspond to characteristic curves from this analysis.

5.2.8 Dynamic light scattering (DLS)

DLS measurements of BSA and ovalbumin denatured by branched surfactants are carried out at room temperature (25 °C) in a Zeta-sizer Nano ZS with a 633 nm wavelength (Malvern-UK). Samples are prepared at 1 mg protein / mL using the same procedure described previously in the preparation of protein-surfactant complexes. DLS is used to characterize the diffusion coefficient (D_f) and the hydrodynamic radius (R_H) of protein-branched surfactant complexes.

5.3 Experimental Results

Vertical PAGE is used to evaluate the performance of branched surfactants in protein separations using 2-EHS, 3,7-DMOS and 2-BOS. Polyacrylamide gels are shown in Fig. 5.1 for eight different proteins with molecular weights ranging from 116 to 6.5 kDa (Table 3.2, Ch. III) that are denatured with 2-EHS (left), 3,7-DMOS (center) and 2-BOS (right). None of the branched surfactants surpass the performance of $SC_{12}S$ or $SC_{10}S$, (homologue linear sulfate surfactants of twelve and ten carbons). However, 2-BOS and 3,7-DMOS show significantly better separations than SC_8S in terms of narrow bands and resolution. Also, there is an erratic migration resulting from the use of 2-BOS and 3,7-DMOS. As a result, the relationship between protein mobility and protein molecular weight is not linear as expected. This outcome has the potential to help enable future applications in 2D surfactant-surfactant gel electrophoresis for membrane proteins[7,21,22].

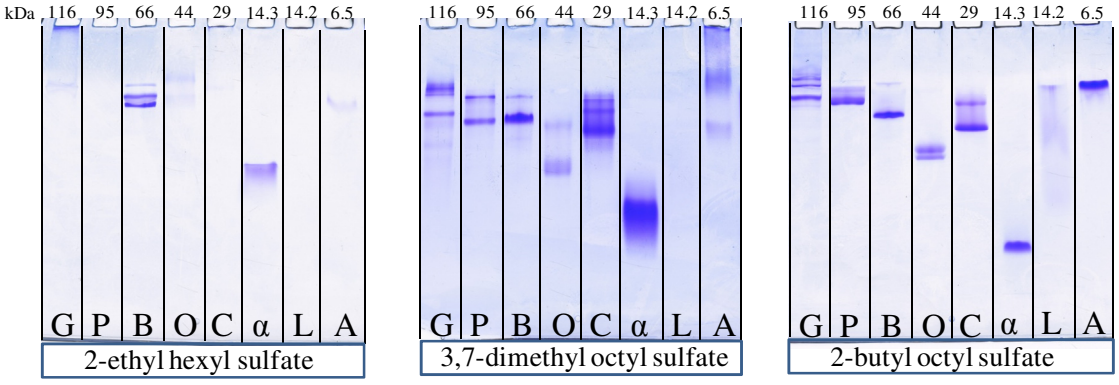

Figure 5. 1. Characteristics images of polyacrylamide gel electrophoresis using branched surfactants 2-EHS (left), 3,7-DMOS (center) and 2-BOS (right).

Additionally, the electrophoresis results of 2-BOS and 3,7-DMOS reveal additional bands, which could be associated to post-translational modifications (e.g. protein glycosylation), or previously undetected contaminants. Additional bands are also observed in previous studies when SC_8S and $SC_{10}S$ are used in PAGE analysis[11]. This leads us to hypothesize that short-tailed surfactants may interact differently with certain proteins than long-tailed surfactants.

Electrophoretic mobilities (Fig. 5.2) are calculated using Eq. 5.1. Error bands represent one standard deviation from three independent experiments. For comparison, electrophoretic mobilities of proteins denatured with $SC_{12}S$ are included in the plots as the gray filled markers.

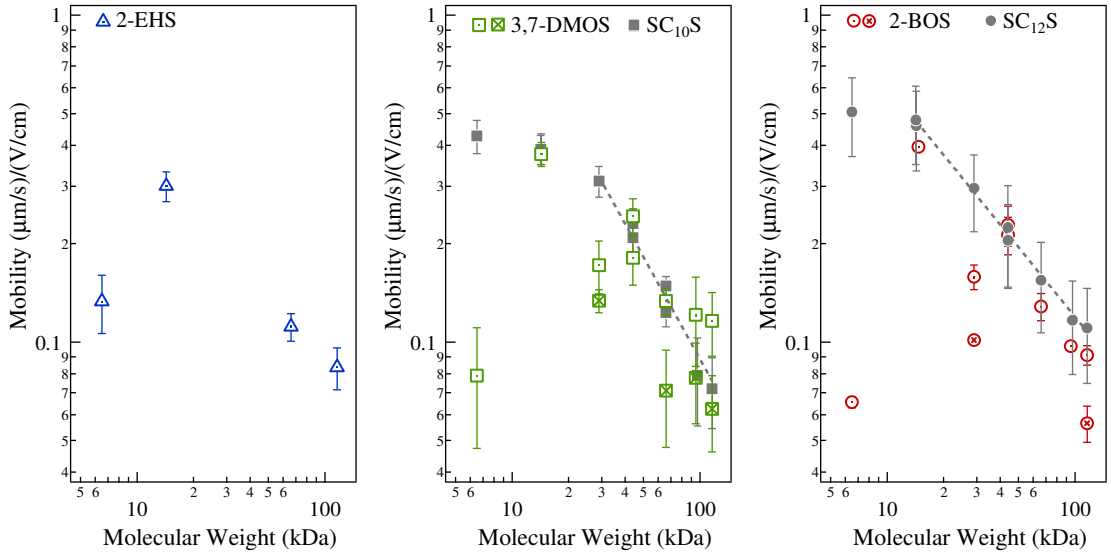

Figure 5. 2. Electrophoretic mobilities of proteins associated with branched surfactants. 2-EHS (left), 37-DMOS (center) and 2-BOS (right). Second bands in β-galactosidase, BSA and carbonic anhydrase are represented by the crossed markers (☒,⊗).

Small angle x-ray scattering (SAXS) is used to characterize the self-assembly of 2-EHS, 3,7-DMOS and 2-BOS and the changes in structural conformation of BSA and ovalbumin when associated with branched surfactants. The raw scattering data is converted into a real space analogue called the pair distance distribution function (PDDF) through an inverse Fourier transformation process with the GIFT code. Representative scattering curves for the micelles in solution formed by each branched surfactant and their respective PDDFs (inset plot) are shown in Fig. 5.3. Micelle diameters in solution (no protein) are determined to be 1.2 nm for 2-EHS, 3 nm for 3,7-DMOS and 3.4 nm for 2-BOS. The difference in the feature in the second upturn in the PDDF curves appears to indicate that 2-BOS micelles have different shape than 3,7-DMOS micelles. The difference in the shape of these micelles is expected given the variation of the type of branches attached to the eight-carbon long tail (n-butyl for 2-BOS and two methyl groups for 3,7-DMOS). From calculations of packing parameters (CPP) it is anticipated that the differences in the surfactant tail volume could generate different shapes of aggregates or micelles. All CPP calculations use the optimal head group area of 0.57 $nm^{2,}$ which is the experimental value given by Israelachvili for sulfate head groups[12]. The volume of the hydrophobic portion of the surfactant v (Eq. 5.6) and the effective length l of the hydrocarbon chain (Eq. 5.7) are functions of the total number of carbons n_T present in the molecule, the number of terminal methyl (CH_3) groups, n_m, and the total number of carbons along the longest segment, n_L. For linear surfactants, n_T is equal to n_L. Equations 5.6 and 5.7 give the packing property (v and l) values in nm^3 and nm respectively.

$$v \approx \left(27.4 n_m + 26.9 \cdot \left(n_T - n_m\right)\right) \times 10^{-3} \quad \textbf{(5. 6)}$$

$$l_c \approx \left(0.154 + 0.1265 \cdot (n_L - 1)\right) \quad \textbf{(5. 7)}$$

The calculated CPP for 2-EHS, 3,7-DMOS and 2-BOS are 0.482, 0.457 and 0.546 respectively. These dimensionless numbers suggest that the critical packing shapes for all three branched surfactants are truncated cones. Which are critical packing shapes that can self-assemble into nonspherical (ellipsoidal) micelles. However, note that the equations from which these values are calculated are not specifically developed for branched surfactants. Thus, it is expected that these values will be rough approximations. According to D.F. Evans (1994) molecules with CPP values that lie between 1/3 and 1/2 can self-assemble into several shapes.[26] It is the task of researchers to determine with additional techniques which shape is favored among the alternatives. The SAXS results from free-micelles in solution and protein-surfactant complexes confirm that branched surfactants form ellipsoidal-like micelles, Fig. 3. It is noteworthy that the PDDF of the 2-BOS, which has the largest CPP value, shows that micelles are substantially more elongated than the others.

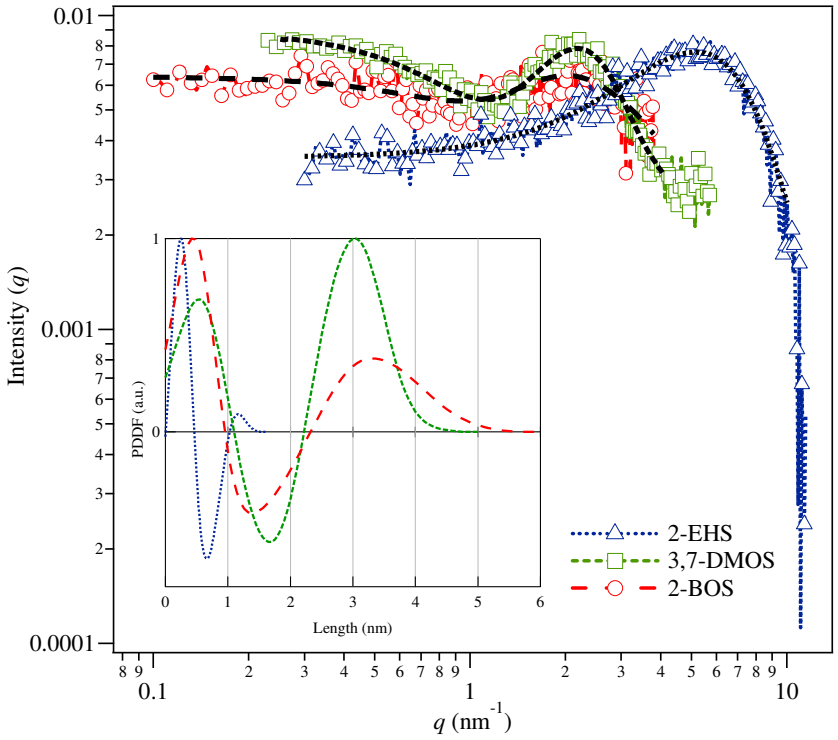

Figure 5. 3. Micelle scattering profiles (markers) and PDDFs (continuous lines) of 2-EHS, 3,7-DMOS and 2-BOS. Scattering fitting curves (black dotted lines). The PDDFs analysis is shown on the inset.

Fig. 5.4 and Fig. 5.5 contain representative scattering curves and the PDDF analyses for BSA and ovalbumin associated to branched surfactants. In Fig. 5.4 markers correspond to the experimental data and lines correspond to the best-fit curves. The resulting PDDF curves for BSA and ovalbumin complexes are shown in Fig. 5.5. For comparison purposes the PDDFs of BSA and ovalbumin denatured with linear $SC_{12}S$ are also included. The shape of the PDDF plots in Fig. 5.5 are typical of pearl-necklace structure (BSA with $SC_{12}S$, 3,7-DMOS and 2-BOS and ovalbumin with $SC_{12}S$) or of oblate globular structures (all proteins with 2-EHS and ovalbumin with 3,7-DMOS and 2-BOS) [18]. The elongation of the BSA complexes does not extend further than 24 nm, while

ovalbumin complexes reach a maximum dimension of 21 nm when associated with 2-EHS.

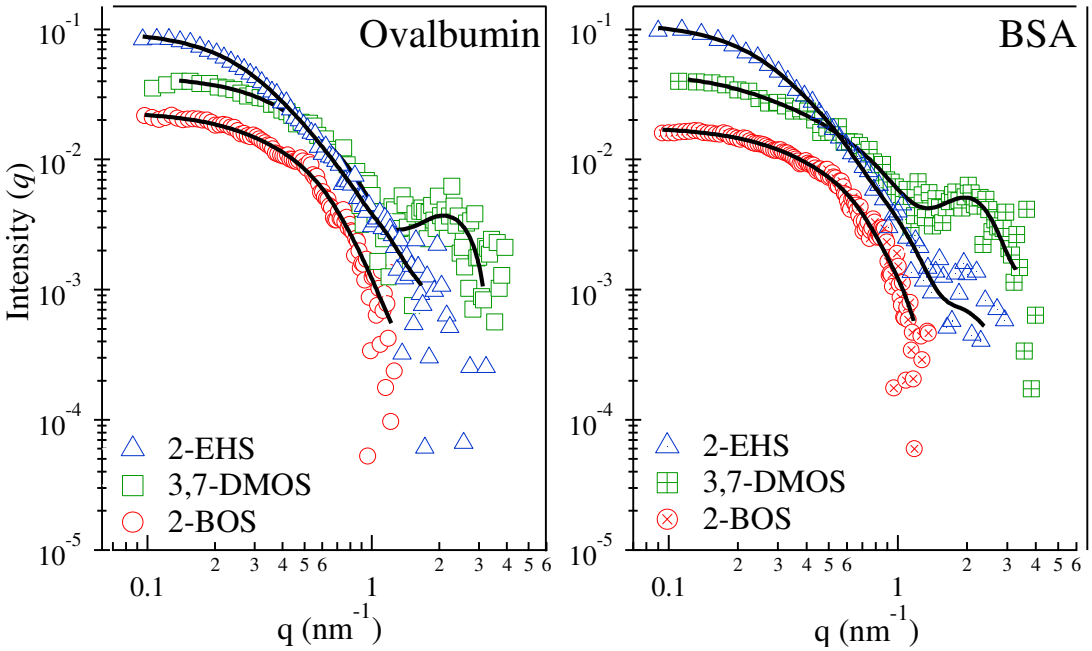

Figure 5. 4. Experimental SAXS data (markers) and approximation from GIFT fit (lines) for ovalbumin (left) and BSA (right) denatured with 2-EHS (△), 3,7-DMOS (□) and 2-BOS (○).

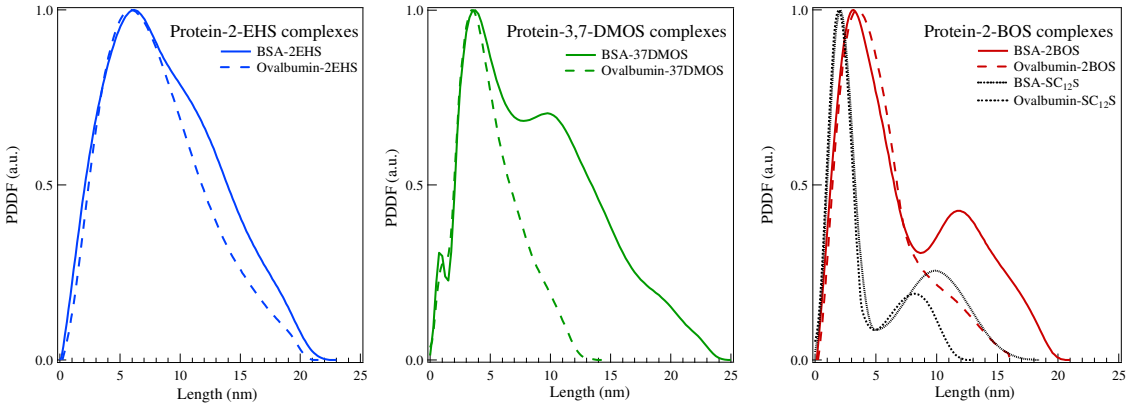

Figure 5. 5. Pair-distance distributions of BSA and ovalbumin-branched surfactant complexes. 2-EHS (left), 3,7-DMOS (center) and 2-BOS (right).

The shape of the PDDFs for ovalbumin associated with branched surfactants (Fig. 5.5) suggests the absence of neighbor micelles within the complex[17,18]. This conformation resembles a globular particle. This is a different result from our previous studies with linear alkyl sulfates where complexes of ovalbumin with SC_xS (*x,* correspond to the number of carbons in a surfactant tail) is always identified as a pear-necklace[11]. Thus, it is inferred that each of the branched surfactants, which have a maximum tail length of six and eight carbons, may have a different adsorption mechanisms and configuration from short-tailed linear surfactants (e.g. SC_8S, $SC_{10}S$).

When associated to 2-BOS (12 carbons, 8 carbon tail), BSA complexes have structures typical of a pearl-necklace shape. However, this changes to a more oblate ellipsoid-like structure when associated to 2-EHS (8 carbons, 6 carbon tail). This indicates that reducing the number of carbons or tail volume causes the formation of a more densely decorated and elongated protein-surfactant complex. The difference in the neighbor micelle distance (*S*), which is one of the structural parameters obtained through PDDF analysis and listed in Table 5.2, between 2-BOS and 3,7-DMOS complexes is 2.2 nm[11,19,20]. This shows that, for shorter tail lengths, the separation between the micelles in the protein-surfactant complex is also smaller. The condensed pearl-necklace conformation of BSA associated to 3,7-DMOS is an intermediate state between a peal-necklace and an oblate ellipsoid-like structure. This is a reflection of a higher density of micelles decorating the protein. Table 5.2 lists other structural parameters obtained from SAXS analysis including the micelle radius ($R_{micelle}$), and the complex lengths (*L*) [11,18–20]. The radii of gyration (R_g) for each protein-branched surfactant complex are also included

from calculations (Eq. 5.8) from the plateau region at the lowest q values corresponding to the Guinier regime.

$$\ln[I(q)] = \ln[a_o] - \frac{R_g^2}{3} q^2 \qquad \textbf{(5. 8)}$$

The diffusion coefficient (D_f) and hydrodynamic radius (R_H) are obtained through dynamic light scattering (DLS). Note that total lengths from SAXS and the hydrodynamic diameter do not need to match. There are several reasons for this but most importantly the hydrodynamic sizes are obtained from the Stokes-Einstein equation under the assumption of spherical shapes, which is clearly not an accurate representation of these structures[13]. In spite of this, DLS is used for quantitative comparisons of the trends in hydrodynamic size with those obtained from scattering results. In general, the D_f obtained for each set of BSA or ovalbumin associated with the branched surfactants indicates that BSA-complexes diffuse slower than ovalbumin complexes. This is expected given the differences in protein molecular weight (BSA: 66 kDa and ovalbumin: 44 kDa). Each set of protein-branched surfactant is analyzed in triplicate. Appendix B contains the corresponding correlation functions for each of the protein-surfactant complex. In contrast to most other samples, when BSA and ovalbumin are denatured by 2-EHS, not much difference is observed. These results suggest the formation of two similar structures despite differences in molecular weight. SAXS analyses of the 2-EHS complexes also show a weak dependence with protein size.

Table 5.2. Structural parameters of BSA and ovalbumin denatured by 2-EHS, 3,7-DMOS and 2-BOS.

Surfactant	Protein	r_m (nm)	L (nm)	S (nm)	R_g (nm)	D_f ($\mu m^2/s$)	R_H (nm)
2-EHS	BSA	6.2	22.0	---	6.1	17.5 ±0.6	14 ±0.4
	Ovalbumin	6.1	20.6	---	5.4	15.1 ± 0.7	15.3 ± 0.8
3,7-DMOS	BSA	3.8	24.5	9.6	4.3	33.2 ±4.7	7.5 ±1.1
	Ovalbumin	3.6	12.5	---	3.6	45.0 ±5.4	5.5 ±0.6
2-BOS	BSA	3.2	20.0	11.8	4.5	20.1 ±2.6	12.5 ±1.8
	Ovalbumin	3.5	16.2	---	3.7	44.4 ±2.7	5.6 ±0.3

r_m, micelle radius; L, protein-surfactant complex length; S, neighbor distance; R_g, radius of gyration; D_f, diffusion coefficient, R_H: hydrodynamic radius.

Circular dichroism (CD) is used to investigate the changes in the secondary structure of the proteins upon adsorption of branched surfactants. Figure 5.6 shows the respective spectra of β-galactosidase, phosphorylase b, BSA, ovalbumin, carbonic anhydrase, α-lactalbumin and aprotinin denatured with 2-EHS (blue triangles), 3,7-DMOS (green squares) and 2-BOS (red circles). Also, for comparison purposes, the CD spectra of the native proteins and the corresponding protein-$SC_{12}S$ complexes are also analyzed.

The results show that the set of studied proteins denatured by branched surfactants all retain some fractions of their intrinsic native structure (α-helical and β-sheets motifs). However, it is also found that 2-BOS disrupts to a much higher extent the secondary structure of β-galactosidase, BSA, ovalbumin, carbonic anhydrase and α-lactalbumin, turning these proteins into a coil-like or unfolded structure[23]. 2-BOS is able to disrupt proteins containing different percentages of α-helix, β-sheet, coil and unordered in the same manner. This indicates the non-preferential adsorption of the surfactant into a

protein of different amino acid composition. On the other hand, 2-EHS and 3,7-DMOS disrupts the secondary structure of the mentioned proteins to a lower extent. For comparison, the CD spectra of 2-EHS and 3,7-DMOS complexes are more similar to changes observed when the same proteins are denatured with the linear surfactant $SC_{12}S$.

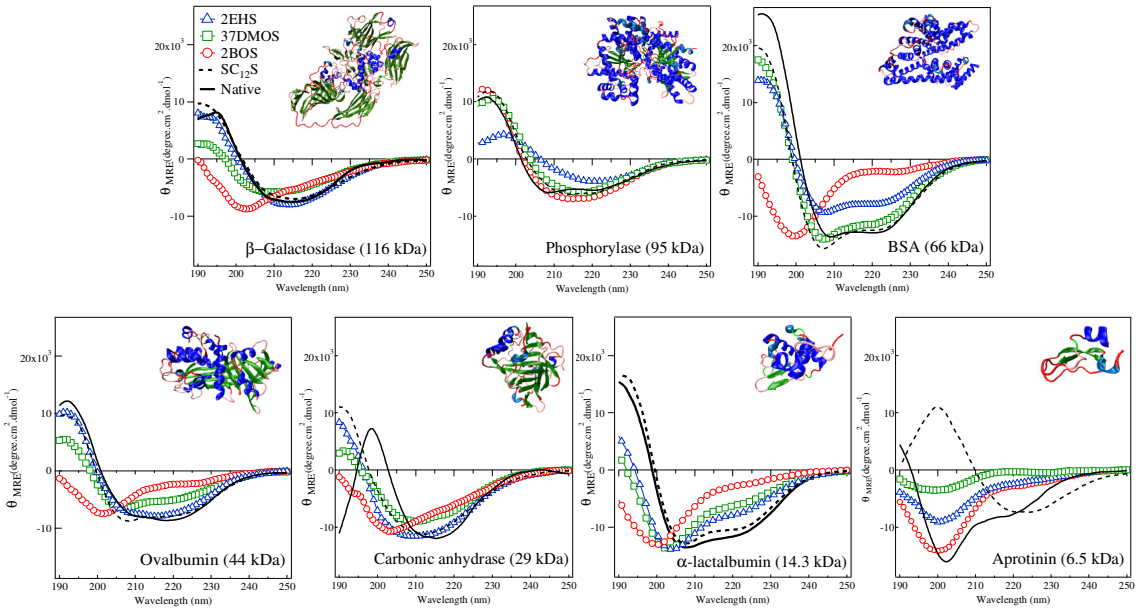

Figure 5. 6. Circular dichroism spectra of proteins denatured by branched surfactants (markers) and sodium dodecyl sulfate, $SC_{12}S$ (dashed lines). Continuous line corresponds to each native protein conformation.

When possible, Dichroweb is used to quantify the CD data in terms of the percentages of the secondary structures (α-helix, β-sheets and un-ordered motifs)[23]. The Dichroweb analysis for the native proteins and the 2-EHS and 3,7-DMOS complexes are shown in Table 5.3. Since this tool is only accurate for the evaluation of proteins with high α-helical and β-sheet conformation, all protein-2-BOS complexes are excluded and omitted in Table 5.3. Dichroweb lacks accuracy to evaluate disordered structures because of the low intensity of these conformations and the low abundance of structural data and

CD spectra for disordered proteins in the databases that Dichroweb uses for reference. Thus, secondary structure calculations of structures that deviate to a large extent from α-helical and β-sheet are challenging and quantification via Dichroweb is inaccurate[16]. Note that among all Dichroweb results shown in Table 5.3, the phosphorylase-3,7-DMOS complex and the native carbonic anhydrase do not meet the NMRSD criteria (values lower than 0.1) so those values are less accurate than the rest.

Table 5. 3. Secondary structure percentages of protein-branched surfactant complexes.

Protein acronym	Surfactant	α-helix (%)	β-sheet (%)	Turns (%)	Unordered (%)	NMRSD
G native	None	12.5	32.1	22.1	33.3	*0.038*
G	2-EHS	14.3	35.1	11.8	38.8	*0.070*
	3,7-DMOS	11.7	32.3	23.3	32.7	*0.055*
P native	None	17.5	32.0	12.5	37.9	*0.043*
P	2-EHS	10.2	38.0	12.5	39.4	*0.072*
	3,7-DMOS	15.1	34.6	20.6	29.6	*0.100*
B native	None	58.0	2.0	17.3	26.8	*0.018*
B	2-EHS	24.7	25.5	13.0	36.8	*0.029*
	3,7-DMOS	30.4	19.6	13.1	37.0	*0.048*
O native	None	21.7	27.0	20.6	30.7	*0.023*
O	2-EHS	18.9	28.5	21.5	31.1	*0.045*
	3,7-DMOS	16.9	30.2	22.5	30.5	*0.065*
C native	None	16.3	27.6	22.3	33.7	*0.169*
C	2-EHS	14.3	27.3	23.9	34.4	*0.079*
	3,7-DMOS	16.6	31.0	12.5	39.9	*0.078*
α native	None	31.4	18.8	20.3	29.5	*0.052*
α	2-EHS	22.2	20.3	24.4	33.2	*0.039*
	3,7-DMOS	19.1	22.1	25.0	33.7	*0.028*
A native	None	13.1	25.6	25.5	35.8	*0.066*
A	2-EHS	11.5	28.9	25.3	34.3	*0.084*
	3,7-DMOS	7.5	35.6	22.9	33.9	*0.307*

G = β-galactosidase, P = phosphorylase, B = bovine serum albumin, O = ovalbumin, C = carbonic anhydrase, α = α-lactabulmin, A = aprotinin. NMRSD: normalized root-mean-square deviation

Fluorescence spectroscopy is also used to evaluate the local polar or non-polar environment near the tryptophan (Trp) residues along the proteins before and after association with branched surfactants. Given the intrinsic chromophore and fluorophore characteristics of the Trp residue, the presence of the Trp residues can be used as reference amino acid to track local conformational changes and association with surfactants. The fluorescence of six proteins (β-galactosidase, phosphorylase b, BSA, ovalbumin, carbonic anhydrase and α-lactalbumin) in their native form and denatured by three branched surfactants (2-EHS, 3,7-DMOS and 2-BOS) and $SC_{12}S$ is evaluated and shown in Fig. 5.7. Aprotinin complexes are not analyzed because of the absence of Trp residues in the protein. Each plot in Fig. 5.7 contains three gray continuous lines in the x-axes at 340 nm, 345 nm and 350 nm to aid in visualizing changes in the fluorescence spectra.

Also, the spectra of each native protein are analyzed to compare changes in the micro-environment surrounding the Trp residues. It is found that complexes branched surfactants with proteins that contain a Trp/Mw ratio higher than 0.24 (Trp/Mw = number of Trp residues / protein molecular weight in kDa) show little variation in the spectrum. This suggests that the presence of multiple Trp residues in a protein causes averaging of many individual signals making it very difficult to analyze changes in local environments. When multiple Trp residues are present, changes in the conformation of the protein can indeed cause transitions in many Trp residues from nonpolar to polar environments and vice versa but all transitions average and reduce our ability to track individual changes in individual Trp residues. When only a few Trp residues are present,

the fluorescence signal has more significant changes because each Trp group contributes more to the total signal.

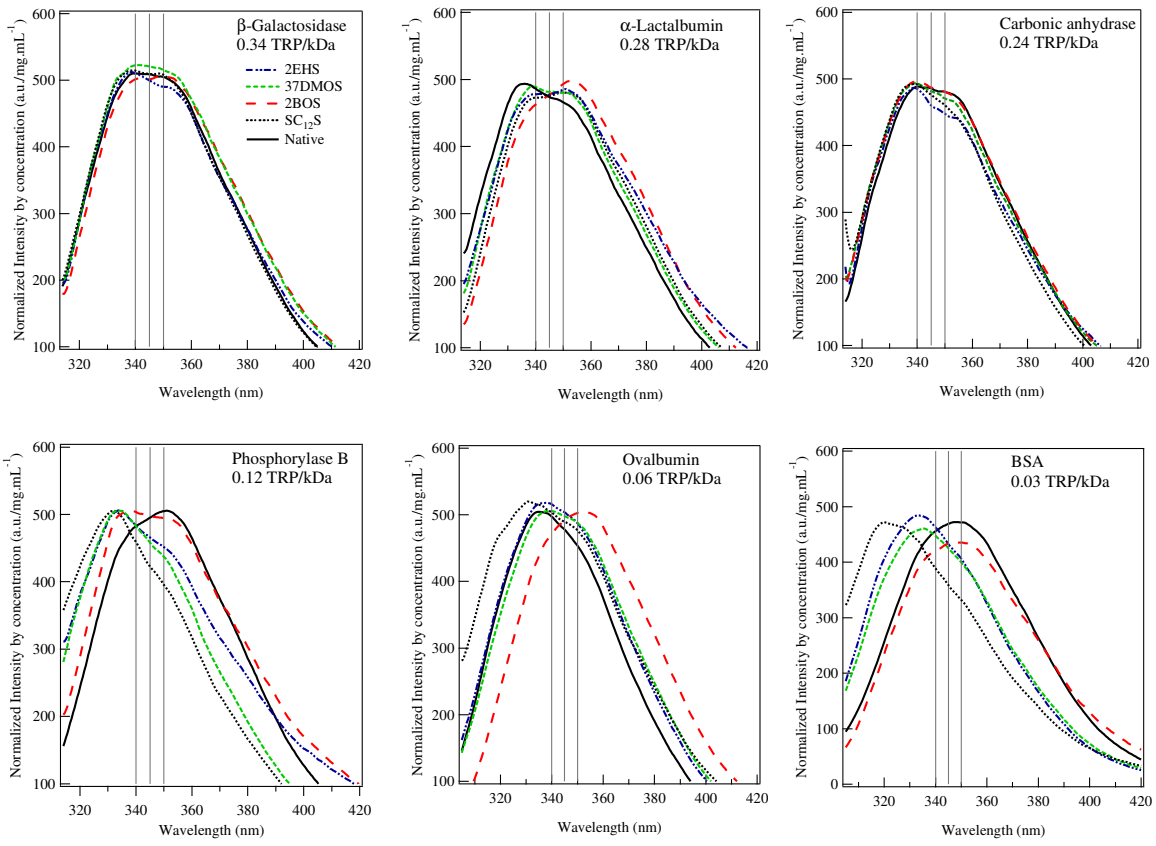

Figure 5. 7. Fluorescence spectra of β-galactosidase, α-lactalbumin, carbonic anhydrase, phosphorylase b, ovalbumin and BSA denatured by 2-EHS (dashed blue line), 3,7-DMOS (dashed green line), 2-BOS (dashed red line) and $SC_{12}S$ (dotted black line). Continuous lines correspond to the fluorescence spectra of each respective native protein.

On the other hand, protein complexes with branched surfactant with lower Trp/Mw ratios (<0.12) show significant variations in the fluorescence spectra upon binding. These results suggest that the limited Trp residues available within phosphorylase b, ovalbumin and BSA, (12, 3 and 2 respectively) contribute more to the changing signals and this allows us to probe the changing local environment of these

residues. In this study, we only attempt to explain conformational changes in BSA and ovalbumin, which are the proteins with the lowest Trp/Mw ratios (0.03 and 0.06 respectively). Although phosphorylase b has a low Trp/Mw ratio (0.12), it is not an easy task to explain average conformational changes in twelve Trp residues.

BSA is a mostly α-helical protein of a relative molecular mass of 66 kDa containing only two Trp residues. From crystallography, Trp-134 and Trp-213 have been located on the surface and inside a hydrophobic fold respectively[24,25]. Therefore, the fluorescence spectrum of BSA in its native state would correspond to the sum of the spectra of the "nonpolar" (Trp-213) and the "polar" (Trp-134) microenvironment surrounding each residue. From Fig. 5.7, the maximum emission wavelength of Trp residues in BSA shifts from 348 nm in its native state to; 348 nm, 336 nm, 334 nm and 324 nm when denatured by 2-BOS, 3,7-DMOS, 2-EHS and $SC_{12}S$ respectively. With the exception of 2-BOS, all surfactants promote blue shifting, which is indicative of a transition of Trp from a polar (e.g. water) to a less polar (e.g. interior of a micelle) environment[26].

The fact that the fluorescence spectrum of BSA-2-BOS complex is similar to the native BSA spectrum, suggest that Trp-213 has either been shielded from water by a 2-BOS micelle or that it is still in a nonpolar environment formed by surrounding hydrophobic residues. If this residue had not remained in a nonpolar microenvironment upon denaturing, Trp-213 would have been exposed to water molecules and the spectrum would have shifted towards the red. Thus, our results suggest that the Trp-213 it is still in a 'buried' state and that the environment around Trp-134 is likely unaltered. If Trp-134 had been affected by the surfactant adsorption the spectrum will have shifted to the left,

which is the fluorescence response of a Trp residue in presence of a nonpolar environment. For the other surfactants associated to BSA (2-EHS, 3,7-DMOS and $SC_{12}S$), the blue shifting suggest that Trp-134 is being covered by surfactants or it has been enclosed within the protein upon the changes in the protein conformation through the denaturing process.

Ovalbumin is a protein of molecular mass of 44 kDa that has an almost equal percentage of α-helix and β-sheet conformations[27]. Ovalbumin contains three buried Trp residues (Trp-150, Trp-184 and Trp-267), which was also confirmed by the maximum emission wavelength difference between ovalbumin and BSA in this study[28]. The difference of 10 nm towards the red in native ovalbumin indicates that more Trp residues are buried within ovalbumin than the Trp residues of native BSA. The maximum fluorescence emission wavelength for native ovalbumin shift from 338 nm to; 351 nm, 342 nm, 338 nm and 334 nm when denatured by 2-BOS, 3,7-DMOS, 2-EHS and $SC_{12}S$ respectively. These transitions suggest that 2-BOS causes the largest conformational change in ovalbumin, moving the Trp residues to more polar microenvironments. The same behavior but to a lower extent was also observed with 3,7-DMOS. On the other hand, when ovalbumin is denatured by 2-EHS, the maximum emission wavelength suggests either no changes in the Trp microenvironment or that 2-EHS is able to shield all three Trp residues. The emission of ovalbumin denatured by $SC_{12}S$ indicates that the adsorption of the surfactant turns one or all Trp residues to a less polar environment.

5.4 Discussion

Scattering, fluorescence spectroscopy and circular dichroism (CD) all suggest that the adsorption of branched surfactants upon protein denaturation is likely changing the conformation of the proteins. However, in most cases proteins are not fully unfolded by the branched surfactants and the presence of secondary structure in each of the protein-surfactant complexes is observed in the CD spectra. The results obtained for 2-EHS and 3,7-DMOS complexes agree with previous authors that have reported that proteins denatured by anionic surfactant do not change to a great degree their secondary structure. Instead, proteins form "looser" conformational states or molten globules that lack the tertiary structure[20,29–32]. On the other hand, it is observed that 2-BOS deviates significantly from this observation. We found that this surfactant can substantially disrupt most of the secondary structure of the studied proteins. This is an interesting result that could have implications and uses beyond protein electrophoresis.

Scattering analyses reveal that adding branches into the surfactant tails contributes to the formation of more ellipsoidal or globular particles, such as in the case of protein-2-EHS complexes. On the other hand, 3,7-DMOS and 2-BOS forms complexes with pearl-necklace shapes that are similar to those formed in linear surfactants[11,20]. However, these complexes are also more densely decorated by micelles than with $SC_{12}S$ and have micelle shapes that approximate globular or ellipsoidal.

Previously, our group has shown that the use of shorter tailed surfactants achieves not only better separations of proteins of low molecular weight but also causes them to form more elongated protein-surfactant complexes. Yet, we also find that separations with very short linear sodium octyl sulfate (SC_8S) are poor and inadequate even though it

also forms larger protein-surfactant complexes. We hypothesize that the loss of resolution for very short surfactants is a result of a decreased association force with the protein. As a result, we focused this work on surfactants with tail lengths shorter or equal to eight carbons aiming to form large protein-surfactant complexes but still maintaining the hydrophobic character by adding branches.

PAGE results with branched surfactants (Fig. 5.1) of 3,7-DMOS and 2-BOS suggest improved proteins separations when compared to SC_8S. This indicates that the branches attached to the eight-carbon long surfactant tails promote stronger binding interactions with the proteins. Nevertheless, our PAGE results are still not superior to protein separations obtained with other linear surfactants $SC_{12}S$ and $SC_{10}S$ of equal number of total carbons[11]. The appearance of anomalous bands in branched surfactants indicates erratic migration of some of the proteins when denatured by 3,7-DMOS and 2-BOS. We hypothesize that the branched architecture promotes different interactions with some of the proteins. This association may be sensitive to the composition of the protein or to the secondary structure. The identification of surfactant properties that could allow us to denature proteins in a different way to sodium dodecyl sulfate ($SC_{12}S$) could be quite powerful for the identification and separation of complex protein mixtures such as membrane proteins[9,21]. The importance of membrane proteins not only relies in the fact of their key role in all metabolic process but also because of the challenges to characterize them. The analysis of membrane proteins is usually done by 2D-PAGE[21]. However because of their low solubility in water, and in the related isoelectric focusing steps, its analysis is not an easy task. Several alternatives have been approached to improve membrane protein stability upon detergent adsorption. Yet, a standard procedure has not

yet been developed for membrane proteins. Among all considered options to target the problems of handling membrane proteins, the design of new surfactants that are able to keep membrane proteins soluble while still increasing the detection fidelity is of much interest[9,33]. To our understanding, the peculiar branching design of 3,7-DMOS and 2-BOS could have the potential of targeting different hydrophobic moieties than the linear surfactants bound to the same proteins. Surfactant-surfactant gel electrophoresis can be used for an optimal membrane protein solubilization. Is been shown that the resolution of 2D surfactant-surfactant gels is affected by the combination of surfactants. In fact, the use of SDS-SDS gel electrophoresis is found with the lowest spot spreading on the gels[34] . However, surfactant-surfactant gel electrophoresis could result in locating the protein spots in the off-diagonal with poor resolution (e.g. different proteins present within the same band). The erratic migrations and selectivity to disrupt in greater extent the secondary structure of 3,7-DMOS and 2-BOS are characteristics that potentially can be used to analyze membrane protein using surfactant-surfactant gel electrophoresis.

The PDDF analysis (Fig. 5.5) also reveals larger protein-surfactant complexes than $SC_{12}S$ for all three branched surfactants. Interestingly, we found a tendency to form more densely packed pearl-necklace structures and some globular complexes. Studies dealing with the migration mechanism of charged polypeptides through random networks indicate that the shape of the particle modifies the motion and friction experienced by the particles migrating through the network[35]. Thus, we hypothesize that different shapes acquired by different protein-surfactant complexes will cause different migration mechanisms through the pores of the gel. Structural differences could cause variations in the electrophoretic mobility such as the ones observed by carbonic anhydrase, which

migrates at a different molecular weight position that it is expected. The fundamental understanding of the specific binding mechanism for branched surfactants with proteins is still a topic of much interest.

The difference in size for complexes of proteins with branched surfactants is also confirmed by diffusion coefficients (Table 5.2). Similarly, the R_g values suggest that BSA complexes are consistently larger than ovalbumin complexes. The use of multiple characterization techniques gives us high confidence in the structures that are probed and the conclusions that are made. SAXS results provide the highest level of detail possible for these structures but the results are also confirmed with independent DLS characterizations[11,19,20,36,37].

The differences between the size and the shape of the micelles in solution (inset Fig. 5.3) and the micelles within the protein-surfactant complex (Fig. 5.3 or Table 5.2) also indicate that each of the branched surfactants interacts in a slightly different way with BSA and ovalbumin. The larger variation is found for 2-EHS aggregates. Here, the radius of 2-EHS micelles in solution is only 1.2 nm while the radii of the globular structures formed with 2-EHS associated to BSA and ovalbumin are 6.2 and 6.1 nm respectively. The radius of the micelles of 3,7-DMOS is also found to be larger in the protein-surfactant complex by 0.7 ± 0.1 nm than in 'free' solution. For 2-BOS micelles, both aggregates in solution and in the protein-surfactant complex appear to be in the same range size (radii around 3.7 nm ± 0.1). Thus, our results suggest that as the surfactant tail volume decreases, the cross-sectional size of the structures formed during protein denaturation increases. Short tail surfactants could bind more dynamically with the protein forming globular aggregates that are larger and do not contain well-defined

micellar structures. In contrast, the association of surfactants with longer tails could be restricted to a similar size compared to the free micelle even when interacting with the protein.

Circular dichroism and fluorescence spectroscopy allow us to track changes in the secondary structure of the proteins upon adsorption of 2-EHS, 3,7-DMOS and 2-BOS. Spectroscopic data for some of the selected proteins seem to only result in small changes when denatured by the three branched surfactants and $SC_{12}S$ (Fig. 5.6 and 5.7). However, these variations are significant in terms of local chromophoric perturbations and conformational changes. CD results suggest that 2-BOS turns almost all proteins into coil-like denatured structures with the exception of phosphorylase b complexes (Fig. 5.6). We hypothesize that the intrinsic characteristics of phosphorylase b is the key to further understand the stronger preservation of secondary structure. Yet, results also show that all branched surfactants tend to disrupt the α-helical motifs of phosphorylase b turning the protein into a more β-sheet structure. This is observed by the absence of the peaks at ~210 nm and ~220 nm in the CD spectra of phosphorylase b-surfactant complexes, which is the emblematic features of α-helical structures[23,38].

On the other hand, the CD spectrum of aprotinin, the smallest protein in the study, indicates minimal changes upon branched surfactant adsorption. The slight blue shifting of the native peak at 203 nm and the reduction in intensity in the wavelengths above 215 nm correspond to a small disruption of the limited α-helix and β-sheets motifs. However, when $SC_{12}S$ is used, the secondary structure turns towards a β-sheet structure. We speculate that $SC_{12}S$ surfactants preferentially adsorb into the limited native α-helical portions of the small protein, turning aprotinin into a β-sheet structure. Preferential

adsorption in α-helical domains and shifting to β-sheet conformations have been also observed when $SC_{12}S$ denatured larger proteins[20]. Dicroweb results (Table 5.3) confirm the secondary structure changes when 2-EHS, 3,7-DMOS and $SC_{12}S$ denatured aprotinin.

The fluorescence study of the local Trp environment shows significant promise as a mechanism to interrogate surfactant association in specific locations along the protein backbone. However, this approach is difficult when multiple Trp residues are part of a protein because individual contributions are averaged. In proteins where Trp residues are not many, it is possible to correlate optical shifts with protein conformational changes in specific locations. Mutations of natural proteins (inclusion of Trp in specific locations) or the use of artificial proteins or peptides could be used to decipher the influence of local amino acid charge hydrophobicity or secondary structure to surfactant binding. Yet, for proteins with high numbers of Trp residues not much can be said from this approach other than conformational changes in proteins are confirmed by fluorescence experiments (Fig. 5.7). These results are also confirmed by the CD spectra, which indicate significant secondary structure modifications but not a complete destruction. Among the six proteins tested with fluorescence spectroscopy, ovalbumin and BSA have the smallest number of Trp residues. The fluorescence spectra of BSA and ovalbumin, proteins with two and three Trp residues respectively, show different protein modifications upon the adsorption of 2-EHS, 3,7-DMOS and 2-BOS. The CD (Fig. 5.6) and fluorescence (Fig. 5.7) spectra of BSA-2-BOS complex indicate the disruption of the α-helical motifs and the adjustment of the environment of Trp-213 by either 2-BOS aggregates or a rearrangement within the protein core. Meanwhile, the blue shift in the association of 2-EHS and 3,7-DMOS to BSA suggests that the microenvironment of the Trp-134 is less polar than in its

original native state. In the fluorescence analysis, blue shifts suggest either folding transitions or less polar microenvironments. This means that Trp residues are embedded in hydrophobic regions that can be hidden within the protein itself or covered by the hydrophobic chains of the surfactant. Additionally, the BSA-$SC_{12}S$ complex, which shifted from 350 nm to 320 nm, indicates a transition to a less polar state.

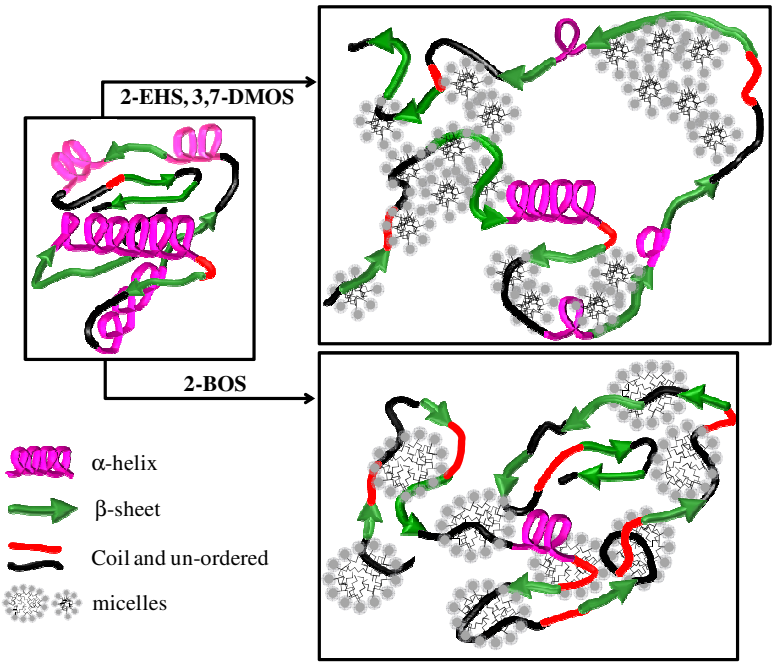

Figure 5. 8. Schematic of protein-branched surfactant complexes

Figure 5.8 shows a representation of the hypothesized interaction of surfactants of different tail structure with the same native protein. This diagram represents the experimental observations that arise from our results from SAXS (Fig. 5.5) and circular dichroism (Fig. 5.6). It shows that the surfactant with the larger tail volume disrupts to a larger extent the secondary structure of the protein but does not result in the largest protein-surfactant complex. The adsorption of the branched surfactant with larger tail volumes (2-BOS) to the proteins turns the α-helical and β-sheet motifs mainly into coils

and disordered structures. In contrast, the surfactant of smaller tail volume (2-EHS) transforms to some extent the α-helical motifs into β-sheet and coil structures but forms a protein complex that maintains a significant amount of secondary structure but is also more elongated. Thus, protein conformations can have differences in size and secondary structure based on the surfactant that is used to denature them. This observation suggests an interesting use of branched surfactants for protein separation with 2D surfactant-surfactant gel electrophoresis[7,9,21,22]. These techniques are especially useful for proteomic analyses involving membrane proteins that are insoluble in buffers used for isoelectric focusing[9,10]. In surfactant-surfactant 2D gel electrophoresis, one dimension of gel electrophoresis could separate proteins by their molecular weight (e.g. $SC_{12}S$), while the second gel electrophoresis dimension could disperse proteins by differences in secondary structure content (e.g. 2-BOS). This is an area that will be researched in the future.

Branched surfactants have substantial potential to be used in new protein electrophoresis separations but their uses would likely be different than simple molecular weight determination. In particular, 2-BOS is the most interesting branched surfactant found in this study because of its ability to modify to a large extent the secondary structure of most proteins and because it leads to narrow bands in gel electrophoresis. The denaturing capacity of this surfactant, beyond electrophoretic uses, should be explored further. Nevertheless, at the moment, the use of any of these surfactants in traditional polyacrylamide gel electrophoresis is not justified and would require further optimization to obtain separations that are competitive with $SC_{12}S$. Future characterization studies with 2-BOS could further clarify its binding mechanisms and its potential as a more effective denaturant. Also, 2D surfactant-surfactant gel

electrophoresis studies of membrane proteins using 2-BOS as one of the surfactants merit further attention.

5.5 Conclusions and outlook

In this work, the interaction of three branched surfactants (2-EHS, 3,7-DMOS and 2-BOS) with a series of proteins of different size and composition are studied and discussed. It is found that the addition of alkyl branches to anionic surfactants drastically affects their performance in proteomic separations. However, PAGE results indicate the need of further optimizations before adopting branched surfactants for this use. In particular, PAGE suggests that 3,7-DMOS and 2-BOS are the more promising alternatives to conduct future proteomic separations while 2-EHS is found to be inadequate. Through CD and fluorescence spectroscopy, we characterize conformational changes in the secondary structure of the proteins and changes to the polar or non-polar microenvironment near the Trp residues. Both techniques indicate a stronger modification of the protein when 2-BOS is used as a denaturing agent. SAXS analysis is used to investigate the size and shape of BSA and ovalbumin when denatured by all branched surfactants. It is found that most surfactants form pearl-necklace or ellipsoidal shapes. The comparison of SAXS results with those of $SC_{12}S$ complexes indicates that branched short-tailed surfactants form larger structures. The findings in this work are valuable for the development of novel surfactant that can tackle diverse characteristics of protein separations and is also valuable for the understanding of the fundamental interactions of branched surfactants with proteins.

5.6 References

(1) Ananthapadmanabhan, K. P.; Dickinson, E.; Goddard, E. D.; Lindman, B.; Strauss, U. P.; Thalberg, K.; Tirrel, M.; Winnik, F. M. *Interactions of Surfactants with Polymers and Proteins*; CRC Press, Inc.: Florida, USA, 1993.

(2) *Protein-Based surfactants*; Nnana, I.; Xia, J., Eds.; Marcel Dekker, Inc.: New York, 2001; p. 290.

(3) Tanford *The hydrophobic effect: formation of micelles and biological membranes*; John Wiley & Sons: New york, USA, 1973.

(4) Lundhal, P.; Greijer, E.; Sandberg, M.; Cardell, S.; Eriksson, K.-O. *Biochimica et Biophysica Acta (BBA)* **1986**, *873*, 20–26.

(5) Reynolds, J. A.; Tanford, C. *The Journal of Biological Chemistry* **1970**, *245*, 5161–5165.

(6) Brown, E. G. *Analytical biochemistry* **1988**, *174*, 337–348.

(7) Hamdan, M.; Righetti, P. G. *Proteomics today. Protein assessment and biomarkers using spectrometry 2D electrophoresis and microarray technology*; John Wiley & Sons: Hoboken, NJ, 2005; p. 426.

(8) Shapiro, A. L.; Viñuela, E.; Maizel, J. V. *Biochemical and Biophysical Research Communications* **1967**, *28*, 815–820.

(9) Rabilloud, T.; Chevallet, M.; Luche, S.; Lelong, C. *Proteomics* **2008**, *8*, 3965–3973.

(10) Rabilloud, T.; Chevallet, M.; Luche, S.; Lelong, C. *Journal of proteomics* **2010**, *73*, 2064–77.

(11) Ospinal-Jimenez, M.; Pozzo, D. C. *Langmuir* **2011**, *27*, 928–935.

(12) Israelachvili, J. *Intermolecular and Surface Forces with application to colloidal and biological systems*; Second.; Academic Press: London, 1985.

(13) Berg, J. *An Introduction to Interfaces & Colloids. The Bridge to Nanoscience*; World Scientific Publishing Co. Pte. Ltd.: Singapore, 2010; p. 785.

(14) Reynolds, J. A.; Tanford, C. *Proceedings of the National Academy of Sciences of the United States of America* **1970**, *66*, 1002–1007.

(15) Whitmore, L.; Wallace, B. A. *Biopolymers* **2008**, *89*, 392–400.

(16) Whitmore, L.; Wallace, B. A. *Nucleic Acid Research* **2004**, *32*, W668–W673.

(17) O.Glatter, O. K. *Academic press* **1982**.

(18) Lindner, P.; Zemb, T. *Elsevier Science B.V.* **2002**.

(19) Franklin, M. J.; Surampudi, L. N.; Ashbaugh, H. S.; Pozzo, D. C. *Langmuir* **2012**, *28*, 12593–12600.

(20) Ospinal-Jiménez, M.; Pozzo, D. C. *Langmuir* **2012**, *28*, 17749–17760.

(21) Bergh, G. Van Den; Arckens, L. *Expert Review Proteomics* **2005**, *2*, 1–10.

(22) Rabilloud, T. *Journal of proteomics* **2010**, *73*, 1562–72.

(23) Ann, W. B.; Janes, R. W. *Modern techniques for circular dichroism and synchrotron radiation circular dichroism spectroscopy.*; IOS Press: The Netherlands, 2009; Vol. 1.

(24) Peterman, B. F.; Laidler, K. J. *Archives of Biochemestry and Biophysics* **1980**, *199*, 158–164.

(25) Viallet, P. M.; Vo-Dinh, T.; Ribou, a C.; Vigo, J.; Salmon, J. M. *Journal of protein chemistry* **2000**, *19*, 431–9.

(26) Moriyama, Y.; Ohta, D.; Hachiya, K.; Mitsui, Y.; Takeda, K. *Journal of Protein Chemistry* **1996**, *15*, 265–272.
(27) Masayuki, Y.; Takahashi, N.; Hirose, M. *The Journal of Biological Chemistry* **2003**, *278*, 35524.
(28) Zemser, M.; Friedman, M.; Katzhendler, J.; Greene, L. L.; Misky, A.; Gorinstein, S. *Journal of protein chemistry* **1994**, *13*, 261–274.
(29) Donnet, C.; Arystarkhova, E.; Sweadner, K. J. *The Journal of biological chemistry* **2001**, *276*, 7357–65.
(30) Krishnamurthy, V. M.; Kaufman, G. K.; Urbach, A. R.; Gitlin, I.; Gudiksen, K. L.; Weibel, D. B.; Whitesides, G. M. *Chemical reviews* **2008**, *108*, 946–1051.
(31) Sabato, A.; Di Cesare, N.; Gryczynski, I.; Rossi, M.; Lakowicz, J. R. *J. Biochem.* **2001**, *130*, 13–18.
(32) Muga, A.; Arrondo, J. L.; Bellon, T.; Sancho, J.; Bernabeu, C. *Archives of Biochemestry and Biophysics* **1993**, *300*, 451–457.
(33) Breyton, C.; Pucci, B.; Popot, J. In *Heterologous Expression of Membrane Proteins, Methods in Molecular Biology*; Mus-Veteau, I., Ed.; Humana Press: Totowa, NJ, 2010; Vol. 601.
(34) Rabilloud, T. *Electrophoresis* **2009**, *30*, S174–80.
(35) Viovy, J.-L. *Reviews of Modern Physics* **2000**, *72*, 813–872.
(36) Hassan, N.; Barbosa, L. R. S.; Itri, R.; Ruso, J. M. *Journal of Colloid and Interface Science* **2011**, *362*, 118.
(37) Pozzo, D. C. *Langmuir* **2009**, *25*, 1558–1565.
(38) Greenfield, N.; Fasman, G. D. *Biochemistry* **1969**, *8*, 4108–16.

CHAPTER VI

STRUCTURAL ANALYSIS OF PROTEIN DENATURATION WITH ALKYL PERFLUORINATED SULFONATES

A final study using short-tailed surfactants with stronger hydrophobic character as denaturing agents is addressed to investigate their interactions with proteins of diverse size and composition. In this case, short-tailed surfactants are fully fluorinated and it is expected that the exchange of hydrogen by fluorine atoms improves the macroscopic separations. In this chapter, scattering and circular dichroism are used to decipher the nano-structural conformation of protein-fluorinated surfactant complexes.

6.1 Background

Polyacrylamide gel electrophoresis (PAGE) is one of the most widely used analytical techniques for proteomic separations and sodium dodecyl sulfate ($SC_{12}S$ or SDS) is the most commonly used denaturing surfactant in this application. However, although this is a well-studied technique it still lacks in resolution and this can frequently result in the misidentification of proteins[1–3]. Importantly, a detailed and accurate proteomic separation can be key to identifying markers for diseases[4,5].

Aspects of this chapter reproduced with permission from Ospinal-Jimenez, M., Pozzo D.C., Langmuir, 28 (51), pp 17749-17760. Copyright 2012. American Chemical Society.

The separation of proteins with gel electrophoresis involving $SC_{12}S$ has been widely studied and the interactions between this surfactant and numerous proteins have been well-documented[1–10]. Unfortunately, the association of alternative surfactants with proteins is still not well developed even though it could allow for gaining a fundamental understanding of these important interactions. Surfactant alternatives to $SC_{12}S$ could also result in improvements in separation efficiency, in additional selectivity for post-translational modifications (e.g. glycosylation) or in the enhancement of complex or difficult separations such as those involving membrane bound proteins[10–12]. Thus, obtaining a better understanding of the principal mechanisms that control and affect the adsorption of surfactants and micelles to denatured proteins is valuable to the general biological field and fundamental studies in this area could promote the intelligent design of novel surfactant chemistries.

In the last decades, several new approaches have been investigated to improve proteomic separations involving gel electrophoresis. New insights related to the interactions that occur between proteins and a variety of surfactants have been found to be of great importance[1,3,13,14]. However, studies of alternative surfactants combining macroscopic and microscopic characterizations are still scarce. In prior work, we found the performance of sodium alkyl sulfates (SC_xS, *x* corresponds to the number of carbons in the surfactant tail) in PAGE to be directly correlated to the size of the surfactant tail [7]. Proteins associated with smaller hydrogenated micelles generally resulted in separations of higher resolution. In Chapter IV, the use of linear hydrogenated surfactants shows that the separation resolution, defined by the sharpness of the protein bands, followed this trend: $SC_{10}S > SC_{12}S > SC_{14}S > SC_{16}S$. However, very small surfactants with tail lengths

shorter than eight carbons (< SC_8S) did not result in good separations. We hypothesized that this is due to a weaker binding force between the surfactant tails and the proteins (i.e. lower hydrophobic interactions). Thus, we also hypothesized that perfluorinated surfactants (PFC_xS) with tail lengths of eight carbons or smaller could be good alternatives to increase the strength of hydrophobic interactions in a protein-surfactant complex while still forming small micelle structures and causing significant unfolding of the proteins.

Fluorinated surfactants are selected based on their high surface activity and strong tendency to self-aggregate into stable assemblies when used in coatings, antifogging agents, and water repellents among other applications[15]. Nevertheless, their use in the biological field is still quite recent[16–19]. The stability of the C-F bond, the most stable bond in organic chemistry, makes fluorocarbons much more thermally and chemically stable than hydrogenated counterparts[16,20]. Many fluorinated molecules also are biologically inert and could make good alternatives for use in biological separations[20].

Previous proteomic and biological studies have also used perfluoroalkylated amphiphiles in a variety of applications including drug delivery, protein extraction, 2D crystallization and separation techniques[16]. Recently, Li et. al, studied the interactions of PFC_8S, PFC_4S and sodium octane-sulfonate with native human serum albumin in solution[21]. From their adsorption and particle size analyses, they concluded that fluorinated surfactants have stronger interactions than sodium octane-sulfonate a hydrogenated surfactant. Despite these important works, the interactions that emerge between fluorinated surfactants and proteins are much less understood that with the hydrogenated counterparts.

It has also been previously shown that the architecture of a polyelectrolyte, in our case a protein-surfactant complex, plays a key role in their electrophoretic migration inside gel matrices[22]. Based on the previous results shown in Ch. IV and V, we also hypothesize that proteins that are more densely decorated with micelles will be stiffer and more extended. According to basic theories of electrophoretic transport, these structures should also show a stronger dependence between mobility and molecular weight[22]. Furthermore, the associated micelles can frequently dominate the hydrodynamic interaction with the hydrogel matrix because they are often larger than the protein backbone. Thus, the structure and transport of a protein-surfactant complex in a gel will depend strongly on the chemical structure of the surfactant that is used and on its binding mechanism to proteins.

The chemical characteristics of a fully denatured protein also depend on the specific amino acid composition and sequence. Since each protein contains a distinctive residue sequence, all protein-surfactant interactions are somewhat unique for each protein and also for different regions of the same protein. Unfortunately, very little is currently known about the influence of the local amino-acid sequence on the association of surfactants to denatured proteins. Fig. 6.1, shows a schematic representation of a very simple protein-surfactant complex forming a pearl-necklace structure. Here, the protein is represented by a random sequence of amino acids that have different characteristics.

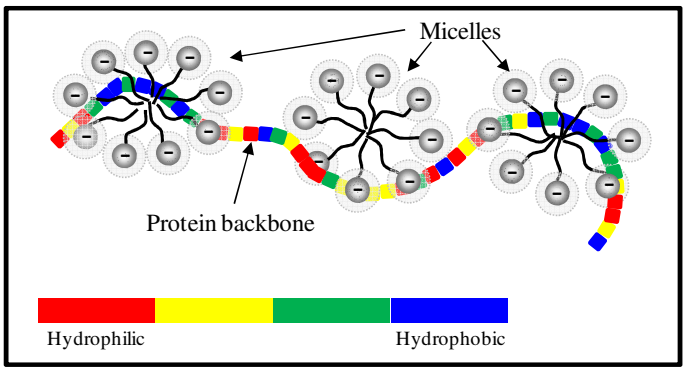

Figure 6. 1. Schematic of a protein-surfactant complex. Three micelles are associated with a protein that contains four types of amino acids of different hydrophobicity and charge. Micelles could show different adsorption mechanisms depending on the local amino acid sequence.

In Fig. 6.1, red blocks represent highly hydrophilic amino acids while blue corresponds to hydrophobic amino acids. If it is assume that surfactant binding is dominated by hydrophobic interactions, the micelles would be expected to associate in local regions of higher hydrophobicity. On the other hand, if electrostatic interactions dominate, micelles are expected to associate head-on to regions in the unfolded protein that contain a net charge that is opposite that of the surfactant, like the middle micelle in Fig. 6.1. Still, it is obvious that this model is highly oversimplified and surfactant association could also depend on the specific secondary structure motifs that are present in the denatured protein. These motifs could also be very different from those found in the native folded state. Furthermore, the local charge of the residues in any region of the protein will also be affected by solution conditions and would likely impact the electrostatic association of the surfactant. Due to the heterogeneity of the protein chain, the binding of surfactants can be affected by hydrogen bonding, Van der Waals interactions, hydrophobic interactions and electrostatic forces[23]. Moreover, some of these

interactions could further be affected by the electric fields that are applied during electrophoresis. Therefore, surfactant association to denatured proteins is a very complex process and systematic characterization is necessary to fully understand this important system.

This study is focused in investigate alkyl fluorinated (PFC_xS) surfactants with eight, six and four carbons in the tail region. Model proteins of different molecular weights are used to analyze the structural changes upon fluorinated surfactants denaturation. Table 3.2 (Ch. III) contains relevant information on the set of model proteins that have been selected for this study[24–36]**.** It is expected to observe differences in surfactant aggregation with molecules of different tail length. Scattering studies have shown that surfactant architecture largely dictates the aggregate shape[37,38]. Oblate and spherical micelles, among other shapes, can form depending on the type of surfactant that binds to the protein[38]. In this case, it is projected that short tail fluorinated surfactants will either form smaller spherical micelles or, due to the larger stiffness of the fluorinated chains, may also aggregate as oblate or ellipsoidal micelles[20,39,40].

Small angle x-ray scattering (SAXS), dynamic light scattering (DLS), gel electrophoresis (PAGE) and circular dichroism (CD) are used as characterization techniques to provide information on protein separation, the conformation of protein-surfactant complexes and to quantify changes in secondary structure. Small angle x-ray scattering is one of the most useful techniques to characterize the structural parameters and shapes of protein-surfactant complexes. Furthermore, scattering techniques have been used in the past to characterize native proteins and complexes of proteins associated with a diverse range of hydrogenated surfactants[7,8,10,41–43]. However, small angle

scattering studies of proteins with fluorinated surfactants are still rather limited. New insights in protein-fluorinated surfactant complexes could contribute to developing novel surfactants for electrophoretic separations using a rational molecular design.

6.2 Materials and methods

Eight proteins and five surfactants; β-galactosidase, phosphorylase-B, bovine serum albumin (BSA), ovalbumin, carbonic anhydrase, lysozyme, α-lactabulmin, aprotinin, sodium dodecyl ($SC_{12}S$), decyl ($SC_{10}S$) and octyl (SC_8S) sulfate, potassium tridecafluoro-1-hexanesulfonate (PFC_6S), potassium nonafluoro-1-butanesulfonate (PFC_4S) are purchased and used as supplied from Sigma Aldrich (St. Louis, MO). Potassium perfluoro-octanesulfonate (PFC_8S) was acquired from TCI America (Portland, OR). Table 3.2 (Ch. III) shows the list of all the studied proteins.

All buffers are prepared in DI water. Buffers A and B contain glycine and trizma-base, purchased from Sigma Aldrich (St. Louis, MO), at concentrations of (0.192 M) and (0.025 M) respectively and a final pH of ~8.5+/-0.2. Buffer B is identical to buffer A, but also contains 0.5 times the critical micelle concentration of each surfactant in order to follow the typical procedures used for SDS-PAGE. Buffer C contains anhydrous glycerol (3.6 M) purchased from JT Baker (Phillipsburg, NJ), trizma hydrochloride (62.5 mM) purchased from Sigma Aldrich (St. Louis, MO) and bromophenol blue as indicator from Bio-Rad (Hercules, CA) and has a final pH of ~8.5 +/- 0.2. Buffer D is also identical to buffer A but contains a low concentration of the corresponding surfactant (25 mM for PFC_4S, 8 mM for PFC_6S and 1 mM for PFC_8S) in order to use it for sample dilutions.

Surfactant is added to buffer D to minimize the potential for "stripping" bound surfactant from the saturated proteins but low levels are used to minimize potential scattering contributions from free micelles. To verify this, the scattering profiles of all buffers were compared with that of the bare buffer (i.e. no added surfactant).

6.2.1 Sample preparation

All samples are initially prepared at a ratio of 3 mg of surfactant / 1 mg of protein. Dithiothreitol (DTT) purchased from Fisher Scientific (Fair Lawn, NJ), is used as the reducing agent. DTT is added in a stoichiometric excess of 5 times the total number of disulfide bonds for each protein sample prepared for SAXS, DLS and CD experiments and at a constant concentration of 200 mM for PAGE samples. All protein samples are then thermally denatured by heating for 4 minutes at 95°C in the presence of surfactant. Final β-galactosidase, bovine serum albumin, ovalbumin and lysozyme concentrations are determined with an Evolution 300 UV-Visible spectrophotometer from Thermo Scientific (Waltham, MA) at 280 nm using the molar extinction coefficients of 20.9, 6.67, 7.25 and 26.4 $mLg^{-1}cm^{-1}$, respectively. The purity of the proteins in solution is also checked with SDS-PAGE. All SAXS, DLS and CD samples are filtered with a 0.45μm Millipore filter before analysis.

6.2.2 Gel electrophoresis

A mini-PROTEAN Tetra cell from Bio-Rad (Hercules, CA) is used to perform all PAGE experiments. Commercial slab gels of 12% polyacrylamide, which do not contain $SC_{12}S$ in the preparation, are purchased from Bio-Rad. The absence of $SC_{12}S$ in the gels is necessary to ensure that the results depend only on the interaction between the proteins and the surfactants of interest. Coomassie brilliant blue and a standard protein ladder are also purchased from Bio-Rad. All protein samples are prepared in buffer C. Gels are run in buffer A (anode) and buffer B (cathode). After each run, gels are fixed in a solution of methanol (Fisher Scientific), acetic acid (J.T. Baker - Center Valley, PA) and DI water at a volume ratio of 40%, 10% and 50% respectively. Each gel is immersed first in fixer solution (2 hours) and then in coomassie brilliant blue (overnight). Gels are then washed with the fixer solution to remove excess coomassie brilliant blue. All gels are scanned and analyzed using the software ImageJ to calculate the electrophoretic mobility using Eq. (6.1). Electrophoretic mobility (μ_E) is given in units of (μm/s)/(V/cm), where ($v_{complex}$) corresponds to the protein-surfactant complex velocity and (E) represents the electric field E across the gel. The applied electrical potential is kept constant at 150 V for all runs and a gel dimension of 6 cm is used to estimate the electric field. Running times are tracked and a protein ladder of 10 purified proteins is used in all gels as a molecular weight reference. All PAGE samples are prepared as is indicated in sample preparation at a concentration of 3.5 mg of protein/mL of solution.

$$\mu_e \approx \frac{v_{complex}}{E} \qquad \textbf{(6. 1)}$$

6.2.3 Small Angle x-ray Scattering (SAXS)

A SAXSess Small Angle X-ray Scattering instrument from Anton Paar (Graz, Austria) is used to perform all SAXS experiments. The instrument uses a CuK_α x-ray source with a wavelength of 1.54 Å with line collimation. Image plates from Fujifilm (Greenwood, SC), cyclone scanner from Perkin-Elmer (Covina, Ca) and the SAXSquant software is used to acquire, correct, and analyze the raw data. The pair-distance distribution functions (PDDF) are calculated using the GIFT analysis package [37,44]. This is a generalized indirect Fourier transformation method that provides structural parameters for protein-surfactant complexes such as the shape of the scattering complex (pearl-necklace, oblate, ellipsoidal, etc), the average maximum extension (L), the micelle diameter (D_m) and the average separation distance between nearest neighbor micelles (S) [7,45]. The scattering vector q is defined in Eq. (6.2), where θ is the scattering angle and λ the x-ray wavelength. In addition, radii of gyration (R_g) for each protein-surfactant complex are calculated using the Guinier approximation (Eq. 6.3) where I_0 is the zero angle intensity [37].

$$q = \frac{4\pi}{\lambda}\sin\theta \qquad \textbf{(6. 2)}$$

$$\ln[I(q)] = \ln[I_0] - \frac{R_g^2}{3}q^2 \qquad \textbf{(6. 3)}$$

Protein-surfactant samples for SAXS are prepared at 15 mg protein/mL of solution and then diluted to 1 mg of protein/mL of solution with their respective buffer D. All protein-PFC_8S, PFC_6S and PFC_4S complexes are analyzed at room temperatures and all are filtered to avoid scattering from precipitated surfactant crystals that sometimes

form in fluorinated surfactants with longer tails. Specifically this is important for the PFC_8S and PFC_6S samples, because they are analyzed below their corresponding Kraft temperatures (see Appendix B). In addition to these measurements, scattering profiles of a dilution series of surfactant are conducted to determine micelle shapes when possible. The scattering of free micelles of PFC_4S, $SC_{12}S$, $SC_{10}S$ and SC_8S are measured at 50 mM, 210 mM, 60 mM and 30 mM respectively. All dilution series are conducted to the point where no changes in the intensity profiles are observed. At this point the absence of correlations between protein-surfactant complexes in the solution implies a structure factor of 1 [44].

6.2.4 Dynamic light scattering (DLS)

DLS measurements are performed in a Zeta-sizer Nano ZS with a 633 nm wavelength (Malvern-UK). Sample preparation is identical to SAXS samples. For DLS, the samples are diluted to 0.5, 1.0 and 1.5 mg protein/mL and compared to verify that dilute conditions had been achieved. DLS is used to characterize the diffusion coefficient and hydrodynamic diameter (D_H) of protein-surfactant complexes. However, note that the values of D_H can only be used for qualitative comparison because they correspond to the diffusion of equivalent spheres following Stokes-Einstein diffusion[38]. This is likely quite different from the expected elongated shape of typical protein-surfactant complexes [7,10]. Therefore, the hydrodynamic dimensions obtained from DLS cannot be compared directly to the dimensions and radii of gyration obtained from SAXS.

6.2.5 Circular dichroism (CD)

Spectra of β-galactosidase, BSA, ovalbumin and lysozyme associated with perfluorinated and hydrogenated alkyl surfactants in the far-UV region (λ ~190-260 nm) are recorded on a Jasco-720 Spectropolarimeter (Easton, MD). All protein-surfactant samples are prepared following the same procedures used for SAXS and DLS. The only exception is the absence of trizma and glycine, which increase the absorption background of the buffer at the far-UV region of the spectrum. Samples are analyzed at 62.5 μg of protein/mL of solution. All spectra are converted into mean residue ellipticity (θ_{MRE}), which is given in (degrees•cm^2•dmol^{-1}) using Eq. (6.4) and (6.5) [46]. Here θ_e is the raw CD data in (millidegrees), c is the concentration in (mg/mL), l is the pathlength of the quartz cell in (mm) and MRW is the mean residue weight of the sample, M_w corresponds to the protein molecular weight in Daltons, and n refers to the number of amino acids in the proteins. The denominator factor in Eq. (6.5) refers to the total number of peptide bonds, which is one less than the total number of residues [46].

All CD spectra are collected in a 1 mm quartz cuvette, at 25 °C, using a data pitch of 0.2 nm in a continuous scanning mode at 100 nm/min and a total accumulation of 8 scans.

$$\theta_{MRE} = \frac{\theta_m \cdot 0.1 \cdot MRW}{c \cdot l} \quad \textbf{(6. 4)}$$

$$MRW = \frac{M_w}{n-1} \quad \textbf{(6. 5)}$$

Analysis of circular dichroism is conducted using the Dichroweb online analysis server [47,48]. CONTIN algorithm and the protein reference dataset SP175 are used for fitting. For all solutions, only those that had values for the normalized root mean square deviation (NRMSD) of 0.1 or less are considered acceptable and are reported.

6.3 Experimental results

Polyacrylamide Gel Electrophoresis (PAGE): PAGE analyses are conducted to explore the potential that fluorinated surfactants have for analytical protein separations. Fig. 6.2 shows the PAGE experiments for the full set of proteins described in Table 3.2 (Ch. III). Proteins are denatured with two kinds of anionic surfactants: fluorinated (PFC_xS) and hydrogenated (SC_xS).

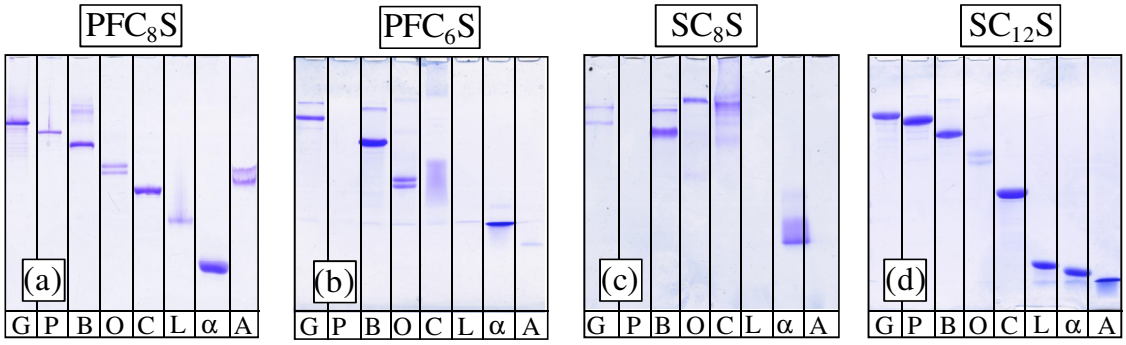

Figure 6. 2. Polyacrylamide gel electrophoresis of commercial gels (12 wt%) with (a) PFC_8S, (b) PFC_6S, (c) SC_8S and (d) $SC_{12}S$. G: β-galactosidase, P: phosphorylase, B: bovine serum albumin, O: ovalbumin, C: carbonic anhydrase, L: lysozyme, α: α-lactabulmin, A: aprotinin

The best performance is found using $SC_{12}S$ (Figure 6.2d) followed by PFC_8S (Fig. 6.2a) and then by PFC_6S (Fig. 6.2b). With PFC_6S it is only possible to identify six

proteins (G, B, O, L, α and A). The carbonic anhydrase sample is only roughly resolved due to significant band dispersion. Still, separations with PFC_6S clearly show better performance than the larger hydrogenated surfactant, SC_8S.

Separations with SC_8S show very poor resolution due to large band dispersion and low mobility values (Fig. 6.2c). Particularly, it is only possible to identify some of the bands in the high protein molecular weight range but, in comparison with the others surfactants, SC_8S shows the poorest proteomic separations. Fig. 6.2 also shows that there are two bands corresponding to ovalbumin when PFC_8S, PFC_6S and $SC_{12}S$ are used in the separation. Separations with PFC_4S are also attempted using these standard conditions but they failed completely and no protein bands could be identified (data not shown). In a qualitative comparison, the identification of proteins with PFC_4S is even weaker than that shown for SC_8S.

In order to quantitatively compare the migration of protein-surfactant complexes, we also calculate the electrophoretic mobilities with both the hydrogenated and fluorinated surfactants using Eq. (6.1). Fig. 6.3 depicts the protein-surfactant mobility as a function of the protein molecular weight. Error bars represent one standard deviation from three independent experiments. The mobilities of the larger proteins for each surfactant are fitted with Power law and the best-fit equations are shown in Fig. 6.3. Proteins with the lowest molecular weight values show deviations from power-law behavior in all surfactants.

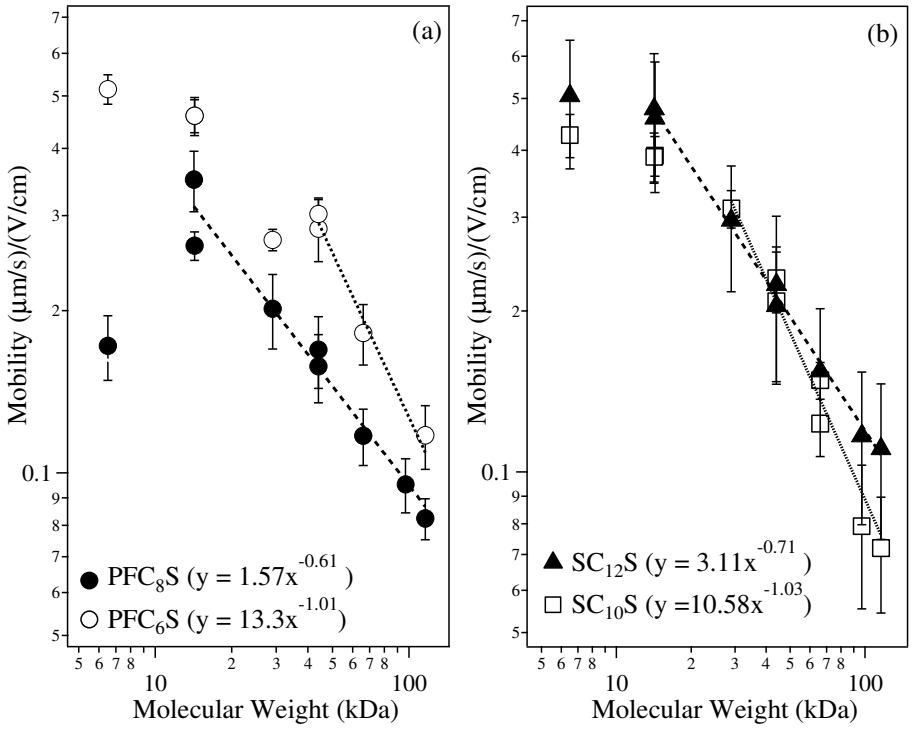

Figure 6. 3. Electrophoretic mobilities of proteins denatured by PFC_8S, PFC_6S (a) and $SC_{12}S$, $SC_{10}S$ (b). Dashed lines correspond to the power law fits.

The power law exponent shown in Fig. 6.3 can be used to quantitatively compare the dependence on molecular weight for each surfactant. When the exponents are larger, better separation resolution will be obtained. The multiplication coefficient, in contrast, can be used to compare the speed of the separation. Again, larger values are better because they represent faster separations. Fig. 6.3 indicates that PFC_6S promotes a faster migration for protein-surfactant complexes between 44 to 116kDa but fails to separate carbonic anhydrase adequately. PFC_6S surpasses the mobility of $SC_{10}S$ complexes at the high molecular weight region. According to the fits, PFC_6S and $SC_{10}S$ appear to be good candidate surfactants for PAGE but it is still necessary to understand why they do not perform better for separations of small proteins. It is also necessary to understand the

nature of the anomalous migration in carbonic anhydrase. It is interesting that lysozyme (14.3 kDa) and α-lactalbumin (14.2 kDa) are well separated in PFC_8S-PAGE. These two proteins have similar molecular weights and have been previously shown minimal differences in mobility in 1D PAGE with hydrogenated surfactants (SC_xS)[7]. Although this is problematic to estimate molecular weights from PAGE, it indicates that there are other parameters of importance to determine protein-surfactant binding and mobility. Furthermore, this dependence could be useful in complex separation techniques such as in surfactant-surfactant 2D electrophoresis of membrane proteins[49,50].

Dynamic light scattering (DLS): DLS tests are performed in order to determine the effect of the surfactant tail length on the self-diffusion of protein-surfactant complexes and also to compare trends in hydrodynamic sizes with structural parameters obtained through SAXS. Fig. 6.4a, 6.4b and 6.4c shows the correlation functions of protein-fluorinated surfactant complexes. Monomodal distributions in all correlation functions are evident and single decays are observed. In Fig. 6.4, markers corresponds to the experimental data and the lines throught the markers represent the respective cumulant fit. As expected, the correlation functions of the complexes of larger proteins decay at slower rates.

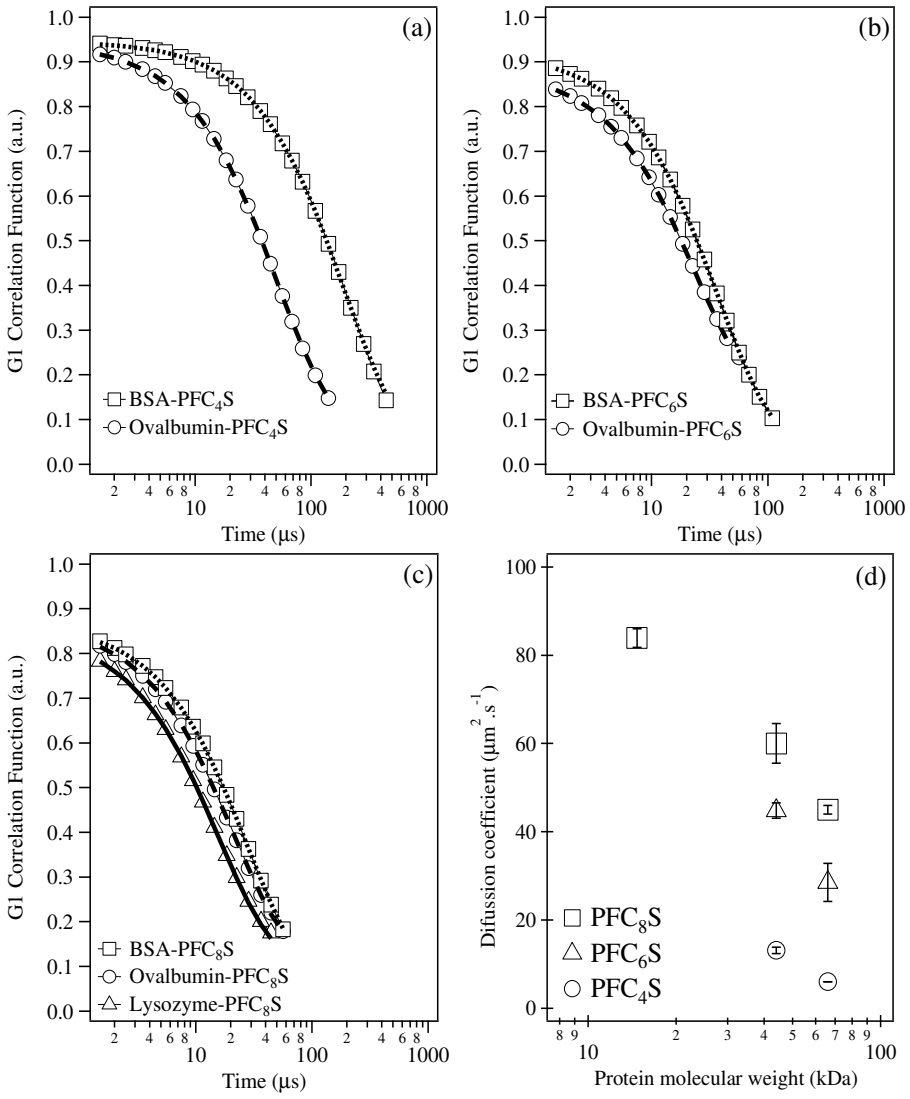

Figure 6. 4. Correlation functions and diffusion coefficients of complexes of protein and fluorinated surfactants (1mg protein/ml solution). a) protein-PFC_4S complexes, b) protein-PFC_6S complexes, c) protein-PFC_8S complexes and d) Diffusion coefficients for complexes of protein and fluorinated surfactant.

The respective cumulant fits are also plotted showing a good aggrement with the raw data. The corresponding diffusion coefficients are also shown in Fig. 6.4d. This shows that the diffusion coefficients of BSA, ovalbumin and lysozyme associated with PFC_8S, PFC_6S and PFC_4S decrease with increasing protein molecular weight. Data for

lysozyme associated with PFC_6S and PFC_4S is not shown because the samples are not stable and the proteins aggregate and flocculate.

Small angle x-ray scattering (SAXS): SAXS is used to study the interactions between three model proteins (BSA, ovalbumin and lysozyme) and three fluorinated surfactants in solution. Micelle sizes and structural parameters of all protein-surfactants are extracted from scattering curves after they are converted into pair-distance distribution functions (PDDF) using the Indirect Fourier Transformation analysis[37]. Fig. 6.5 compares the pair-distance distribution functions (PDDF) corresponding to free micelles for three types of hydrogenated surfactants ($SC_{12}S$, $SC_{10}S$ and SC_8S) and one of the fluorinated surfactants (PFC_4S). Free micelles of PFC_6S and PFC_8S could not be analyzed with SAXS because their Kraft temperatures are above room temperature, which is the experimental condition for PAGE and SAXS experiments. Both PFC_8S and PFC_6S have solubility limits at room temperature below their CMCs. Still, although free micelles cannot form at room temperature, the surfactant can associate with the protein. The solubility diagrams for both surfactants have been collected and are shown in the Appendix B.

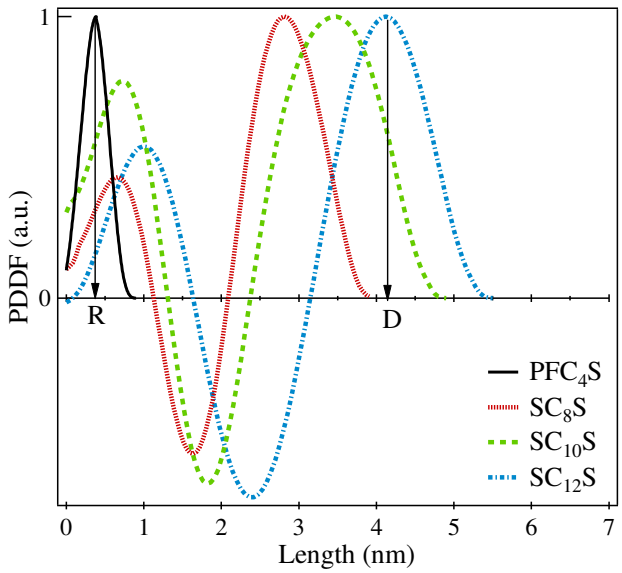

Figure 6. 5. Pair-distance distribution functions and diameters of single micelles of PFC_4S (0.8 nm), SC_8S (2.8 nm), $SC_{10}S$ (3.4 nm) and $SC_{12}S$ (4.1 nm) extracted from SAXS scattering profiles.

Our results show that PFC_4S forms very small spherical aggregates of less than 1 nm in diameter. For comparison, the diameters of the spherical micelles of hydrogenated surfactants range between 2.8 and 4.1 nm. It is important to note that the difference in shape of SAXS profiles for hydrogenated and fluorinated micelles originate from the different electron density contrasts between the core, shell and solvent for each system. The proper interpretation of these curves has been discussed in detail in previous chapters and this is also highlighted in Appendix A[7,37,44,45]. Specifically, the differences in the shape of the PDDFs are due to the electron density of the fluorine and hydrogen atoms in the micelle core. In recent work, our group has also shown that for hydrogenated surfactants the position of the second peak is directly correlated to the micelle diameter[45]. The relationship between the tail length and the micelle size of hydrogenated surfactant is

also discussed in Chapter IV[7]. The formation of spherical micelles of PFC_4S has also been observed by other authors but the size of the aggregates is not mentioned [15,20,51]. The length of a PFC_4S monomer based on bond lengths, angles and the assumption of a fully extended hydrophobic chain is estimated as ~1.05 nm. From this, one can estimate the upper bound micelle size to be 2.1 nm in diameter. However, this estimated micelle size does not consider changes to the arrangement of the tail atoms, interdigitation or electrostatic interactions[15,17,20]. Nevertheless, SAXS demonstrates the formation of extremely small micelle aggregates for PFC_4S.

Fig. 6.6 contains representative curves of SAXS profiles for all complexes of proteins and fluorinated surfactants. The lysozyme-PFC_6S and lysozyme-PFC_4S are absent in the figure because they aggregate and flocculate during the sample preparation. The markers represent the raw SAXS data and the dotted lines correspond to the best-fit curves from GIFT analysis. All SAXS curves show a scattering plateau at low q, which indicates that the resolution of the instrument (~90 nm) is appropriate to characterize the maximum lengths of the protein-surfactant complexes.

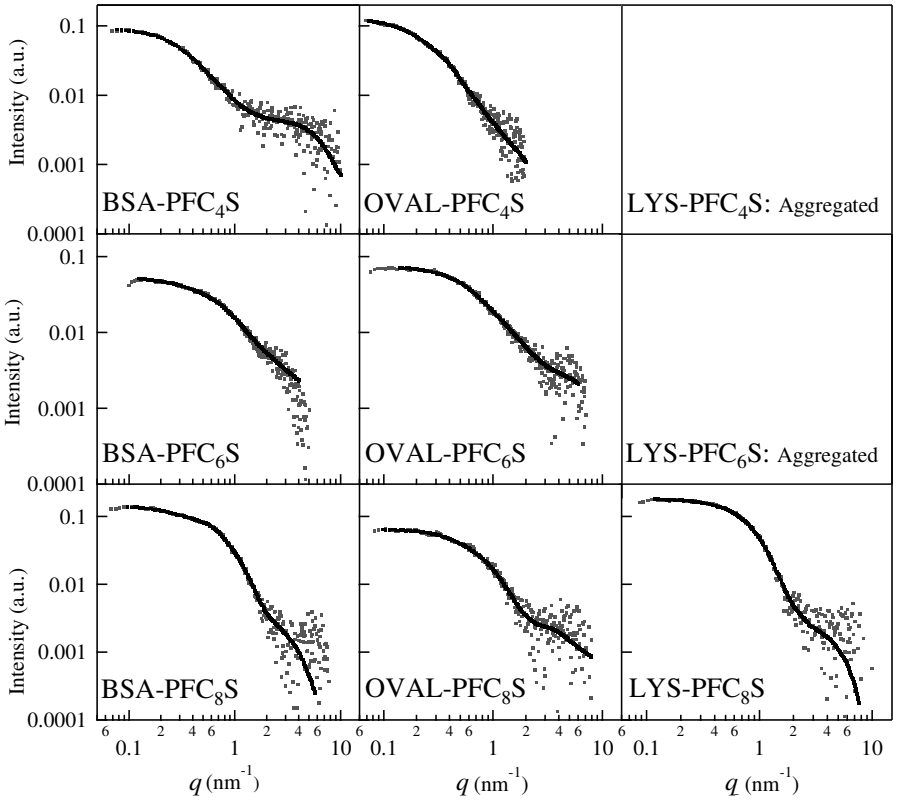

Figure 6. 6. Experimental SAXS profiles (markers) and approximation from GIFT fit (dashed -lines) for all protein complexes with fluorinated surfactants.

The scattering curves for stable protein-surfactant complexes are analyzed with GIFT and pair-distance distribution functions (PDDF) are calculated and plotted in Fig. 6.7[52]. In these PDDFs, the first peak corresponds to the size of the micelles in the complex; the second peak represents the average micelle separation distance and the point where the curve crosses the lower axis is related to the length of the complex[45]. The radius of gyration, R_g, for each protein-surfactant complex is also calculated from the lower *q* region of the scattering data using Guinier analysis (see Table 6.1) [44].

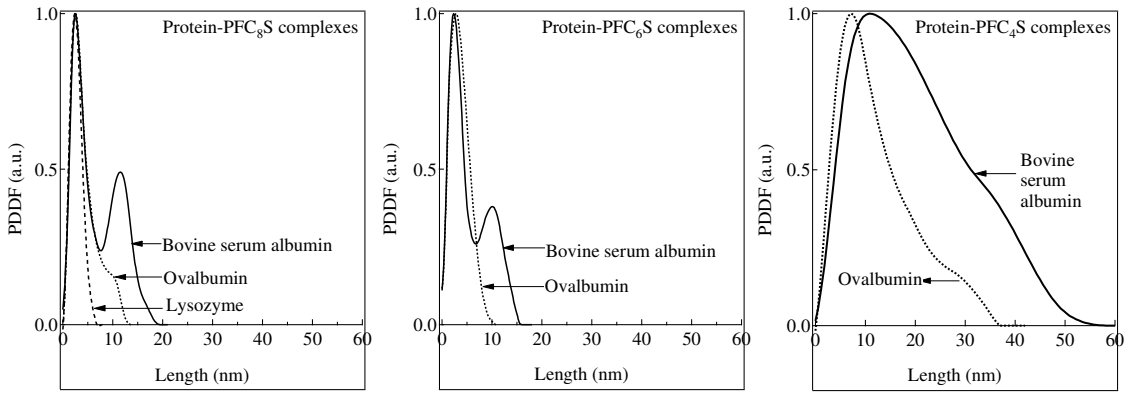

Figure 6. 7. Pair-distance distribution functions of protein-fluorinated surfactant complexes. From left to right: PFC_8S, PFC_6S and PFC_4S

As expected, the resulting curves show systematic changes in length as the protein molecular weight increases. Complexes of BSA have the longest extension followed by ovalbumin and lysozyme. Also, the shape of the PDDF indicates that the BSA-PFC_6S or BSA-PFC_8S form necklace-like structures. However, the PDDFs for ovalbumin and lysozyme complexes suggest the absence of neighbor micelles within the complex. This indicates that only one micelle is associated with these proteins. The adsorption of one micelle into the smallest protein (lysozyme) is expected because a small protein size is directly associated with a limited region suitable for micelle interactions. However, the extension of complexes of lysozyme-PFC_8S (6.8 nm) is larger than for lysozyme-$SC_{10}S$ (3.8 nm)[7]. In Chapter IV, it is also discussed that the overall length of the lysozyme complex increases with increasing surfactant tail length. A summary of the structural parameters obtained through SAXS (complex length, neighbor distance, micelle radius and radius of gyration) and the hydrodynamic size obtained with DLS for all complexes of proteins and fluorinated surfactants are listed in Table 6.1.

Table 6. 1. Summary of structural parameters for protein-surfactant complexes

Complex name (protein-surfactant)	Complex length [a] (nm)	Neighbor distance [a] (nm)	r_m [a] (nm)	R_g [a] (nm)	D_H [b] (nm)
BSA-PFC_8S	19.4	11.5	2.6	3.2	10.1
Ovalbumin-PFC_8S	13.5	Single micelle	2.6	2.7	8.1
Lysozyme-PFC_8S	6.8	Single micelle	2.4	2.2	6.1
BSA-PFC_6S	15.8	10.1	2.3	2.8	13.1
Ovalbumin- PFC_6S	10.7	Single micelle	2.8	2.3	9.7
BSA-PFC_4S	52.0	**---**	---	7.6	68.7
Ovalbumin- PFC_4S	37.0	**---**	---	5.9	18.7

Determined by SAXS [a], determined by DLS [b]

Note that the reported hydrodynamic diameter values correspond to the equivalent diameter of a hard sphere. The expected micelle diameters for fluorinated surfactants of six and eight carbons, assuming fully extended chains, are 3.1 and 4.2 nm respectively. The micelle diameter of complexes of BSA with PFC_6S and PFC_8S obtained through PDDF analysis are 4.6 and 5.2 nm respectively. It is expected that, as the tail length increases, the micelle size will increase but there could also be changes in shape that could affect this relationship. The indication of two peaks for BSA with PFC_6S and PFC_8S confirms the presence of multiple micelles attached to the backbone. The shape of the PDDFs of ovalbumin and BSA with PFC_4S could indicate the formation of a much more elongated structure or the formation of stable multi-protein aggregates that do not flocculate.

Circular dichroism (CD): CD measurements are performed to obtain information on changes in the secondary structure of proteins thermally denatured by fluorinated and hydrogenated surfactants. Fig. 6.8 contains characteristic curves of CD spectra. The CD spectrum for the native protein is shown as a solid line.

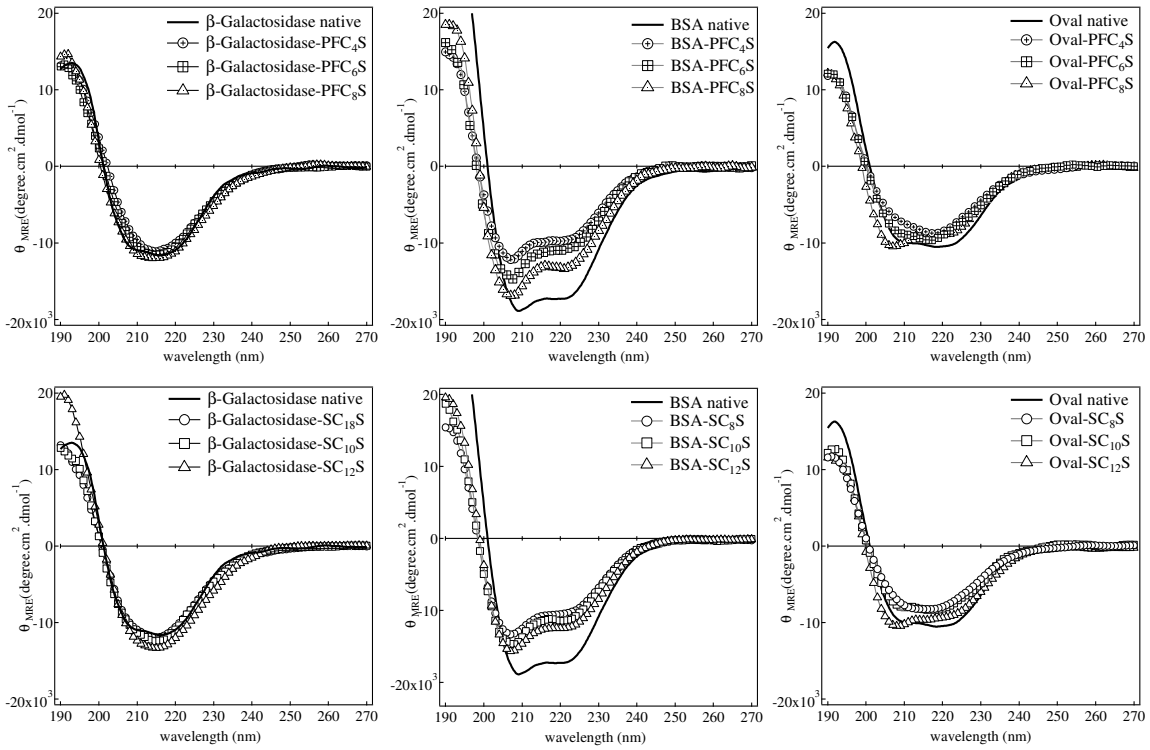

Figure 6. 8. Far UV-CD spectra of β-galactosidase (left), BSA (center) and ovalbumin (right) denatured with perfluorinated, PFC_xS (top) and hydrogenated, SC_xS (bottom) surfactants.

Each secondary structure composition (α-helix, β-sheet, turns and coil) is qualitatively described by the features occurring in the far UV region of the CD spectrum[46]. It is evident that the stability of the folded shape (native protein) has been modified by the interactions of proteins with both types of surfactants: PFC_xS and SC_xS. The results also suggest that, as the tail becomes smaller, the extent of alteration to the secondary structure becomes stronger. Surfactants with longer tails disturb the secondary structure of both proteins to a much lesser extent.

A typical α-helical protein is described with two negative peaks at ~222 nm and ~208 nm and a positive peak at ~190 nm. A β-sheet protein shows a negative peak

around 215 nm and a positive peak at ~195 nm[46,53]. Fig. 6.8 shows slight shifting towards blue at 206 nm and 220 nm for the BSA-surfactant complexes. The ovalbumin spectra also show shifting of the peaks to the blue region when the protein is associated with the longest tailed surfactants (i.e. PFC_8S and $SC_{12}S$). β-galactosidase complexes show the smallest changes of all three proteins that are analyzed by CD. Here, the α-helical peaks (208 and 222 nm) shift very slightly towards 215nm. CD experiments show that the different surfactants affect the secondary structure of the proteins in different ways.

The online server Dichroweb is used to estimate the secondary structure composition of the denatured protein-surfactant complexes[47]. Fig. 6.9 shows the estimated percentages for β-galactosidase, BSA and ovalbumin complexes. The results suggest that PFC_4S and SC_8S, the surfactants of smaller tail lengths, alter the secondary structure more effectively. However, note that β-galactosidase and ovalbumin-surfactant complexes show less significant changes than BSA-surfactant complexes. The reduction of α-helix and increase in β-sheet of BSA complexes is significantly larger.

The reliability of the analysis was ensured by only considering fits with a low NRMSD value. This is the most useful measure to judge goodness of fit between theoretical and experimental CD data. Ideally, values of less than 0.1 indicate good approximations [47]. All fits show NMRSD values lower than 0.075.

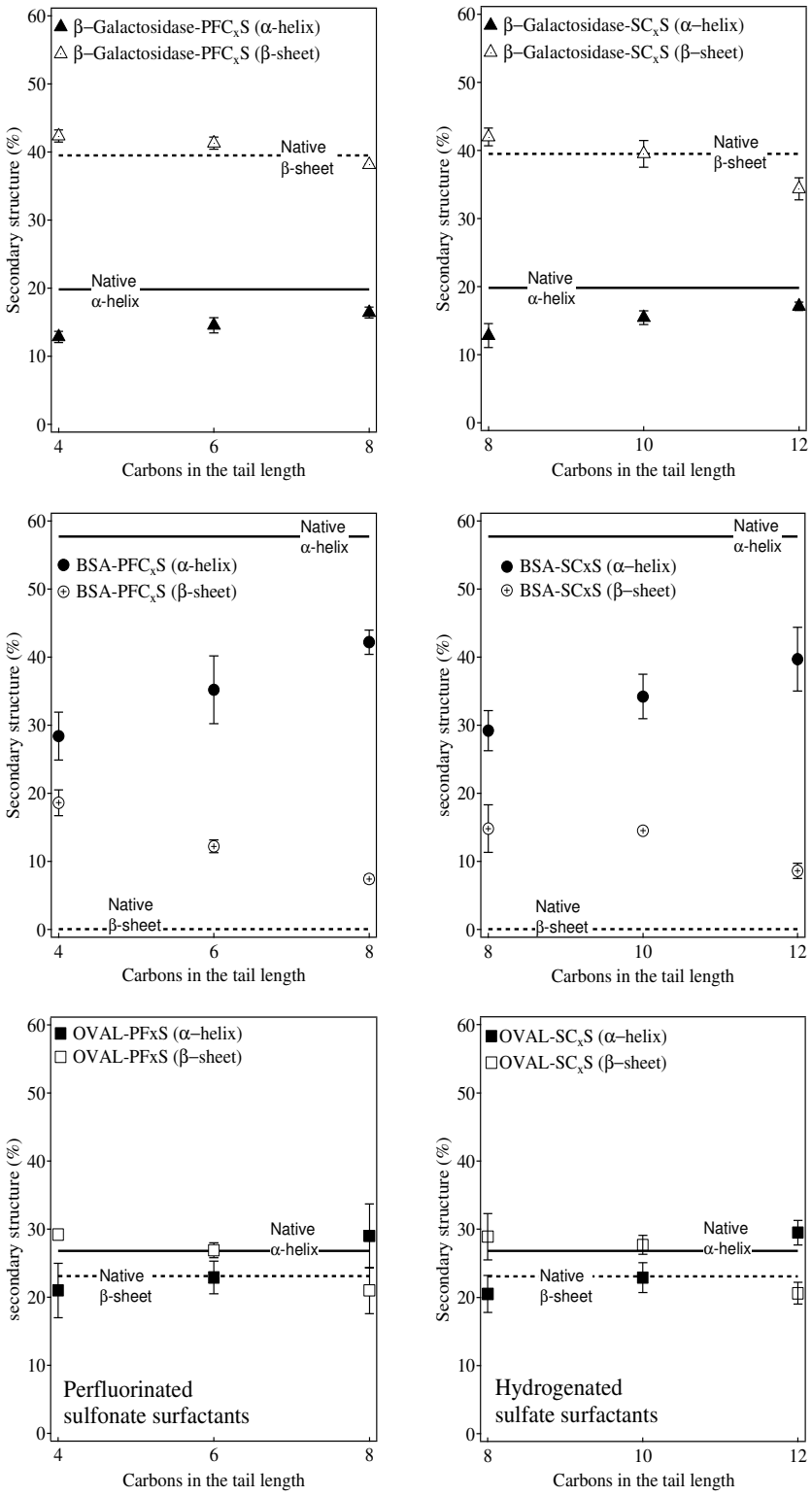

Figure 6. 9. α-helix and β-sheet content. β-galactosidase (triangles), bovine serum albumin (circles), ovalbumin (squares). Values calculated from Dichroweb[49].

6.4 Discussion

The electrophoretic separation (PAGE) of model proteins with fluorinated surfactants confirmed the viability of using fluorinated surfactants for protein separations. In terms of achieving a better resolution for the identification of proteins, PFC_8S and PFC_6S show significantly better performance than SC_8S assessed by the resolution of the peaks and the correlation of mobility to protein molecular weight (Fig. 6.2 and 6.3). This suggests that the exchange of hydrogen by fluorine atoms in surfactants of eight and six carbons in their chain promotes stronger hydrophobic interactions with proteins when compared to their hydrogenated counterparts and results in better proteomic separations for surfactants of equal size. However, within the set of fluorinated surfactants, PFC_8S and PFC_6S are the only ones that could be practically useful for this application after significant optimization is performed. At this point, none of the alternative surfactants that are evaluated show improved separation efficiency when compared to $SC_{12}S$ or $SC_{10}S$. Although optimization of new buffers and gel compositions is outside the scope of this initial study, it is possible that this could further improve the separation performance of fluorinated surfactants.

Previously, it is also mentioned that similarly sized proteins can co-migrate and that variations in experimental conditions could potentially induce changes in protein mobility that reduce or alter the overlapping migration of proteins with similar molecular weight[1,2]. The observation that PFC_8S causes a markedly different migration for lysozyme (14.3 kDa) and α-lactalbumin (14.2 kDa) shows that it may be a promising candidate for use in separations of membrane proteins through 2D surfactant-surfactant electrophoresis[49,50]. This particular application takes advantage of differences in

association of a protein to different types of surfactant to modify their migration and help in protein identification when isoelectric focusing in the native state is not possible due to poor solubility. This topic is still an open area of research and analysis of other proteins of similar size would be necessary to evaluate the potential in this application.

Recent work by Ruso et al., showed no significant differences in the interactions of lysozyme with perfluorooctanoate or hydrogenated surfactants, with the exception of finding a higher Gibbs free energy of unfolding[17]. However, in that work the proteins were not fully denatured in the same way as it is typically done for electrophoresis by breaking all disulfide bonds and heating the sample. Their studies focused on identifying the effects of saturating a native protein with these surfactants. They also concluded that the role of the four disulfide bonds in the protein contributed to reducing the total interactions between lysozyme and perfluorooctanoate. We found that lysozyme reduced with DTT and denatured by heating in the presence of PFC_8S forms much larger structures (Fig. 6.7) than when the same process is repeated with hydrogenated surfactants[7]. In both cases: lysozyme-PFC_8S and lysozyme-SC_8S are identified as protein-surfactant complexes of only one micelle but the length of the complexes are different.

In contrast, the presence of additional peaks in the PDDF (Fig. 6.7) for BSA associated with either PFC_8S or PFC_6S indicates that neighbor micelles are present, which is a signal to describe the formation of “pearl-necklace” structures. On the contrary, in all ovalbumin-PFC_xS complexes the absence of the second peak, the increase in the micelle radius and the appearance of a shoulder at the end of the curve, suggests the formation of elongated shapes such as ellipsoidal or oblate micelles. The increase in

the position of the first peak as the surfactant tail decreases could indicate that the reduction in tail size is altering the packing conformation and the complex structure to form elongated shapes.

The very different shapes and sizes that are found between free spherical PFC_4S micelles (Fig. 6.5) and the highly elongated large protein-PFC_4S complexes (Fig. 6.7) suggest that PFC_4S structures are dramatically affected after binding to proteins. Unfortunately, at this time it is not possible to determine if these large structures are a result of surfactant association to a single protein that is highly elongated or if they result from the stable aggregation of multiple denatured proteins. Furthermore, Table 6.1 shows that complexes of BSA and ovalbumin associated with PFC_8S and PFC_6S may not be fully unfolded as they are significantly shorter than complexes of the same proteins associated with PFC_4S. The marked difference in the size of protein-PFC_4S complexes (Fig. 6.7) and the small changes that are observed in CD spectra of larger surfactants (Fig. 6.8) also suggests that BSA-PFC_8S, BSA-PFC_6S, ovalbumin-PFC_8S and ovalbumin-PFC_6S retain significant secondary structure. These changes in size are also confirmed in the DLS correlation function (Fig. 6.4a, 6.4b and 6.4c) of all protein-PFC_xS complexes. The slower decays observed in the correlation functions of the protein-PFC_4S samples describe much larger particles. Our results are also in agreement with previous authors that find that the presence of fluorinated surfactants only partially unfolds proteins[17].

Fig. 6.10 describes an example of a native protein denatured with two surfactants of short and large tails. The diagram illustrates the observations that arise from the SAXS and CD results. It shows the effect of the surfactant tail length when a protein is denatured by a series of surfactants. Even after reduction and heating, all proteins keep

some secondary structure but the relative content can change considerably. Results from SAXS (Fig. 6.7) and CD (Fig. 6.8 and 6.9) show that shorter tailed surfactants are more effective at unfolding the proteins and lead to elongated complexes. Still, even these samples retain a considerable amount of secondary structure.

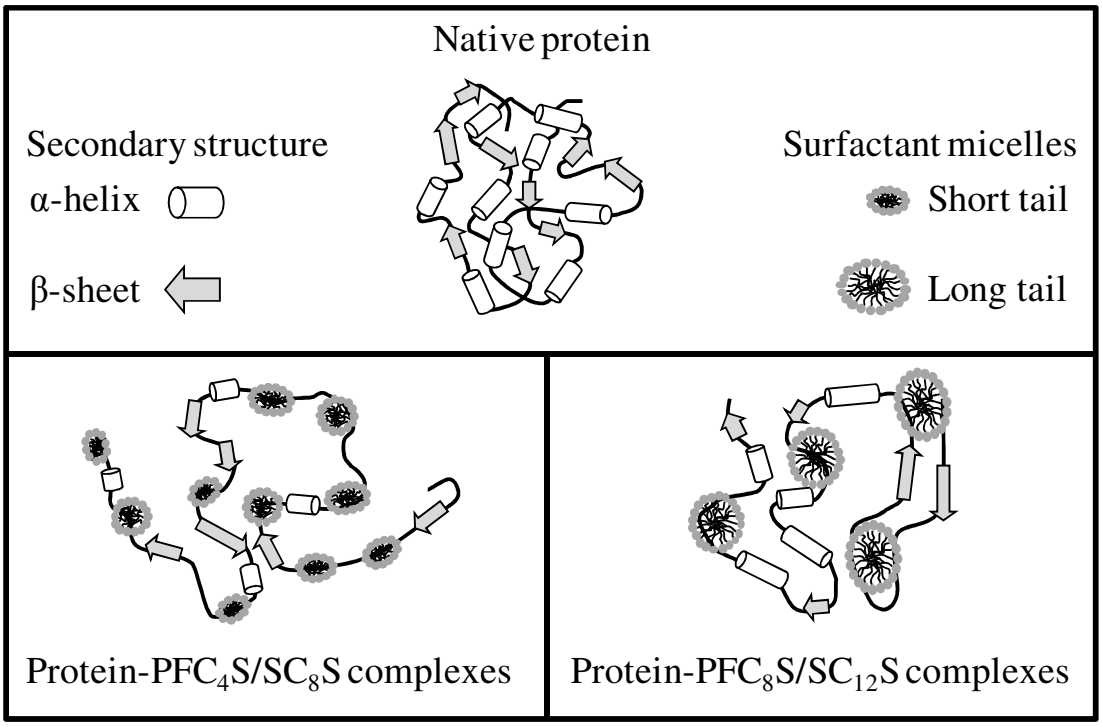

Figure 6. 10. Schematic of protein-surfactant complexes of fluorinated (PFC_xS) and hydrogenated surfactants (SC_xS) of different tail length associated with the same hypothetical protein.

Interestingly, the α-helical content is usually found to decrease while the β-sheet content increases upon denaturation with shorter surfactant tails. This effect is more pronounced when the native protein has larger α-helix content. According to the protein data bank (PDB), native ovalbumin (PDB ID: 1UHG) is characterized by roughly equal amounts of α-helix and β-sheet proportions (~31%), the native BSA (PDB ID: 3V03) is described as a primarily helical structure (74%) and the native β-galactosidase (PDB ID:

3VD3) is primarily β-sheet (39%) but still has a significant α-helix (13%) portion[24,26,27,36].

The estimates of the secondary structure content for the native β-galactosidase, BSA and ovalbumin obtained in this study from CD spectra are in reasonable agreement with the reported values in the PDB[24,26,27]. After denaturation, the α-helix content of BSA decreases to values as low as 28.4% and the β-sheet content increases to 18.6%. The changes in β-galactosidase and ovalbumin are significantly smaller but keep the same trends where longer tailed surfactants disrupt to a lesser extent the secondary structures. Furthermore, the same trends are observed for fluorinated and for hydrogenated surfactants but they are shifted to different tail sizes (Fig. 6.9).

On the other hand, the aggregation of lysozyme in the presence of PFC_4S and PFC_6S (Fig. 6.6) indicates that binding of surfactant to proteins is not only affected by the surfactant type and the specific experimental conditions but also by the composition of each protein. Fig. 6.1 shows a simple schematic that illustrates the role of the amino acid sequence on the binding of micelles. In this study, because of their high isoelectric point, lysozyme and aprotinin (pI: 10.5 and 11.3 respectively) are the only two proteins that carry a net positive charge at the experimental conditions that are used (pH ~7.5 ± 0.2). This is highlighted by a schematic showing the charge of all proteins at the experimental conditions in the Appendix B. The aggregation of lysozyme and the abnormal migration of aprotinin suggest that electrostatic forces dominate interactions with PFC_6S and PFC_4S and micelle adsorption to these proteins could be significantly different than to other proteins due to this effect. Another possible explanation for the aggregation is related to

the small protein sizes. This could result in only a limited number of protein moieties that are suitable for interaction with surfactant micelles. The abnormal migration of proteins denatured with hydrogenated surfactants has also been discussed by other authors suggesting that mobility is affected not only by the saturation of the protein with detergent but also by their effective size[6,9].

In conclusion we have shown that, by learning about the association mechanisms of proteins and fluorinated surfactants, it is viable to improve proteomic separations. Fluorinated surfactants such as PFC_8S and PFC_6S could indeed be promising alternative surfactants to perform electrophoresis separations in the future. However, as studied in this chapter, these surfactants are not yet ready to replace $SC_{12}S$ (SDS) without the optimization of other separation parameters (e.g. buffer compositions and gel concentration). The optimization of other separation parameters is suggested as part of a future work. Still, the observation of structural changes that occur in proteins denatured by different surfactants and the specific association mechanisms have been carefully analyzed in this work and merit further attention in the future. Studies using synthetic polypeptides of different size and composition (e.g. with controllable hydrophobic regions) could also clarify the specific mechanisms that control interactions of fluorinated surfactants with complex proteins.

6.5 Conclusion and outlook

This chapter shows that proteomic separations are feasible with the use of the perfluorinated anionic surfactant PFC_8S. The interactions between proteins and fluorinated surfactants with six and eight carbons have also been evaluated and determined to be stronger than for their hydrogenated counterpart surfactants in gel electrophoresis. It was found that proteomic separations with surfactants of shorter tails are possible as long as the hydrophobic interactions between micelles and proteins achieve a minimum binding strength to resist the applied electrical potential during gel electrophoresis. Also, the results from this study shown that, for shorter tail lengths, the disruption of the secondary structure is stronger for both types of surfactants (i.e. hydrogenated or fluorinated). Gel electrophoresis, scattering analysis and circular dichroism all suggest that fluorinated surfactants enhance protein denaturation but that these still retain some of the secondary structure. Moreover, results suggest that binding of surfactants to proteins is affected by the specific protein sequence and composition. These findings are expected to be useful to guide the design of new nanostructures based on the association mechanisms between protein and alternative surfactants to improve protein separations for reliable protein identification.

6.6 References

(1) Brown, E. G. *Analytical biochemistry* **1988**, *174*, 337–348.
(2) López, M. F.; Patton, W. F.; Utterback, B. L.; Chung-Welch, N.; Barry, P.; Skea, W. M.; Cambria, R. P. *Analytical biochemistry* **1991**, *199*, 35–44.
(3) Tung, J.-S.; Knight, C. A. *Analytical biochemistry* **1972**, *48*, 153–163.
(4) Durand, G.; Seta, N. *Clinical Chemistry* **2000**, *46*, 795.
(5) Hirsch, J.; Hansen, K. C.; Burlingame, A. L.; Matthay, M. A. *American Journal of Physiology. Lung Cellular and Molecular Physiology* **2003**, *287*, L1–L23.
(6) Su, Y.-Y. T.; Jirgensons, B. *Archives of Biochemistry and Biophisics* **1977**, *181*, 137–146.
(7) Ospinal-Jimenez, M.; Pozzo, D. C. *Langmuir* **2011**, *27*, 928–935.
(8) Pozzo, D. C. *Langmuir* **2009**, *25*, 1558–1565.
(9) Mattice, W.; Riser, J. M.; Clark, D. S. *Biochemistry* **1976**, *15*, 4264–4272.
(10) Reynolds, J. A.; Tanford, C. *Proceedings of the National Academy of Sciences of the United States of America* **1970**, *66*, 1002–1007.
(11) Kashino, Y. *Journal of Chromatography B* **2003**, *797*, 191.
(12) Chandramouli, K.; Qian, P.-Y. *Human Genomics and Proteomics* **2009**, *2009*, 1–22.
(13) Muto, Y.; Esumi, K.; Meguro, K.; Zana, R. *Journal of Colloid and Interface Science* **1987**, *120*, 162–171.
(14) Andersen, K. K.; Otzen, D. E. *J. Phys. Chem. B* **2009**, *113*, 13942–13952.
(15) Kissa, E. *Fluorinated surfactants and repellents*; series, S. science, Ed.; 2nd ed.; Marcel Dekker: New York, 2001.
(16) Krafft, M. P. *Advanced Drug Delivery Reviews* **2001**, *47*, 209.
(17) Ruso, J. M.; González-Pérez, A.; Prieto, G.; Sarmiento, F. *Internation Journal of Biological Macromolecules* **2003**, *33*, 67–73.
(18) Hassan, N.; Barbosa, L. R. S.; Itri, R.; Ruso, J. M. *Journal of Colloid and Interface Science* **2011**, *362*, 118.
(19) Vieira, D. B.; Crowell, A. M. J.; Doucette, A. A. *Rapid Commun. Mass Spectrom* **2011**, *26*, 523–531.
(20) Kissa, E. *Fluorinated surfactants: Synthesis·Properties·Applications*; Marcel Dekker, INC: New york, USA, 1994; Vol. 50.
(21) Li, L.; Xu, Z. S.; Song, G. W. *Journal of Fluorine Chemistry* **2009**, *130*, 225.
(22) Viovy, J.-L. *Reviews of Modern Physics* **2000**, *72*, 813–872.
(23) Otzen, D. *Biochimica et Biophysica Acta* **2011**, *1814*, 562–591.
(24) Wheatley, R. W.; Kapperlhoff, J. C.; Hahn, J. N.; Dugdale, M. L.; Dutkoski, M. J.; Tamman, S. D.; Fraser, M. E.; Huber, R. E. *Archives of Biochemestry and Biophysics* **2012**, *521*, 51–61.
(25) Gregoriou, M.; Noble, M. E. M.; Watson, K. A.; Garman, E. F.; Krulle, T. M.; De la Fuente, C.; Fleet, G. W. J.; Oikonomakos, N. G.; Johnson, L. N. *Protein science* **1998**, *7*.
(26) Majorek, K. A.; Porebski, P. J.; Dayal, A.; Zimmerman, M. D.; Jablonska, K.; Stewart, A. J.; Chruszcz, M.; Minor, W. *Mol. Immunology* **2012**, *52*, 174–182.
(27) Masayuki, Y.; Takahashi, N.; Hirose, M. *The Journal of Biological Chemistry* **2003**, *278*, 35524.

(28) Saito, R.; Sato, T.; Ikai, A.; Tanaka, N. *Acta Crystallogra. Sect. D* **2004**, *60*.
(29) Cipriani, F.; Rower, M.; Landret, C.; Zander, U.; Felisaz, F.; Marquez, J. A. *Acta Crystallogr. Sect. D* **2012**, *68*, 1393–1399.
(30) Chrysina, E. D.; Brew, K.; Acharya, K. R. *J. Biol. Chem.* **2000**, *275*.
(31) Yang, I. S.; Kim, T. G.; Park, B. S.; Cho, K. J.; Lee, J. H.; Park, Y.; Kim, K. H. *Biochemical and Biophysical Research Communications* **2010**, *397*, 429–435.
(32) Craven, G.; Steers, E.; Anfinsen, C. *The Journal of Biological Chemistry* **1965**, *240*, 2468.
(33) Battell, M. L.; Zarkadas, C. G.; Smillie, L. B.; Madsen, N. B. *The Journal of Biological Chemistry* **1968**, *243*, 6202.
(34) Gold, A. M. *Biochemistry 7*, 2106.
(35) Wong, K.-P.; Tanford, C. *The Journal of Biological Chemistry* **1973**, *248*, 8518–8523.
(36) Berman, H. M.; Westbrook, J.; Feng, Z.; Gilliland, G.; Bhat, T. N.; Weissig, H.; Shindyalov, I. N.; Bourne, P. E. *Nucleic Acid Research* **2000**, *28*, 235.
(37) O.Glatter, O. K. *Academic press* **1982**.
(38) Berg, J. *An Introduction to Interfaces & Colloids. The Bridge to Nanoscience*; World Scientific Publishing Co. Pte. Ltd.: Singapore, 2010; p. 785.
(39) Tiddy, G. J. T. Concentrated surfactant systems. *Modern Trends of Colloid Science in Chemistry and Biology* **1985**, 148–156.
(40) Matsuoka, K.; Moroi, Y. *Current Opinion in Colloid and Interface Science* **2003**, *8*, 227–235.
(41) Sonia F. Santos Hannes Fischer, Rosangela Itri, D. Z. *Journal of Colloid and Interface Science* **2003**, *262*, 400–408.
(42) Chen, S.-H.; Teixeira, J. *Physical Review Letters* **1986**, *57*, 2583–2586.
(43) Malmon, A. G. *Biochimica et Biophysica Acta* **1957**, *26*, 233–240.
(44) Lindner, P.; Zemb, T. *Elsevier Science B.V.* **2002**.
(45) Franklin, M. J.; Surampudi, L. N.; Ashbaugh, H. S.; Pozzo, D. C. *Langmuir* **2012**, *28*, 12593–12600.
(46) Ann, W. B.; Janes, R. W. *Modern techniques for circular dichroism and synchrotron radiation circular dichroism spectroscopy.*; IOS Press: The Netherlands, 2009; Vol. 1.
(47) Whitmore, L.; Wallace, B. A. *Nucleic Acid Research* **2004**, *32*, W668–W673.
(48) Whitmore, L.; Wallace, B. A. *Biopolymers* **2008**, *89*, 392–400.
(49) Hartinger, J.; Stenius, K.; Högemann, D.; Jahn, R. *Analytical biochemistry* **1996**, *240*, 126–33.
(50) Rabilloud, T.; Chevallet, M.; Luche, S.; Lelong, C. *Proteomics* **2008**, *8*, 3965–3973.
(51) Gao, J. Y.; Dubin, P. L. *Biopolymers* **1998**, *49*, 185.
(52) Fritz, G.; Bergmann, A.; Glatter, O. *Journal of Chemicals Physics* **2000**, *113*, 9733–9740.
(53) Kelly, S. M.; Jess, T. J.; Price, N. C. *Biochimica et Biophysica Acta* **2005**, *1751*, 119–139.

CHAPTER VII

CONCLUSIONS AND RECOMMENDATIONS

7.1 Key results

The present experimental study was undertaken to investigate the influence of different surfactant architectures on protein denaturation and separation. Specifically, three groups of surfactants were selected: linear, branched and fully fluorinated surfactants. The primary goals of this thesis, outlined in Section 1.5, are met through systematic structural analysis and macroscopic characterization. In this work, we have shown that surfactant architecture not only plays a key role for protein separations but also it confers distinctive interactions with proteins. Furthermore, we have established that small angle scattering techniques are effective methods to interpret the structural changes that occur in protein-surfactant systems. Also, we show that most proteins interacting with linear, branched and fluorinated surfactants will likely form pearl-necklace structures. Lastly, we determined the feasibility of tuning the surfactant architecture in order to create competitive surfactant alternatives to sodium dodecyl sulfate ($SC_{12}S$). Additional conclusions for each study are summarized as follows:

In Chapter IV we presented a systematic study of the interaction of a series of sodium alkyl sulfates with proteins of diverse size and composition. Scattering analysis indicates that most protein-surfactant complexes form pearl-necklace structures. Moreover, smaller tail length surfactant micelles decorate more homogeneously the proteins. We demonstrated that by using sodium octyl (SC_8S) or decyl sulfate ($SC_{10}S$),

the protein-surfactant complexes resulted in larger complexes than when sodium dodecyl sulfate or larger surfactants were used. Performance metrics in electrophoresis also improved systematically as the surfactant tail was reduced. However, polyacrylamide gel electrophoresis results also indicate that the shorter tail length surfactant (SC_8S) failed to produce good protein separations. We inferred that the reduction of the tail length affected the surfactant binding strength to proteins. On the other hand, for proteins of small molecular weight, $SC_{10}S$ results in a better surfactant to conduct protein separations in terms of obtaining narrow bands and faster migration. Scattering analysis demonstrates that $SC_{10}S$ forms larger protein-surfactant complexes than the ones obtained with $SC_{12}S$ and larger surfactants. Circular dichroism (CD) also confirms the presence of ordered structures (α-helix and β-sheet motifs) in proteins denatured by SC_8S, $SC_{10}S$ and $SC_{12}S$. However, CD also shows that between these three surfactants, there is a trend between the carbon tail and their effect on disrupting the secondary structure. It was found that, as the surfactant tail reduces, the α-helical content decreases and the β-sheet increases. This trend was observed for three different proteins that contain not only different compositions but also diverse secondary structure conformations.

In Chapter V we examined, the effect of branching short-tailed surfactants for protein separations. Specifically three branched surfactants were studied: 2-EHS (a six carbon-tailed) and 3,7-DMOS and 2-BOS (eight-carbon tailed). It was found that adding branches to an eight carbon-tailed surfactant (3,7-DMOS and 2-BOS) significantly improved their performance in polyacrylamide gel electrophoresis. Yet, the resulting protein separations are still not as good as when the linear ten ($SC_{10}S$) and twelve-carbon ($SC_{12}S$) tailed surfactants are used as denaturing agents. Thus, PAGE results suggest that,

after further technical optimization, 3,7-DMOS and 2-BOS could indeed be promising alternatives to conduct protein separations. Circular dichroism (CD) and fluorescence spectroscopy indicate a stronger modification of the protein when 2-BOS is used as denaturing surfactant. Moreover, CD results show that 2-BOS modify to larger extent the secondary structure of most of the proteins, turning them into proteins of higher disordered conformations (e.g coils, turns, etc). Scattering analysis establishes that proteins and branched surfactants form condensed pearl-necklace and ellipsoidal structures. Scattering comparison with $SC_{12}S$ also reveals that branched surfactants form larger complexes.

In Chapter IV and V it was found that the shorter hydrocarbon-tailed surfactants are not adequate to conduct good protein separations (e.g. SC_8S and 2-EHS). It was hypothesized that the reduction in the surfactant tail reduces the binding strength between micelles and proteins. As a result, upon the application of the electric potential during gel electrophoresis, the proteins are striped of surfactant and are badly resolved. In Chapter VI we investigated the use of three short-tailed fluorinated surfactants aiming to increase the hydrophobic character of the surfactant through the presence of the fluorine atoms. We demonstrated that six and eight carbon fluorinated surfactants have stronger interactions with proteins than their hydrogenated counterparts. We also have shown that good protein separations are possible with short-tailed surfactants as long as the hydrophobic interaction between micelles and proteins achieves minimum binding strength to resist the applied electrical potential during the protein analysis. Circular dichroism indicates that, as the surfactant tail length decreases, the secondary structure turns into less α-helical and more β-sheet conformation. Scattering results also show the

conformation of pearl-necklace and ellipsoidal structures. Again, it was found that the shorter-tailed surfactant (PFC_4S) forms the larger protein-surfactant complexes.

The results from this thesis work all are expected to be important for the development of surfactants for protein electrophoresis. Moreover, the findings in these studies are valuable for the engineering design of new nanostructures and to guide further fundamental studies in the interactions between proteins and alternative surfactants. The progress in protein identification is not only a continuous and needed area of research but is also a challenging task given the diverse nature of proteins and the difficulties associated to their separation and identification (e.g. mislabeling).

7.2 Recommendations for future studies

In this dissertation we correlated the nano-structural parameters of a series of protein- surfactant complexes with their performance during gel electrophoresis and we determined that alternative surfactant architectures can enhance protein separations. This highlights the promising field of engineering novel surfactants to improve the low fidelity of certain protein separations when $SC_{12}S$ is used. In the series of studied surfactants, some enhance the separation of proteins while others produce weak and poor protein separations. Given that the protein separation methods used in this dissertation were not optimized, it is recommended to pursue additional analyses that include optimization of the buffer systems, gels structures, and experimental conditions (temperatures and pHs). Electrophoretic separations can be further enhanced by tuning the experimental method and this has been demonstrated with the standard surfactant, $SC_{12}S$[1,2]. Therefore,

optimization studies that could further improve the potential of some of the studied surfactants are strongly recommended. In particular, we recommend the use of capillary gel electrophoresis (CGE) instead of slab-gel PAGE to take advantage of the CGE automation and the higher resolution that is achievable. CGE is a versatile, prompt and automatic technique that allows conducting multiple accurate gel electrophoresis tests in shorter intervals and with very little human interaction.

As was mentioned in Chap. V and VI, in this dissertation the studied branched and fluorinated surfactants could have great potential to improve membrane protein separations. Our results indicated that because of their intrinsic hydrophobic character and their diverse architecture, these surfactants interact differently with many proteins. Two-dimensional gel electrophoresis (2D-PAGE), an essential proteomic method to analyze complex protein mixtures (e.g. serum), takes advantage of separating proteins by two different properties to maximize resolution. For example, proteins can be separated by their net charge in the first dimension through the differences in the protein isoelectric points (called isoelectric focusing or IEF). Then, in a direction orthogonal to the first dimension, the second separation occurs in most of the cases by SDS-PAGE. Thus, proteins are also differentiated by their molecular mass. The challenge associated to 2D-PAGE in the separation of membrane proteins, which are hydrophobic proteins, are associated to the need of using hydrophobic detergents in both dimensions to allow for protein solubilization[3–6]. In this dissertation, we have explored the use of surfactants of different hydrophobic character in 1D electrophoresis. Among these studies, we found that surfactants of higher hydrophobic character can improve protein separations. We also found that some surfactants appear to selectively disrupt to a greater extent the secondary

structure of most proteins (e.g. 2-BOS). Thus, we suggest to explore the use of 2D-PAGE (surfactant-surfactant) by using a combination hydrophobic surfactants, such as the perfluorinated PFC_8S, and the branched surfactant 2-BOS. Also, we recommend studying other 2D-PAGE surfactant combinations such as SDS/2-BOS, SDS/ PFC_8S, etc. It is also recommended to explore and compare different staining methods to better visualize proteins (e.g. Silver-staining, coomassie brilliant blue, fluorescence detection systems, etc)[7]. Fig. 7.1 contains an illustration of three alternative 2D electrophoresis techniques: IEF/SDS-PAGE (left), SDS/SDS-PAGE (center) and SDS/alternative surfactant-PAGE (right).

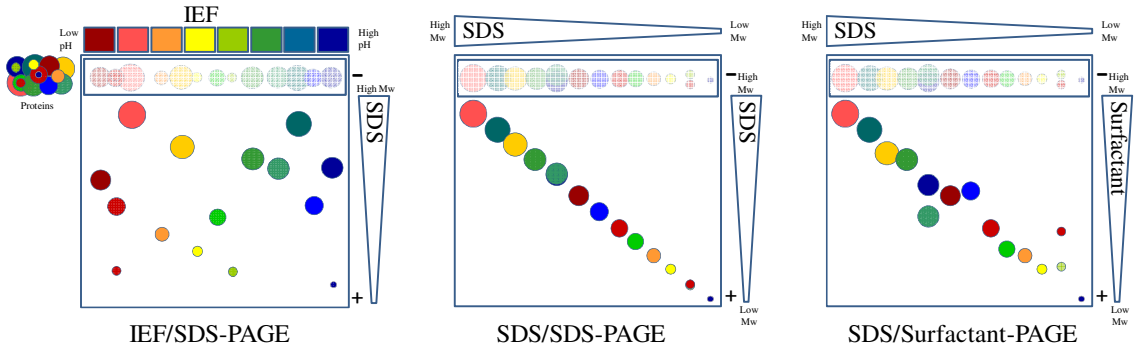

Figure 7.1. Illustration of two dimensional (2D) polyacrylamide gel electrophoresis alternatives.

Each colored circle represents a unique protein. The colors in each of them symbolize the differences in their net charge while the diameter of the circles denotes the size of the proteins. Thus, bigger circles correspond to bigger size proteins. If proteins are separated by their net charge, it is expected to obtain a random distribution of the circles organized by their colors, in this case from left to right as red to blue. On the other hand, when proteins are separated by SDS-PAGE the proteins will distribute according with their size. Note that when SDS is used in both dimensions, the migration of the proteins should be on a 45° line so that this is not a desired approach. In contrast, when using

surfactants that target alternative intrinsic properties such as 2-BOS, these could spread proteins after the second dimension so that they do not fall in the diagonal. Since this separation always takes place in the presence of surfactant, it would be useful in the identification of membrane proteins by 2D-PAGE.

The use of alternative surfactants to enhance protein separations is and will continue being an area of great interest[8–10]. Throughout the years, the use of the most common surfactant, $SC_{12}S$ or SDS, has been challenged in several examples by the use of alternative surfactants or by combinations of surfactants[10–13]. The need to have reliable protein separations, motivate the interest to identify technical improvements such as the use of alternative surfactants to improve fidelity in protein identification. In this dissertation, the results obtained with short tailed, fully hydrogenated and fully fluorinated surfactants encourage us to further expand the use of alternative surfactants such as partially fluorinated surfactants and to different head-groups. The presence of fluorine atoms in a short-tailed surfactant increases its intrinsic hydrophobic character, while promoting the formation of elongated protein-surfactant complexes. Also, it is anticipated that the interactions of hemi-fluorinated surfactants when in contact with proteins should be different and of interest to further understand the interaction of proteins with novel surfactants. During this project a couple of hemi-fluorinated surfactants were synthesized and these could be used to continue further protein denaturation studies. Table 7.1 contains parameters for the synthesized partially fluorinated surfactants. The synthesis was done accordingly to the procedure established by Missel *et. al* which was also used to synthesize two branched surfactants (3,7-DMOS and 2-BOS)[14].

Table 7. 1. Synthesized linear hemi-fluorinated surfactants.

Surfactant name	Molecular weight (g/mole)	Structural formula
1H,1H,7H-dodecafluoroheptyl sulfate	430.1	$CHF_2(CF_2)_5CH_2SO_4$
1H,1H,2H,2H-perfluoro octyl sulfate	443.2	$CF_3(CF_2)_5CH_2CH_2SO_4$
1H,1H-perfluoro-octyl sulfate	479.1	$CF_3(CF_2)_6CH_2SO_4$
1H,1H-Perfluoro-decyl sulfate	579.2	$CF_3(CF_2)_8CH_2SO_4$

On the other hand, advancements in the creation of synthetic polypeptides have opened the opportunity to mimic natural proteins but with controlled composition[15–18]. Nowadays, the versatility and availability of the polymerization that is associated to synthetic polypeptides has moved from fundamental studies focused on preparation to the synthesis of complex self-assembling molecules with controlled sequences and composition of amino acids[19,20]. Although, synthesized polypeptides do not approach the size of natural proteins they do mimics their composition, charge and self-assembly[20]. Chemical peptide synthesis would facilitate the inclusion of desired sequences that allow controlling the distribution of hydrophobic and hydrophilic segments within the synthetic peptide. Accordingly, because proteins and surfactants share the characteristics of both having charged groups and hydrophobic regions, it is feasible to consider experiments using synthetic peptides or proteins to study their binding interactions with surfactants during protein denaturation. It is understood that above the critical micelle concentration, surfactant aggregates or micelles bind proteins along the protein backbone primarily by hydrophobic and hydrophilic forces[21–23]. Therefore, the study of the interaction of surfactants with synthetic proteins of specific and limited hydrophobic sites will elucidate the specific adsorption of these alternative surfactants into the protein on specific regions in the peptide or protein. It is suggested to use small angle scattering, circular dichroism,

and fluorescence as some of the characterization methods for this study. In particular, tryptophan fluorescence could be especially powerful when these groups are added in controlled and variable locations on the polypeptide to probe surfactant binding. The results from these studies would contribute to understanding the fundamental aspects of the formation and nano-structure of protein-surfactant complexes.

Finally, to our knowledge, nano-structural studies of protein-surfactant complexes during gel electrophoresis are scarce[24]. Preliminary studies using small angle neutron scattering to characterize the nano-structure of protein-surfactant complexes during gel electrophoresis were achieved during this dissertation. The experiment consisted in tracking the structural changes of BSA denatured by a series of alkyl sodium sulfates under the effect of different electric fields. The preliminary scattering results showed almost no changes in the scattering profiles of each BSA-surfactant complex that was tested. However, we did verify the feasibility of this type of analysis. Therefore, it is suggested to conduct comprehensives studies using small angle x-ray and neutron scattering with proteins denatured by fluorinated and branched surfactants during gel electrophoresis since these are the structures that are present in a real separation. The results from these studies will elucidate the ensemble average of the conformational changes that each protein-surfactant complex would undergo in the presence of an electric field.

7.3 References

(1) Rabilloud, T. *Journal of proteomics* **2010**, *73*, 1562–72.
(2) Westermeier, R. *Electrophoresis in practice. A guide to methods and applications of DNA and protein separations*; 4th ed.; Wiley-Vch Verlag & Co. KGaA: Germany, 2005; p. 406.
(3) Bergh, G. Van Den; Arckens, L. *Expert Review Proteomics* **2005**, *2*, 1–10.

(4) Hamdan, M.; Righetti, P. G. *Proteomics today. Protein assessment and biomarkers using spectrometry 2D electrophoresis and microarray technology*; John Wiley & Sons: Hoboken, NJ, 2005; p. 426.
(5) Rabilloud, T.; Chevallet, M.; Luche, S.; Lelong, C. *Proteomics* **2008**, *8*, 3965–3973.
(6) Rabilloud, T. *Electrophoresis* **2009**, *30*, S174–80.
(7) Hirsch, J.; Hansen, K. C.; Burlingame, A. L.; Matthay, M. A. *American Journal of Physiology. Lung Cellular and Molecular Physiology* **2003**, *287*, L1–L23.
(8) Starita-Geribaldi, M.; Thebault, P.; Taffin de Givenchy, E.; Guittard, F.; Geribaldi, S. *Electrophoresis* **2007**, *28*, 2489–97.
(9) Breyton, C.; Pucci, B.; Popot, J. In *Heterologous Expression of Membrane Proteins, Methods in Molecular Biology*; Mus-Veteau, I., Ed.; Humana Press: Totowa, NJ, 2010; Vol. 601.
(10) Ross, A.; Lee, P.; Smith, D.; Langridge, J.; Whetton, A.; Gaskell, S. *Proteomics* **2002**, *2*, 928–936.
(11) Brown, E. G. *Analytical biochemistry* **1988**, *174*, 337–348.
(12) Root, B. E.; Zhang, B.; Barron, A. E. *Electrophoresis* **2009**, *30*, 2117–2122.
(13) López, M. F.; Patton, W. F.; Utterback, B. L.; Chung-Welch, N.; Barry, P.; Skea, W. M.; Cambria, R. P. *Analytical biochemistry* **1991**, *199*, 35–44.
(14) Missel, P. J.; Mazer, N. A.; Benedek, G. B.; Carey, M. C. *The Journal of Physical Chemistry* **1983**, *87*, 1264–1277.
(15) Dawson, P. E.; Muir, T. W.; Clark-lewis, I.; Kent, S. B. H. *Science* **1994**, *266*, 776–779.
(16) Nilsson, B. L.; Soellner, M. B.; Raines, R. T. *Annu. Rev. Biophys. Biomol Struct.* **2010**, *34*, 91–118.
(17) Deming, T. J. *Progress in Polymer Science* **2007**, *32*, 858–875.
(18) Bellomo, E. G.; Wyrsta, M. D.; Pakstis, L.; Pochan, D. J.; Deming, T. J. *Nature materials* **2004**, *3*, 244–8.
(19) Dawson, P. E.; Muir, T. W.; Clark-lewis, I.; Kent, S. B. H. *Science* **1994**, *266*, 776–779.
(20) Deming, T. J. *Progress in Polymer Science* **2007**, *32*, 858–875.
(21) Chen, S.-H.; Teixeira, J. *Physical Review Letters* **1986**, *57*, 2583–2586.
(22) Chodankar, S.; Aswal, V. K.; Kohlbrecher, J.; Vavrin, R.; Wagh, a G. *Journal of Physics: Condensed Matter* **2007**, *19*, 12pp.
(23) Ibel, K.; May, R. P.; Kirschner, K.; Szadkowski, H.; Mascher, E.; Lundahl, P. *European journal of biochemistry / FEBS* **1990**, *190*, 311–8.
(24) Pozzo, D. C. *Langmuir* **2009**, *25*, 1558–1565.

Appendix A

PDDF of homogeneous spheres and inhomogeneous core-shell spheres

Figure A1, shows typical PDDF curves for homogeneous spheres and for in-homogeneous core-shell spheres as would be characterized by SAXS for fluorinated and hydrogenated surfactant micelles respectively. The PDDF models were calculated using the program Singlebody that utilizes a Monte Carlo approach for the calculation [1]. The differences in shape originate from the relative contrasts between the electron densities in the solvent, head groups and tails.

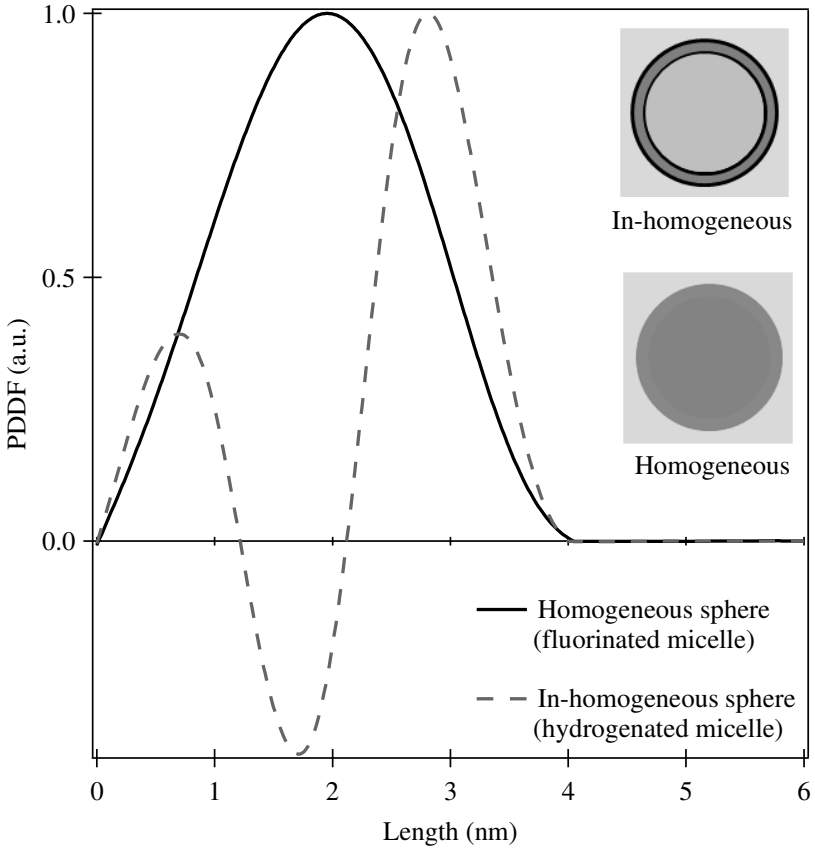

Figure A1. Characteristic PDDF for a homogeneous sphere (continuous line) and an in-homogeneous (dotted line) core-shell sphere with an identical radius (2 nm).

The electron density of the fluorinated surfactant tail is larger than the hydrogenated solvents (e.g. buffers). In contrast, for hydrogenated surfactants, the tails and the hydrogenated solvent do not have a large difference in electron density (or scattering length density). The negative feature in the in-homogeneous PDDF (hydrogenated surfactant) reflects that the contrast between the surroundings (e.g. buffer) and the micelle core (e.g. hydrocarbon chain tail) is smaller than the shell. Equation A1 (re-stated Eq. 2.4) shows the relationship that describes the PDDF calculation where $\Delta\rho(r)$ corresponds to the scattering length density differences between the continuous phase and that at position r.

$$PDDF \approx r^2 \cdot \left\langle \int_V \Delta\rho(r_1) \cdot \Delta\rho(r_1 - r) dr_1 \right\rangle \qquad \text{Equation A1}$$

Reference

1. Fritz, G. Singlebody MC. http://physchem.kfunigraz.ac.at/sm/

Appendix B

Additional characterizations of protein-surfactant complexes: DLS, phase diagrams and isoelectric points

Figure B1, shows the respective correlation functions of the protein-branched surfactant complexes analyzed in Ch. V. Dynamic light scattering analysis shows the monomodal distributions in all correlations and single decays. Markers correspond to the experimental data and lines represent the cumulant fit for each curve. The correlation functions show that larger protein-surfactant complexes decay at slower rates. Also, the correlations for 2-EHS complexes suggest that BSA and ovalbumin complexes decay at analogous rates.

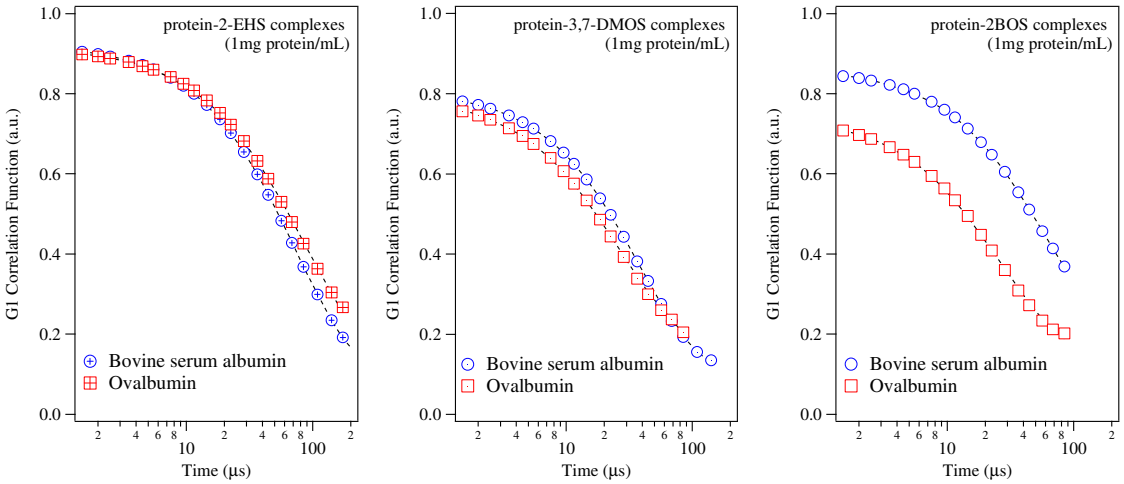

Figure B1. Correlation functions of complexes of protein and branched surfactants.

Figure B2 shows optical phase diagrams used to determine the solubility of PFC_6S and PFC_8S (Ch. VI). These measurements along with SAXS experiments indicate that both surfactants: PFC_6S and PFC_8S are below their Kraft temperature at the experimental conditions of this work.

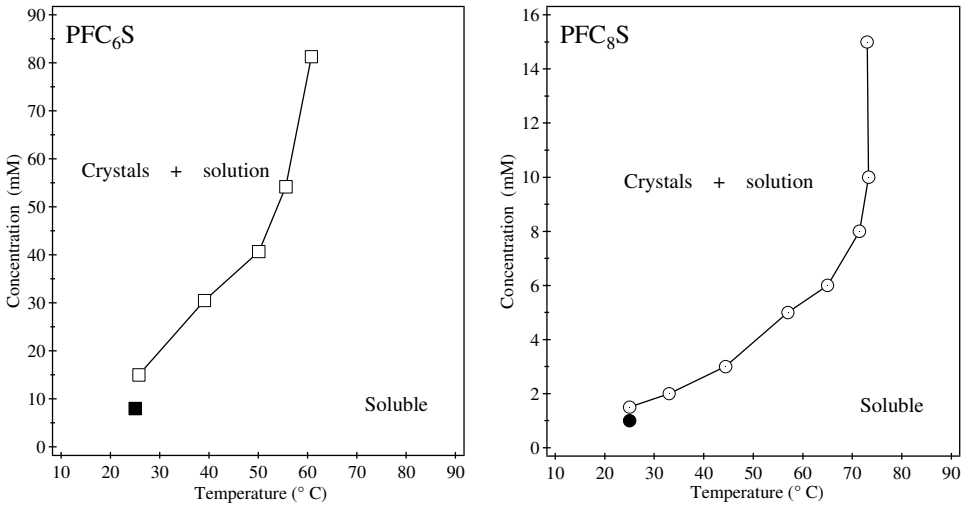

Figure B2. Phase diagram of PFC_6S and PFC_8S dissolved in trizma-glycine buffer. Filled square and circle corresponds to the temperature and buffer concentration (buffer D) used in the experiments of Ch. VI

The isoelectric points and the sign of the net charge for the eight model proteins at the experimental conditions used in all PAGE, SAXS, CD and DLS experiments done in this thesis work are shown in Fig. B3. This plot illustrates that aprotinin and lysozyme carry a net positive charge at our experimental conditions. Thus, it is expected that electrostatic forces could dominate protein-surfactant interactions.

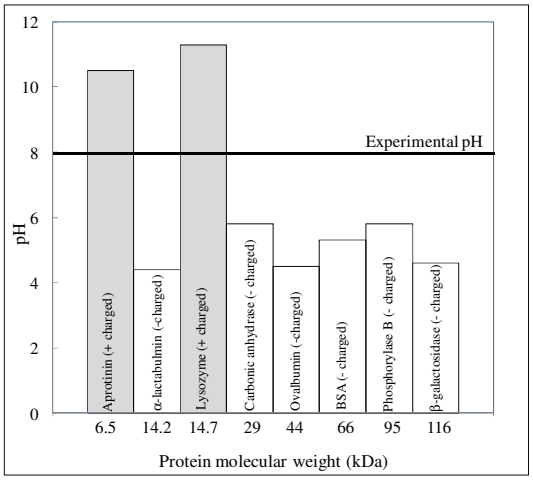

Figure B3. Isoelectric points of the model proteins that are analyzed with polyacrylamide gel electrophoresis.

Bibliography

Ahmed, N.; Oliva, K. T.; Barker, G.; Hoffmann, P.; Reeve, S.; Smith, I. A.; Quinn, M. A.; Rice, G. E. Proteomic tracking of serum protein isoforms as screening biomarkers of ovarian cancer. *Proteomics,* 2005, 5, 4625–4636.

Ananthapadmanabhan, K. P.; Dickinson, E.; Goddard, E. D.; Lindman, B.; Strauss, U. P.; Thalberg, K.; Tirrel, M.; Winnik, F. M. *Interactions of Surfactants with Polymers and Proteins.* CRC Press, Inc.: Florida, USA, 1993.

Andersen, K. K.; Otzen, D. E. J. Phys. Chem. B. 2009, 113 (42), 13942-13952.

Ann, W. B.; Janes, R. W. *Advances in Biomedical Spectroscopy Modern techniques for circular dichroism and synchrotron radiation circular dichroism spectroscopy*. IOS Press: The Netherlands, 2009; Vol. 1.

Battell, M. L.; Zarkadas, C. G.; Smillie, L. B.; Madsen, N. B. The sulfhydryl groups of muscle phosphorylase.*The Journal of Biological Chemistry,* 1968, 243 (23), 6202-6209.

Bellomo, E. G.; Wyrsta, M. D.; Pakstis, L.; Pochan, D. J.; Deming, T. J. Stimuli-responsive polypeptide vesicles by conformation-specific assembly. *Nature materials*, 2004, 3(4), 244–248.

Berg, J. An *Introduction to Interfaces & Colloids: The Bridge to Nanoscience*. World Scientific Publishing Co.: Singapore, 2010.

Bergh, G. Van Den; Arckens, L. Recent advances in 2D electrophoresis: an array of possibilities. *Expert Review Proteomics*, 2005, 2, 1–10.

Berman, H. M.; Westbrook, J.; Feng, Z.; Gilliland, G.; Bhat, T. N.; Weissig, H.; Shindyalov, I. N.; Bourne, P. E. The Protein Data Bank. *Nucleic Acid Research*, 2000, 28(1), 235-242.

Bezzobotnov, V. Y.; Borbély, S.; Cser, L.; Faragó, B.; Gladkih, I. A.; Ostanevich, Y. M.; Vass, S. Temperature and concentration dependence of properties of sodium dodecyl sulfate micelles determined from small-angle neutron scattering experiments. *Journal of Physical Chemistry*, 1988, 92, 5738–5743.

Bowers, J., Butts, C.P., Martin, P.J., Vergara-Gutierrez, M.C. Aggregation behavior of aqueous solutions of ionic liquids. *Langmuir* 2004, 20(6), 2191-2198.

Brechlin, P.; Jahn, O.; Steinacker, P.; Cepek, L.; Kratzin, H.; Lehnert, S.; Jesse, S.; Mollenhauer, B.; Kretzschmar, H. A.; Wiltfang, J.; Otto, M. Cerebrospinal fluid-optimized two-dimensional difference gel electrophoresis (2-D DIGE) facilitates the differential diagnosis of Creutzfeldt-Jakob disease. *Proteomics*, 2008, 8, 4357–4366.

Breyton, C.; Pucci, B.; Popot, J. Amphipols and Fluorinated Surfactants: Two Alternatives to Detergents for Studying Membrane Proteins In vitro. *Methods in Molecular Biology,* 2010, Vol. 601, 219-245.

Brown, E. G. Mixed anionic detergent/aliphatic alcohol-polyacrylamide gel electrophoresis alters the separation of proteins relative to conventional sodium dodecyl sulfate-polyacrylamide gel electrophoresis. *Analytical biochemistry,* 1988, 174, 337–348.

Casals, C.; Miguel, E.; Perez-Gil, J. Tryptophan fluorescence study on the interaction of pulmonary surfactant protein A with phospholipid vesicles. *Biochemical Journal* 1993, 296, 585–593.

Chandramouli, K.; Qian, P.-Y. Proteomics: Challenges, Techniques and Possibilities to Overcome Biological Sample Complexity. *Human Genomics and Proteomics,* 2009, 1-22.

Chattopadhyay, A. K.; Mittal, K. L. *Surfactants in Solution. Surfactant science series* 1996, 64, 415.

Chen, S.-H.; Teixeira, Structure and fractal dimension of protein-detergent complexes. *Physical Review Letters*, 1986, 57, 2583–2586.

Chodankar, S.; Aswal, V. K.; Kohlbrecher, J.; Vavrin, R.; Wagh, a G. Surfactant-induced protein unfolding as studied by small-angle neutron scattering and dynamic light scattering. *Journal of Physics: Condensed Matter*, 2007, 19, 326102, 12pp.

Chodankar, S.; Aswal, V. K.; Kohlbrecher, J.; Vavrin, R.; Wagh, A. G. Structural study of coacervation in protein-polyelectrolyte complexes. *Physical Review E*, 2008, 78(3), 031913-1:031913-8.

Chodankar, S., Hassan, P.A., A.G. Wagh, V K Aswal. Structure of protein-surfactant complexes as studied by small-angle neutron scattering and dynamic light scattering. *Physica B: Condensed Matter*, 2007, 398: 112–117.

Chrambach, A.; Rodbard, D. Polyacrylamide gel electrophoresis. *Science*, 1971, 172 (3982), 440–451.

Chrysina, E. D.; Brew, K.; Acharya, K. R. Crystal structure of apo- and holo-bovine alpha-lactalbumin at 2.2 -A resolution reveal an effect of calcium on inter-lobe interactions. *Journal of Biological Chemistry*, 2000, 275(47), 37021-37029.

Cipriani, F.; Rower, M.; Landret, C.; Zander, U.; Felisaz, F.; Marquez, J. A. Crystal direct: a new method for automated crystal harvesting based on laser-induced photoablation of thin films. *Acta Crystallographica Section D,* 2012, 68, 1393-1399.

Craven, G.; Steers, E.; Anfinsen, C. Purification, composition and molecular weight of the B-galactosidase of Escherichia coli K12. *The Journal of Biological Chemistry* 1965, 240 (69), 2468-2477.

D'Auria, S., Di Cesare, N., Gryczynski, I., Rossi, M., Lakowicz, J.R. On the Effect of Sodium Dodecyl Sulfate on the Structure of beta- Galactosidase from Escherichia colt: a fluorescence study. *Journal of Biochemistry,* 2001, 130(1), 13–18.

Dawson, P. E.; Muir, T. W.; Clark-lewis, I.; Kent, S. B. H. Synthesis of proteins by native chemical ligation. *Science*, 1994, 266(5186), 776–779.

Deep, S., Ahluwalia, J.C. Interaction of bovine serum albumin with anionic surfactants. *Physical Chemistry Chemical Physics*, 2001, 3, 4583-4591.

Deming, T. J. Synthetic polypeptides for biomedical applications. *Progress in Polymer Science*, 2007, 32(8-9), 858–875.

Dolnik, V.; Gurske, W. A. Chemical modification of proteins to improve the accuracy of their relative molecular mass determination by electrophoresis. *Electrophoresis,* 2011, 32(20), 2893–2897.

Donnet, C.; Arystarkhova, E.; Sweadner, K. J. Thermal denaturation of the Na,K-ATPase provides evidence for alpha-alpha oligomeric interaction and gamma subunit association with the C-terminal domain. *Journal of Biological Chemistry,* 2001, 276(10), 7357–7365.

Durand, G.; Seta, N. Protein glycosylation and diseases: Blood and urinary oligosaccharides as markers for diagnosis and therapeutic monitoring. *Clinical Chemistry*, 2000, 46(6), 795-805.

Evans, F. D.; Wennerstrom, H. *The Colloidal Domain where Physics, Chemistry, Biology and Technology meet*; 1st ed.; VCH Publishers, Inc.: New York, USA, 1994.

Franklin, M. J.; Surampudi, L. N.; Ashbaugh, H. S.; Pozzo, D. C. Numerical validation of IFT in the analysis of protein-surfactant complexes with SAXS and SANS. *Langmuir*, 2012, 28(34), 12593-12600.

Fritz, G.; Bergmann, A.; Glatter, O. Evaluation of Small-Angle Scattering Data of Charged Particles Using the Generalized Indirect Fourier Transformation (GIFT) Technique. *Journal of Chemicals Physics*, 2000, 113(21), 9733-9740.

Fritz, G.; Bergmann, A. Interpretation of small-angle scattering data of inhomogeneous ellipsoids. *Journal of Applied Crystallography*, 2004, 37(5), 815-822.

Gao, J. Y.; Dubin, P. L. Binding of Proteins to Copolymers of Varying Hydrophobicity. *Biopolymers*, 1998, 49, 185-193.

Gargi B.R., Chakraborty, I., Soumen G., Moulik, S.P. A critical and comprehensive assessment of interfacial and bulk properties of aqueous binary mixtures of anionic surfactants, sodium dodecylsulfate, and sodium dodecylbenzenesulfonate. *Colloid Polymer Science,* 2007, 285, 457-469.

Gibbons, G. H.; Liew, C. C.; Goodarzi, M. O.; Rotter, J. I.; Hsueh, W. A.; Siragy, H. M.; Pratt, R.; Dzau, V. J. Genetic Markers: Progress and potential for Cardiovascular Disease. *Circulation, Journal of the American Heart Association,* 2004, 109(IV), 47–58.

Gimel, J. C.; Brown, W. A light scattering investigation of the sodium dodecyl sulfate-lysozyme system. *Journal of Chemical Physics,* 1996, 104(20), 8112–8117.

Glatter, O. The interpretation of Real-Space information from small-angle scattering experiments. *Journal of Applied Crystallography.* 1979, 12, 166-175.

Glatter, O., Kratky, O. *Small Angle X-ray Scattering*. Academic press: London, 1982.

Gold, A. M. Sulfhydryl groups of rabbit muscle glycogen phosphorylase b. Reaction with dinitrophenylating agents. *Biochemistry*, 1968, 7(6), 2106-2115.

Gorg, A.; Weiss, W.; Dunn, M. Current two-dimensional electrophoresis technology for proteomics. *Proteomics* 2004, 4, 3665–3685.

Greenfield, N, and G D Fasman. Computed circular dichroism spectra for the evaluation of protein conformation. *Biochemistry,* 1968, 8(10): 4108–16.

Gregoriou, M.; Noble, M. E. M.; Watson, K. A.; Garman, E. F.; Krulle, T. M.; De la Fuente, C.; Fleet, G. W. J.; Oikonomakos, N. G.; Johnson, L. N. The structure of a glycogen phosphoylase glucopyranose spirohydantoin complex at 1.8 A resolution and 100 K: the role of the water structure and its contribution to binding. *Protein Science*, 1998, 7(4), 915-927.

Groth, C., Nyden, M., Holmberg, K., Kanicky, J.R., Shah, D.O. Kinetics of the Self-Assembly of Gemini Surfactants. *Journal of Surfactants and Detergents,* 2004, 7(3), 247-255.

Gull, N., Aswal, V.K., Chodankar, S. and Kabir-UD-DIN. Small angle neutron scattering studies on the interaction of cationic surfactants with bovine serum albumin. *Pramana- Journal of Physics,* 2008, 71(5): 1027–1031.

Hamdan, M.; Righetti, P. G. *Proteomics today. Protein assessment and biomarkers using spectrometry 2D electrophoresis and microarray technology*. John Wiley & Sons: Hoboken, USA, 2005.

Hartinger, J.; Stenius, K.; Högemann, D.; Jahn, R. 16-BAC/SDS-PAGE: a two-dimensional gel electrophoresis system suitable for the separation of integral membrane proteins. *Analytical biochemistry*, 1996, 240(1), 126–133.

Hassan, N.; Barbosa, L. R. S.; Itri, R.; Ruso, J. M. Fibrinogen stability under surfactant interaction. *Journal of Colloid and Interface Science*, 2011, 362(1), 118-126.

Hirsch, J.; Hansen, K. C.; Burlingame, A. L.; Matthay, M. A. Proteomics: current techniques and potential applications to lung disease. *American Journal of Physiology. Lung Cellular and Molecular Physiology*, 2003, 287, L1–L23.

Ibel, K.; May, R. P.; Kirschner, K.; Szadkowski, H.; Mascher, E.; Lundahl, P. Protein-decorated micelle structure of sodium-dodecyl-sulfate-protein complexes as determined by neutron scattering. *European journal of biochemistry / FEBS* 1990, 190(2), 311–318.

Israelachvili, J. *Intermolecular and Surface Forces with Application to Colloidal and Biological Systems*; 3rd ed.; Academic Press. USA, 2011.

Jin, T.; Hu, L.-S.; Chang, M.; Wu, J.; Winblad, B.; Zhu, Proteomic identification of potential protein markers in cerebrospinal fluid of GBS patients. *European Journal of Neurology*, 2007, 14(5), 563–568.

Jones, M. N.; Skinner, H. a; Tipping, E. The interaction between bovine serum albumin and surfactants. *Biochemical Journal,* 1975, 147(2), 229–34.

Jones, M. N. A theoretical approach to the binding of amphypathic molecules to globular proteins. *Biochemical Journal,* 1975, 151(1), 109-114.

Kashino, Y. Separation methods in the analysis of protein membrane complexes. *Journal of Chromatography B*, 2003, 797(1-2), 191-216.

Kayser, M.; De Knijff, P. Improving human forensics through advances in genetics, genomics and molecular biology. *Nature Reviews Genetics,* 2011, 12(3), 179–192.

Kelly, S. M.; Jess, T. J.; Price, N. C. How to study proteins by circular dichroism. *Biochimica et Biophysica Acta*, 2005, 1751(2), 119–139.

Kissa, E. *Fluorinated surfactants: Synthesis•Properties•Applications*; Marcel Dekker, INC: New York, USA, 1994, Vol. 50.

Kissa, E. *Fluorinated Surfactants and Repellents*; *Surfactant science series*, 2nd ed.; Marcel Dekker: New York, 2001.

Kline, S. R. Reduction and analysis of SANS and USANS data using IGOR pro. *Journal of Applied Crystallography*, 2006, 39, 895-900.

Krafft, M. P. Fluorocarbons and fluorinated amphiphiles in drug delivery and biomedical research. *Advanced Drug Delivery Reviews,* 2001, 47(2-3), 209-228.

Krishnamurthy, V. M.; Kaufman, G. K.; Urbach, A. R.; Gitlin, I.; Gudiksen, K. L.; Weibel, D. B.; Whitesides, G. M. Carbonic anhydrase as a model for biophysical and physical-organic studies of proteins and protein-ligand binding. *Chemical reviews* 2008, 108, 946–1051.

Kwak, J. C. T. *Polymer-Surfactant Systems. Surfactant science series*. Marcel Dekker, INC: New York, USA, 1998

Lerman, L. S.; Frisch, H. L. Why does the electrophoretic mobility of DNA in gels vary with the length of the molecule?. *Biopolymers*, 1982, 21(5), 995–997.

Li, H.; Li, C.; Wu, H.; Zhang, T.; Wang, J.; Wang, S.; Chang, J. Identification of Apo-A1 as a biomarker for early diagnosis of bladder transitional cell carcinoma. *Proteome Science,* 2011, 9(21), 1–11.

Li, L.; Xu, Z. S.; Song, G. W. Study on the langmuir aggregation of fluorinated surfactants on protein. *Journal of Fluorine Chemistry,* 2009, 130(2), 225-230.

Li, Y., Wang, X., Wang, Y. Comparative studies on interactions of bovine serum albumin with cationic gemini and single-chain surfactants. *Journal of Physical Chemistry B,* 2006, 110(16), 8499-8505.

Lindner, P.; Zemb, T. *Neutrons, X-rays and light: Scattering Methods Applied to Soft Condensed Matter.* 1st ed., Elsevier Science B.V.: The Netherlands, 2002.

López, M. F.; Patton, W. F.; Utterback, B. L.; Chung-Welch, N.; Barry, P.; Skea, W. M.; Cambria, R. P. Effect of various detergents on protein migration in the second dimension of two dimensional gels. *Analytical biochemistry*, 1991, 199(1), 35-44.

Lumpkin, O. J.; Zimm, B. H. Mobility of DNA in gel electrophoresis. *Biopolymers,* 1982, 21(11), 2315–2316.

Lundhal, P.; Greijer, E.; Sandberg, M.; Cardell, S.; Eriksson, K.-O. A model for ionic and hydrophobic interactions and hydrogen-bonding in sodium dodecyl sulfate-protein complexes. *Biochimica et Biophysica Acta*, 1986, 873(1), 20–26.

Majorek, K. A.; Porebski, P. J.; Chruszcz, M.; Almo, S. C.; Minor, W. Structural and immunologic characterization of bovine, horse, and rabbit serum albumins. *Molecular Immunology*, 2012, 52(3-4), 174–182.

Malmon, A. G. Small Angle X-ray Scattering Studies of the Size, Shape and Hydration of Catalase. *Biochimica et Biophysica Acta,* 1957, 26(2), 233-240.

Masayuki, Y.; Takahashi, N.; Hirose, M. Crystal structure of S-ovalbumin as a non-loop-inserted thermostabilized serpin Form. *The Journal of Biological Chemistry,* 2003, 278(37), 35524-35530.

Matsuoka, K.; Moroi, Y. Micellization of fluorinated amphiphile. Current *Opinion in Colloid and Interface Science*, 2003, 8(3), 227–235.

Mattice, W.; Riser, J. M.; Clark, D. S. Conformational properties of the complexes formed by proteins and sodium dodecyl-sulfate. *Biochemistry*, 1976, 15(19), 4264–4272.

Messina, P.V., Prieto, G., Ruso, J.M., Sarmiento, F. Conformational changes in human serum albumin induced by sodium perfluorooctanoate. *Journal of Physical Chemistry B*, 2005, 109(32), 15566–15573.

Missel, P. J.; Mazer, N. A.; Benedek, G. B.; Carey, M. C. Influence of chain length on the spehere to rod transition in alkyl sulfate micelles. *The Journal of Physical Chemistry,* 1983, 87(7), 1264–1277.

Mobasheri, A. Osteoarthritis year 2012 in review: biomarkers. *Osteoarthritis and Cartilage,* 2012, 20(12), 1451–1464.

Moriyama, Y.; Ohta, D.; Hachiya, K.; Mitsui, Y.; Takeda, K. fluorescence behavior of Tryptophan residues of bovine and human serum albumins in ionic surfactant solutions: A comparative study of the two and one tryptophan(s) of bovine and human albumins. *Journal of Protein Chemistry,* 1996, 15(3), 265–272.

Muga, A., Arrondo, J.L., Bellon, T., Sancho, J., Bernabeu, C. Structural and functional studies on the interactions of sds with galactosidase. *Archives of Biochemestry and Biophysics*, 1993, 300(1), 451–457.

Muller, K.; Laggner, P.; Glatter, O.; Kostner, G. The structure of Human-Plasma low density lipoprotein B. An X-ray Small Angle Scattering study. *European Journal of Biochemistry,* 1978, 82(1), 73–90.

Muto, Y.; Esumi, K.; Meguro, K.; Zana, R. Aggregation behavior of mixed fluorocarbon and hydrocarbon surfactants in aqueous solutions. *Journal of Colloid and Interface Science,* 1987, 120(1), 162-171.

Myers, D. *Surfactant Science and Technology.* 3rd ed. VCH Publishers, Inc.: New York, USA. 1988.

Narayanan, J.; Abdul Rasheed, A. S.; Bellare, J. R. A small-angle X-ray scattering study of the structure of lysozyme-sodium dodecyl sulfate complexes. *Journal of colloid and interface science,* 2008, 328(1), 67–72.

Nelson, C. A. The binding of Detergents to Proteins. *The Journal of Biological Chemistry* 1971, 246(12), 3895–3901.

Nielsen, A. D.; Arleth, L.; Westh, P. Analysis of protein-surfactant interactions-a titration calorimetric and fluorescence spectroscopic investigation of interactions between Humicola insolens cutinase and an anionic surfactant. *Biochimica et Biophysica Acta*, 2005, 1752, 124–132.

Nilsson, B. L.; Soellner, M. B.; Raines, R. T. Chemical Synthesis of Proteins. *Annual Review of Biophysics and Biomolecular Structure,* 2010, 34, 91–118.

Nnana, I., and Xia, J. *Protein-Based surfactants. Synthesis, physicochemical properties, and applications.* Surfactant science series, Vol. 101. Marcel Dekker, Inc.: New York, USA. 2001.

Ospinal-Jimenez, M.; Pozzo, D. C. Structural analysis of protein complexes with sodium alkyl sulfates by small-angle scattering and polyacrylamide gel electrophoresis. *Langmuir* 2011, 27(3), 928–935.

Ospinal-Jiménez, M.; Pozzo, D. C. Structural analysis of protein denaturation with alkyl perfluorinated sulfonates. *Langmuir*, 2012, 28(51), 17749–17760.

Otzen, D. Protein-surfactant interactions: A tale of many states. *Biochimica et Biophysica Acta*, 2011, 1814(5), 562–591.

Peng, J.; Gygi, S. P. Proteomics: the move to mixtures. *Journal of mass spectrometry,* 2001, 36(10), 1083–1091.

Peterman, B. F.; Laidler, K. J. Study of Reactivity of Tryptophan Residues in Serum Albumins and Lysozyme by N-Bromosuccinamide Fluorescence Quenching. *Archives of Biochemistry and Biophysics,* 1980, 199(1), 158–164.

Pozzo, D. C. Neutron-scattering probe of complexes of Sodium dodecyl sulfate and serum albumin during polyacrylamide gel electrophoresis. *Langmuir*, 2009, 25(3), 1558–1565.

Privalov, P. L. Cold denaturation of Proteins. *Critical Reviews in Biochemistry and Molecular Biology*, 1990, 25(4), 281–306.

Rabilloud, T.; Chevallet, M.; Luche, S.; Lelong, C. Fully denaturing two-dimensional electrophoresis of membrane proteins: A critical update. *Proteomics*, 2008, 8(19), 3965–3973.

Rabilloud, T. Two-dimensional gel electrophoresis in proteomics: Past, present and future. *Journal of Proteomics,* 2010, 73(11), 1562–72.

Rabilloud, T.; Variations on a theme: changes to electrophoretic separations that can make a difference. *Journal of Proteomics,* 2010, 73(8): 1562–72

Reynolds, J. A.; Tanford, C. Binding of dodecyl sulfate to proteins at high binding ratios. Possible implications for the state of proteins in biological membranes. *Proceedings of the National Academy of Sciences of the United States of America.* 1970, 66(3), 1002–1007.

Reynolds, J. A.; Tanford, C. The gross conformation of protein-sodium dodecyl sulfate complexes. *The Journal of Biological Chemistry*, 1970, 245(19), 5161–5165.

Root, B. E.; Barron, A. E.; Zhang, B. Size-based protein separations by microchip electrophoresis using an acid-labile surfactant as a replacement for SDS *Electrophoresis* 2009, 30(12), 2117-2122.

Rossi, S., Karlsson, G., Ristori, S., Martini, G., Edwards, K. Aggregate Structures in a Dilute Aqueous Dispersion of a Fluorinated/Hydrogenated Surfactant System. A Cryo-Transmission Electron Microscopy Study. *Langmuir*, 2001, 17, 2340–2345.

Ruiz-Peña, M.; Comas-Rojas, H.; Rodriguez-Calvo, S.; Perez-Gramatges, A. Self-association behaviour of protein: surfactant systems in alcohol/water mixtures *IEE. Proceedings-Nanobiotechnology* 2005, 152(5), 177-181.

Ruso, J. M.; Gonzáez-Pérez, A.; Prieto, G.; Sarmiento, F. Study of the interaction between lysozyme and sodium octanoate in aqueous solutions. *Colloids and Surfaces A,* 2004, 249(1-3), 45–50.

Ruso, J. M.; González-Pérez, A.; Prieto, G.; Sarmiento, F. Study of the interactions between lysozyme and a fully-fluorinated surfactant in aqueous solution at different surfactant-protein ratios. *International Journal of Biological Macromolecules,* 2003, 33(1-3), 67–73.

Saito, R.; Sato, T.; Ikai, A.; Tanaka, N. Crystal structure analysis of bovine carbonic anhydrase II. *Acta Crystallographica D: Biological Crystallography,* 2004, 60 (4), 792-795.

Samsó, M.; Daban, J. R.; Hansen, S.; Jones, G. R. Evidence for sodium dodecyl sulfate/protein complexes adopting a necklace structure. *European Journal of Biochemistry,* 1995, 232(3), 818–824.

Samyn, B.; Sergeant, K.; Memmi, S.; Debyser, G.; Devreese, B.; Van Beeumen, J. MALDI-TOF/TOF de novo sequence analysis of 2-D PAGE-separated proteins from Halorhodospira halophila, a bacterium with unsequenced genome. *Electrophoresis,* 2006, 27(13), 2702–2711.

Santos. S.F., Zanette, D., Fischer, H., Itri, R. A systematic study of bovine serum albumin (BSA) and sodium dodecyl sulfate (SDS) interactions by surface tension and small angle X-ray scattering. *Journal of Colloid and Interface Science,* 2003, 262(2), 400–408.

Sauer, M.; Hofkens, J.; Enderlein, J. *Handbook of Fluorescence Spectroscopy and Imaging*. Wiley-Vch Verlag & Co. KGaA: Germany, 2011.

Scattering length density calculator http://www.ncnr.nist.gov/resources/sldcalc.html.

Schramm, L. L. *Surfactants: Fundamentals and Applications in the Petroleum Industry.* Cambridge University Press: Cambridge, UK, 2000.

Shapiro, A. L.; Viñuela, E.; Maizel, J. V. Molecular weight estimation of polypeptide chains by electrophoresis in SDS-polyacrylamide gels. *Biochemical and Biophysical Research Communications*, 1967, 28(5), 815–820.

Starita-Geribaldi, M.; Thebault, P.; Taffin de Givenchy, E.; Guittard, F.; Geribaldi, S. 2-DE using hemi-fluorinated surfactants. *Electrophoresis*, 2007, 28(14), 2489–2497.

Stenstam, A.; Khan, A.; Wennerstrom, H. The Lysozyme-Dodecyl Sulfate System. An example of Protein-Surfactant Aggregation. *Langmuir*, 2001, 17(24), 7513–7520.

Stjerndahl, M., Lundberg, D., Zhang, H., Menger, F. *Journal of Physical Chemistry B* 2007, 111(8), 2008-2014.

Su, Y.-Y. T.; Jirgensons, B. Further Studies on Detergent-Induced Conformational Transitions in Proteins. *Archives of Biochemistry and Biophysics* 1977, 181(1), 137-146.

Tanford, C. Micelle Shape and Size. *Journal of Physical Chemistry,* 1972, 76(21), 3020–3024.

Tanford, C. *The Hydrophobic Effect: formation of micelles and biological membranes*, John Wiley & Sons: New York, USA, 1973.

Tiddy, G. J. T. *Concentrated Surfactant Systems. Modern Trends of Colloid Science in Chemistry and Biology* 1985, 148–156.

Tung, J.-S.; Knight, C. A. Relative importance of some factors affecting the electrophoretic migration of proteins in sodium dodecyl sulfate-polyacrylamide gels. *Analytical biochemistry*, 1972, 48(1), 153-163.

Turro, N. J.; Lei, X.-G.; Ananthapadmanabhan, K. P.; Aronson, M. Spectroscopic probe analysis of protein-surfactant interactions: the BSA/SDS system. *Langmuir*, 1995, 11(7), 2525–2533.

Valstar, A.; Almgren, M.; Brown, W. The interaction of bovine serum albumin with surfactants studied by light scattering. *Langmuir,* 2000, 16(3), 922-927.

Vasilescu, M., Angelescu, D. *Langmuir* 1999, 15(8), 2635-2643.

Verrills, N. M. Clinical Proteomics: Present and Future Prospects. *Clinical Biochemist Reviews,* 2006, 27, 99–116.

Viallet, P. M.; Vo-Dinh, T.; Ribou, a C.; Vigo, J.; Salmon, J. M. Native fluorescence and mag-indo-1-protein interaction as tools for probing unfolding and refolding sequences of the bovine serum albumin subdomain in the presence of guanidine hydrochloride. *Journal of Protein Chemistry,* 2000, 19(6), 431–439.

Vieira, D. B.; Crowell, A. M. J.; Doucette, A. A. Perfluorooctanoic acid and ammonium perfluorooctanoate volative surfactants for proteome analysis?. *Rapid Communication in Mass Spectrometry,* 2011, 26(5), 523-531.

Viovy, J.-L. Electrophoresis of DNA and other polyelectrolytes: Physical mechanisms. *Reviews of Modern Physics,* 2000, 72(3), 813–872.

Vivian, J. T.; Callis, P. R. Mechanisms of Tryptophan Fluorescence Shifts in Proteins *Biophysical Journal,* 2001, 80(5), 2093–2109.

Weber, K.; Osborn, M. The Reliability of Molecular Weight Determinations by Dodecyl Sulfate-Polyacrylamide Gel Electrophoresis. *Journal of Biological Chemistry,* 1969, 244(16), 4406–4412.

Westermeier, R. *Electrophoresis in practice. A guide to methods and applications of DNA and protein separations.* 4th ed. Wiley-VCH Verlag & Co. KGaA: Germany, 2005.

Witte, F.M., Enghberts, J.B.F.N. Perturbation of SDS and CTAB micelles by complexation with poly(ethylene oxide) and poly(propylene oxide). *The Journal of Organic Chemistry*, 1987, 52(21), 4767-4772.

Wheatley, R. W.; Kapperlhoff, J. C.; Hahn, J. N.; Dugdale, M. L.; Dutkoski, M. J.; Tamman, S. D.; Fraser, M. E.; Huber, R. E. Substitution for Asn460 cripple beta-galactosidase (Escherichia coli) by increasing substrate affinity and decreasing transition state stability. *Archives of Biochemistry and Biophysics,* 2012, 521(1-2), 51-61.

Whitmore, L.; Wallace, B. A. DICHROWEB, an online server for protein secondary structure analysis from circular dichroism spectroscopic data. *Nucleic Acid Research*, 2004, 32(2), W668–W673.

Whitmore, L.; Wallace, B. A. Protein secondary structure analyses from Circular Dichroism spectroscopy: Methods and reference databases. *Biopolymers*, 2007, 89(5), 392–400.

Wong, K.-P.; Tanford, C. Denaturation of Bovine Carbonic Anhydrase B by Guanidine Hydrochloride. *Journal of Biological Chemistry,* 1973, 248(24), 8518-8523.

Yang, I. S.; Kim, T. G.; Park, B. S.; Cho, K. J.; Lee, J. H.; Park, Y.; Kim, K. H. Crystal structures of aprotinin and its complex with sucrose octasulfate reveal multiple modes of interactions with implications for heparin binding. *Biochemical and Biophysical Research Communications*, 2010, 397(3), 429-435.

Zemser, M.; Friedman, M.; Katzhendler, J.; Greene, L. L.; Misky, A.; Gorinstein, S. Relationship between functional properties and structure of ovalbumin." Journal of protein chemistry. *Journal of Protein Chemistry,* 1994, 13(2), 261–274.

Curriculum Vitae

Mónica Ospinal-Jiménez, PhD.

EDUCATION

University of Washington, Ph.D. in Chemical Engineering July 2013
Thesis Title: *Engineering protein electrophoresis through surfactant design*
Advisor: Prof. Danilo C. Pozzo, PhD.

University of Washington, MS., Chemical Engineering Dec 2010

University of Puerto Rico, MS., Chemical Engineering Jun 2006
Thesis Title: *Hydrogen Production Study using Autothermal Reforming of Biodiesel and other Hydrocarbons for Fuel Cell Applications.*
Advisor: Prof. José A. Colucci, PhD.

Universidad del Valle, B.S., Chemical Engineering May2002
Thesis Title: *Uso, Manejo y Disposición de Tricloroetileno Empleado en un Proceso de Lavado de Partes de Aluminio*
Advisor: Prof. Juan P. Silva, PhD.

Awards/Honors
University of Washington Scholarship (Sep 2007 – Jun 2012)
University of Puerto Rico Scholarship (Jan 2003 – Jun 2006)
Universidad del Valle Honor Scholarship (June 1997- Mar 2001)

PROFESSIONAL EXPERIENCE

University of Washington, Department of Chemical Engineering, Seattle, WA
Graduate Research Assistant Jan. 2008-Present

- Performed research investigating the effect of surfactant architecture for proteomic separations.
- Developed relationships between surfactant architecture and protein separation
- Characterized linear, branched and fluorinated anionic surfactants.
- Mentored five undergraduate students

Teaching Assistant Sep. 2008-Dec 2012

- Instructor of colloid and surface science laboratory sections
- Developed and led laboratory experiments
- Assisted in grading of exams, laboratory reports and presentations.

Puerto Rico Math & Science Partnership, University of Puerto Rico, Mayaguez, PR
Project Manager Assistant July 2006-June 2007

- Assisted program manager in all programmatic issues for 48 schools that were part of a NSF funded research project focused in a preparing teachers to be experts in science and mathematics.

University of Puerto Rico, Department of Chemical Engineering, Mayaguez, PR
Graduate Research Assistant Jan. 2003-June 2006

- Established the feasibility of using two new catalysts to convert hydrocarbons to a hydrogen rich product gas.
- Assisted in the monthly reports to Argonne National Laboratory and Department of Energy
- Assisted in the transterification and commercialization of biodiesel in Latin America.
- Evaluated biodiesel, glycerin and ethanol for hydrogen production.
- Designed and complete auto-thermal reforming experiments
- Mentored and supervised 25+ undergraduate students

Teaching Assistant

- Supervised and advised undergraduate students. Instructor of unit operation lab, mass and energy balance, mass transfer

Johnson & Johnson, Medical Division, Cali, Colombia
Quality Control Engineer July 2002-Jan. 2003

- Evaluated and wrote new SOP's to improve the safety and environmental practices. Ensured regulatory compliance in the production lines of Cidex solution and plaster bandages.
- Developed training modules in GMP and performed quality control auditing.

Pfizer pharmaceuticals, Quality Control department, Cali, Colombia
Quality Control Analyst May 2001-Apr. 2002

- Executed and interpreted more than 700 specific chemical tests according with the USP (United Standard Pharmacopeias).
- Accepted and rejected raw materials.

Gillette de Colombia, Manufacturing, Cali, Colombia
Co-op student engineer Mar 2000-Jun 2001

- Implemented a new procedure to use and dispose more than 2750 gal of toxic residues of trichloroethylene and perchloroethylene used in a razorblade and ballpoint pen processes. Contributed in the achievement of the ISO-14000 certification.
- Worked with suppliers to qualify products.

PUBLICATIONS

1. Ospinal-Jiménez, M.; Pozzo, C.D., Proteomic denaturation by branched alkyl sodium sulfates. In preparation.
2. Ospinal-Jiménez, M.; Pozzo, C.D., Structural analysis of protein denaturation with alkyl perfluorinated sulfonates. Langmuir 28 (51) (2012).
3. Ospinal-Jiménez, M.; Pozzo, C.D.; Structural Analysis of Protein Complexes with Sodium Alkyl Sulfates by Small-Angle Scattering and Polyacrylamide gel electrophoresis. Langmuir 27 (3) (2010).
4. Ospinal-Jiménez, M.; Colucci, J.A., Hydrogen production using auto-thermal reforming of biodiesel and other hydrocarbons for fuel cell applications. Proceedings ISEC (2006).
5. Ospinal-Jimenez, M. Colucci, J.A., Hydrogen production using auto-thermal reforming of biodiesel and other hydrocarbons for fuel cell applications. Thesis. University of Puerto Rico (2006).
6. Ospinal-Jiménez, M.; Guezlan, H., Silva, JP.; Uso, manejo y disposición del tricloroetileno empleado en un proceso de lavado de partes de aluminio. Tesis. Universidad del Valle (2001).

PRESENTATIONS

1. Ospinal-Jimenez, M., Pozzo, C.D.; "Protein surfactant nanostructures for enhanced electrophoretic separations". UW Chemical Engineering Graduate Symposium. Sept. 2011, Poster.
2. Ospinal-Jiménez, M.; Pozzo, C.D.; "Engineering Protein Electrophoresis through Surfactant Design: The Role of Nanostructure" AIChE Annual Meeting. Nov. 2010, Presentation.
3. Ospinal-Jimenez, M., Pozzo, D.C., "Protein surfactant nanostructures for enhanced electrophoretic separations". International Conference on Neutron Scattering, May 2009, Poster.
4. Ospinal-Jiménez, M., Colucci, J.A. "Hydrogren Production by means of autothermal reforming for fuel cell automotive applications". AIChE Annual Meeting. Nov 2005, Poster. (Awarded 3rd place in Fuels and Petrochemicals Poster section)
5. Ospinal-Jimenez, M. Colucci, J.A. "Hydrogren Production Study using Autothermal Reforming of biodiesel and other Hydrocarbons for fuel cell applications". UPRM Chemical Engineering Graduate Seminar Series. April 2005, Presentation.
6. Ospinal-Jimenez, M., Rodriguez, C., Colucci, J.A. "ATR of Methanol: Catalyst vs. Thermal reforming. AIChE Annual Meeting. Nov 2004, Poster.
7. Ospinal-Jimenez, M., Lopez, D., Colucci, J.A., "Autothermal reforming of biodiesel with a Rh and Pt-based catalyst". AIChE Annual Meeting. Nov 2004, Poster.
8. Ospinal-Jimenez, M., Morales, S., Colucci, J.A., "Commertialization of biodiesel in Central and South America". AIChE Annual Meeting. Nov 2004, Poster.